UNIVERSIDADE DE LISBOA
FACULDADE DE CIÊNCIAS
DEPARTAMENTO GEOLOGIA

Analogue Modelling of Upper Crustal Strike-Slip Fault Propagation Across Morphological and/or Rheological Obstacles

Afonso Duarte Silva Gomes

Mestrado em Geologia
Especialização em Geologia Estrutural

Dissertação orientada por:
Filipe Medeiros Rosas

2019

Acknowledgements

I would like to thank my supervisor, Prof. Filipe Rosas, for the opportunity of participating in this project and for his support and continuous commitment.

I thank Dr. João Duarte for fruitful discussions related to this work, all co-authors for thorough and insightful revisions to the article, and Carlos Nogueira for helping me with the inner-workings of the LATTEX lab.

I acknowledge the LATTEX analogue Modelling lab of the IDL institute (Geology Department, Faculty of Science, University of Lisbon), for providing the infrastructure and materials needed for the experiments.

I acknowledge the European Geoscience Union and their Roland Schlich Early Career Scientist's Travel Support for partially funding my attendance to the EGU General Assembly 2018, where I presented an earlier version of this work.

The final version of this thesis also benefited from the lively, fruitful discussion with all members of the M.Sc. jury, and in particular from the rigorous constructive criticism of Prof. Rui Dias, Dr. Marta Neres and Prof. João Cabral.

Lastly, I'd like to express my gratitude to my parents, João and Manuela, without whose support the continuing of my studies wouldn't have been possible.

Resumo

O manuscrito agora submetido é constituído por duas partes. Uma primeira onde se procura contextualizar sucintamente a metodologia laboratorial de modelação análoga, tanto numa perspectiva histórica, como tendo em vista a sua relevância e utilidade em geologia estrutural. Uma segunda, mais extensa, consistindo no essencial do presente trabalho (entretanto submetido à revista *Journal of Structural Geology*), que incide na aplicação dessa mesma metodologia a um problema específico, conceptual, de geologia estrutural.

O projecto experimental agora apresentado pretendeu estudar, com recurso a modelação análoga, o efeito da presença de heterogeneidades morfológicas e/ou reológicas na formação e modificação do padrão estrutural típico de uma zona de cisalhamento frágil supra-crustal. A heterogeneidade (anomalia) reológica considerada consiste num corpo com um comportamento mecânico (reológico) viscoso, de geometria oblata, disposto sub-horizontalmente ("inter-estratificado" nas rochas da crosta), e.g. correspondendo a um diapiro salino ou uma a uma câmara magmática (pré-tectónica) em arrefecimento. A heterogeneidade morfológica, por sua vez, corresponde a um relevo topográfico alongado (e.g. a uma crista ou cordilheira). O aparato experimental utilizado representa uma variação de uma experiência clássica de Riedel (e.g. Naylor, *et al.*, 1986), consistindo numa caixa de deformação com duas placas basais, horizontalmente justapostas e deslizando lateralmente uma em relação à outra (materializando uma falha vertical de desligamento direito). No decurso da experiência, o movimento ao longo desta falha basal é transmitido a uma cobertura de areia sobrejacente, que acomoda a deformação implicada de um modo frágil. Esta configuração experimental pretende simular genericamente a reactivação de uma falha de desligamento num soco subjacente a uma cobertura sedimentar. Areia quártzica é utilizada como análogo mecânico da crosta superior, e silicone transparente (PDMS) é empregue para representar a anomalia viscosa supra-crustal. São investigadas experimentalmente as seguintes variáveis: a) presença/ausência de uma anomalia viscosa; b) presença/ausência de uma crista topográfica; c) diferente ângulo de interferência da crista topográfica com a direção da falha basal (90º ou 120º no sentido retrógrado). Em concordância, levaram-se a cabo três conjuntos de experiências nos quais se conjugam diferentes combinações destas variáveis: um primeiro no qual se considera somente a anomalia reológica (viscosa); um segundo, no qual a anomalia viscosa está ausente e a direcção da falha basal (DFB) intersecta uma crista topográfica segundo um ângulo de 90º ou 120º; e um terceiro, no qual se consideram, simultaneamente, a anomalia viscosa (interestratificada), e a crista topográfica (com as mesmas orientações anteriormente consideradas). Adicionalmente, foram ainda realizadas uma experiência na qual a anomalia reológica não foi coberta de areia (i.e., aflora ao nível da superfície da cobertura) e uma experiência de controlo, em relação à qual se se comparam os resultados obtidos, consistindo simplesmente numa experiência clássica de Reidel.

Os resultados da experiência de controlo são compatíveis com aqueles obtidos noutras experiências do tipo Riedel (Naylor, *et al.*, 1986; Dooley and Schreurs, 2012) e demonstram o mesmo desenvolvimento típico de estruturas, começando com o propagação de falhas sintéticas *en-échelon* (normalmente designadas de *Riedel shears* ou *R-shears*), com ângulos de ~17º-20º (sentido horário) em relação à DFB. Os *R-shears* tornam-se progressivamente inactivos, dando lugar ao desenvolvimento, a partir das suas extremidades (ou entre *R-shears* sobrepostos) de falhas sintéticas de baixo ângulo (<17º) (designadas de *low-angle synthetic shears* ou *LAS shears*), eventualmente estas últimas estruturas coalescem para formar uma zona de cisalhamento principal que afecta a totalidade do modelo (designada *Y-shear*) e que acomoda toda a movimentação, rejeitando as estruturas previamente desenvolvidas. A geometria helicoidal enraizada na descontinuidade basal, característica dos *R-shears*, é observada em corte, dando origem a um padrão estrutural de falhas "*em flor"* (*flower structures*).

Os resultados do primeiro conjunto de experiências mostram uma interrupção da continuidade da zona de deformação frágil à superfície, revelando uma segmentação do correspondente padrão estrutural na área sobreposta à anomalia viscosa. Esta interrupção é marcada, a topo da anomalia, pela inibição da formação de *R-shears* e por um atraso significativo na propagação de *LAS shears*. Nesta mesma área, este tipo de estruturas acaba por formar-se de um modo mais disperso ou deslocalizado, evidenciando um padrão caracterizado por um maior número de falhas que acomodam individualmente menos movimentação, em claro contraste com o carácter mais localizado, ou discreto, do resto da zona de cisalhamento. Em corte observa-se que estes *LAS shears* enraízam no topo da anomalia viscosa.

No caso do segundo conjunto de experiências, independentemente do ângulo (de 90º ou 120º) considerado para a interferência entre a crista e a DFB, observa-se sempre a formação de uma falha que corta este alto morfológico e que é mais longa, e acomoda mais movimentação, do que as restantes (que materializam a zona de cisalhamento frágil fora deste relevo). Nestas experiências, não é visível nenhum atraso na propagação de *Riedel* ou *LAS shears* através do alto morfológico.

No terceiro conjunto, em ambas as experiências (interferência a 90º ou 120º), é visível uma obstrução à propagação de *R-shears* através da barreira morfo-reológica prescrita (compreendendo à anomalia viscosa e alto morfológico), bem como um atraso na propagação de *LAS* e *Y-shears*. Observa-se também a formação, em ambos os casos, de falhas normais em quadrantes opostos da anomalia viscosa, compatíveis com a direcção de tensão principal mínima (σ_3) implicada no regime geral de cisalhamento simples. Estas falhas delimitam estruturas extensivas (*pull-apart*), que se verificam ser de maiores dimensões na experiência cujo ângulo entre a crista e a DFB é de 120º. Nesta experiência (120º), também se desenvolvem cavalgamentos, que afloram à superfície do modelo preferencialmente ao longo da base dos degraus morfológicos que delimitam a crista (nos quadrantes opostos, i.e., aproximadamente a 90º, das estruturas de *pull-apart*). Estes cavalgamentos estão ausentes, ou são incipientes, nas experiências em que se considerou a crista a 90º da DFB. Os cortes obtidos a partir dos modelos no estado final da deformação mostram que tanto as estruturas extensivas como as compressivas enraízam em profundidade na interface *dúctil-frágil* materializada pelo contacto vertical entre o silicone e a areia.

Na experiência adicional também se observa o desenvolvimento em quadrantes opostos de estruturas extensivas e compressivas, associadas a diferentes orientações das interfaces de contacto entre a areia e o corpo viscoso. Este sofre deformação adoptando progressivamente uma geometria sigmoidal, com encurtamento acomodado à superfície pelo desenvolvimento de dobras de charneiras alinhadas, e estiradas, aproximadamente segundo a direcção do o eixo maior da elipse de deformação finita. Esta geometria sigmóidal do corpo viscoso é também inferida por via da reconstituição dos cortes seriados obtidos no final das experiências do primeiro e terceiro conjuntos de experiências.

Em todas as experiências destes três conjuntos, os padrões estruturais, desenvolvidos nos domínios do modelo afastados das heterogenias morfológicas e/reológicas (i.e., fora da sua influência), são semelhantes àquele obtido na experiência de controlo.

Destes resultados experimentais infere-se que a presença de um corpo viscoso intercalado numa cobertura frágil (supra-crustal) sobreposta a uma falha de desligamento basal, afetando um soco rígido subjacente, exerce um efeito de atenuação e deslocalização na propagação vertical da deformação implicada no movimento da falha. Isto é revelado nas experiências levadas a cabo pela ausência de *R-shears* a topo das anomalias viscosas, e pelo atraso no desenvolvimento à superfície de um padrão deslocalizado de *LAS shears*. O contraste reológico (entre o corpo viscoso e a areia), que controla o diferente modo de acomodação da deformação através da espessura da cobertura, produz também um efeito semelhante na horizontal, ditado pelo contacto lateral entre a anomalia viscosa e o meio frágil

envolvente condicionando, neste caso, a distribuição de estruturas extensivas e compressivas em torno de quadrantes opostos da referida anomalia.

Na ausência de um corpo viscoso, o desenvolvimento preferencial de praticamente uma única estrutura principal (mais longa) a atravessar o alto morfológico é interpretado como o resultado da maior espessura da cobertura na zona topograficamente elevada, e é compatível com relações empíricas de proporcionalidade entre espessura da cobertura e comprimento das estruturas, anteriormente reportadas (e.g. Naylor, *et al.*, 1986).

Do conjunto de experiências em que se consideraram obstáculos morfo-reológicos, apenas na experiência com a crista topográfica a 120º da DFB se observam estruturas compressivas de direcção ortogonal a σ_1. Este resultado mostra que o desenvolvimento deste tipo de estruturas é não apenas controlado pela existência das interfaces de contacto lateral (contraste reológico) entre o corpo viscoso e a areia, mas também, criticamente, pela orientação dos degraus morfológicas que delimitam as cristas. Uma crista topográfica representa uma transição abrupta (interface) entre domínios adjacentes com diferentes cargas litostáticas e compactação. Na experiência com a crista a 120º, a orientação mais ortogonal desta interface em relação a σ_1 (75º) é interpretada como sendo mais favorável à formação e enraizamento de cavalgamentos segundo essa direção. O facto destas estruturas enraizarem na interface areia-silicone e aflorarem alinhadas com a base da crista evidencia a acção recíproca entre os dois tipos de obstáculos. Contrariamente, na experiência com a crista a 90º, a direcção dos degraus morfológicos correspondentes é mais oblíqua em relação a σ_1 (45º), não propiciando a formação destas estruturas.

Os resultados experimentais obtidos são ainda preliminarmente discutidos em vista de alguns exemplos naturais genéricos, nos quais se procura reconhecer os padrões estruturais revelados pelas experiências realizadas.

Palavras-chave:
Modelação análoga; Zona de cisalhamento frágil; Tectónica transcorrente; Anomalia reológica supra-crustal; Padrão morfo-estrutural.

Abstract

The experimental project here portrayed aims to study the effect on the propagation, and ensuing structural pattern, of an upper-crustal brittle shear zone caused by the existence of a topographical and/or rheological anomaly. The experimental apparatus is a variation of the classical Riedel experiment and consists of a quartz sand overburden (brittle upper crust analogue) overlaying two horizontally juxtaposed rigid baseplates, materializing a right-lateral basement fault. The relative horizontal movement between these baseplates is transmitted to the overburden, deforming it. Three different main variables are studied: 1) the presence on an interstratified oblate viscous body, made of a silicone polymer (PDMS) mixed with wolframite powder, centred above the basement fault, simulating a salt pillow or a cooling magma chamber; 2) the presence of a topographical crest; 3) the angle between this crest and the basement fault direction (BFD) (either 90º or 120º clockwise). Three experimental sets, comprising different combinations of these variables are established: a) the first only considers the existence of a crustal interstratified viscous body; b) the second considers solely the presence of a topographical crest, either at 90º or 120º from the BFD; c) the third set represents a combination of the previous two and considers the coincidence of an interstratified viscous body with an overlaying topographical crest (again either at 90º or 120º from the BFD). A control experiment, where no heterogeneities are prescribed, and a supplementary experiment where the viscous anomaly is exposed at the surface (i.e., there is no sand overburden above it) were also performed.

Experimental results fundamentally show that: 1) the propagation of brittle structures is either delayed or inhibited atop the viscous anomaly, producing a delocalized structural pattern; 2) the propagation of structures atop the solely-morphological perturbations is not delayed, these are also longer and accommodate more displacement than others formed elsewhere; 3) compressive (pop-up) and extensional (pull-apart) structures are formed, bounding the viscous anomaly along opposite quarters, in the supplementary experiment and in the experiment where this anomaly is combined with a crest at 120º form the BFD (in this case thrust faults develop at the surface along the base of the crest); 4) similar (although smaller) extensional structures are also formed in the experiment with the viscous anomaly and a crest at 90º from the BFD; 5) in both experiments of the third set, cross sections show normal faults associated with the pull-aparts rooting in the lateral (vertical) boundary between the viscous anomaly and the brittle medium, in the experiment with the crest at 120º the same is also observed for the thrust faults; 6) the viscous anomaly is deformed into a sigmoid shape in all experiments in which it was prescribed.

The contrasting structural pattern in the brittle medium above the viscous anomaly is interpreted as the result of diffuse (viscous) strain accommodation along the whole volume of the anomaly, inhibiting the upwards propagation (from the basement fault to the surface) of discrete brittle structures. This same diffuse propagation of deformation in the viscous anomaly, in contrast with the near instantaneous propagation in the brittle medium is also responsible for horizontal velocity contrasts between the two mediums, that promote the formation of either extensional or compressive structures. This is clearly put in evidence by the fact that thrust and normal faults bound the viscous anomaly and that these structures root in the sand-silicone interface. The fact that, in the third set of experiments, thrust faults only formed in the experiment with the crest at 120º from the BFD shows that not only does the presence of a topographical barrier, but also its angle to the BFD, influence the structural pattern. The formation of these thrusts is interpreted as resulting from the crest being more favourably orientated to (i.e., more orthogonal to) the maximum compression direction (σ1) implied by the bulk simple-shear regime; in this case σ1 is at 75º from the crest, while in the other experiment, with the crest at 90º form the BFD, this barrier is only at 45º to σ1. The fact that the thrusts outcrop along the base of the crest

(which is at 120º from the BFD) and root in the sand-silicone interface further demonstrates the interplay between topographical and rheological barriers in the resulting structural pattern.

The experimental results of the supplementary experiment are further compared and preliminarily discussed in view of different natural examples of outcropping salt diapirs and pre-tectonic magmatic batholiths affected by crustal shear zones

Keywords:

Analogue modelling; Basement strike-slip fault; Brittle shear zone; Upper crustal viscous anomaly; Morpho-structural distribution pattern.

Table of Contents

Figure and Table Index

Abbreviations and Symbols

BFD – basement fault direction.

BFT – basement fault trace.

BF – basement fault.

PDMS – polydimetilsiloxane.

σ_1 – maximum principle stress direction.

σ_3 – minimum principle stress direction.

PIV – particle image velocimetry.

PTV – particle tracking velocimetry.

FT – feature tracking.

X-ray CT – X-ray Computed Tomography

WB – Weak viscous body.

R – Riedel shear.

LAS shear – lower angle synthetic shear.

P – P shear.

TF – thrust fault.

PA – pull-apart.

GC – Gulf of Cadiz.

TMR – Tore-Madeira Rise.

SWIM – SW Iberian Margin fault-system.

1. Introduction

The present dissertation corresponds to the scientific report of the work undertaken in order to obtain a **MSc degree in Geology (Structural Geology branch) by the University of Lisbon** (Geology Department, Faculty of Science). It consisted on the study of upper crustal strike-slip fault propagation across morphological and/or rheological barriers (heterogeneities) such as salt diapirs or cooling laccolithic magma chambers. This was addressed through an analogue modelling experimental approach, which conceptually and systematically considered different possible scenarios/configurations, to gain a general mechanical insight on the main processes at stake. A brief discussion in view of some natural examples was also carried out. All experiments were carried out in the **LATTEX analogue Modelling lab of the IDL institute** (Geology Department, Faculty of Science, University of Lisbon), using all the appropriate lab materials and equipment resources.

All preformed experiments, a detailed description of the employed methodology, the main obtained results and conclusions, were submitted in the form of a paper to the *Journal of Structural Geology*, which constitutes the body of the present thesis (section 2 below). A brief context of the employed analogue modelling approach, and of the critical relevance of this laboratory methodology for the field of Structural Geology and Tectonics is given beforehand in section 1.1.

1.1. Analogue Modelling as a laboratory methodology in Earth Sciences

Analogue modelling is presently a widely used laboratory methodology in modern Earth Sciences, in particular in the fields of Structural Geology and Tectonics in which, together with numerical modelling, it gives rise to the so-called *Geodynamic Modelling*. Such designation although possibly employed with slightly different meanings, sustains the recognized purpose of addressing targeted tectonic objects (e.g. geological structures at different scales, different tectonic settings such as continental rifting or subduction zones) from the point of view of the dynamics at stake. This is, aiming to go beyond the simple geometrical or even kinematical description, and to try to gain a quantitative insight about the mechanics governing the different implied processes. One of the main aspects of this is to understand how different rheological configurations influence the different natural observed geometries and inferred kinematics.

In the next sections (1.2 through 1.4) a brief account of some key aspects of historical and present-day relevance of analogue modelling techniques is presented, to grant some context to the performed experimental work.

1.1.1. Relevance in Structural Geology and Tectonics

In geoscience, analogue modelling refers to a methodology that aims to study a large variety of geological processes at various scales, from outcrop (10^{-1} to 10^{0} m) to mantle convection (10^{5} to 10^{6} m), by means of laboratory-scale physical experiments. This methodology encompasses a wide range of laboratory techniques that make use of modelling materials whose deformation, at a manageable (human) scale of space and time, is considered to be analogous to the deformation of natural rocks at much larger (geological) scales. This is, if a model is correctly envisaged (scaled), it should go through an evolutive process (i.e. it should deform) in the same way as the natural rocks being studied (often referred to as the *prototype*) but at a conveniently observable and measurable scale (Ranalli, 2001).

But why does the need arise to build a laboratory proxy of nature, instead of merely studying the natural object itself? To answer this question several arguments can be made to attest the validity of analogue modelling:

1) Unlike other scientific areas, in geoscience the direct observation of complete processes is often impossible simply because most geologic processes do not unfold at an observable rate (in geology time is generally measured in Ma) and/or do not occur in areas where direct sampling or observation are possible (e.g.: the mantle). This also means that, for these processes, there is no way to directly test hypotheses; however, analogue modelling allows for the possibility to indirectly subject hypotheses to controlled empirical testing (Koyi, 1997; Schellart and Strak, 2016). This possibility is perhaps the most relevant aspect of analogue modelling.

2) While a field geologist can only be confronted with the end result of deformation on any particular case and has to compare it with other cases where deformation is at a different stage in order to obtain a fragmented view of the geodynamic process, an analogue modeller can observe and quantify deformation continuously, from onset to conclusion and in all directions of space (3D). This allows for the reconstruction of deformation evolutive history and understanding of the complete underlaying processes (Koyi, 1997; Schellart and Strak, 2016). This said, the input from the natural case is essential in analogue modelling in order for the models to have any significance.

3) While in rock mechanics it is simple to determine the mechanical properties of a rock (its rheology) for human time scales, because many of these properties are time dependant, it is much harder to estimate rheologies for large time scales (Koyi, 1997)[(1)]. This means that there is still a relative level of uncertainty regarding the large-scale rheology of rocks. However, with physical models it is possible to constrain certain deformation styles to certain rheologies or rheological contrasts; this is, it is possible to study how a given deformation style is dependent on a well know rheology, which in turn allows the extrapolation of the geological-scale rheology of natural rocks based on their deformed state or deformation style (Koyi, 1997). This constitutes a feedback relation where the constant comparison of results with the natural case allows for a better understanding of rheology, which in turn allows for more realistic models.

4) The natural case may also display a great level of complexity, with a great number of variables or factors that may be poorly known or constrained. This may render postulating from field analysis alone too difficult or uncertain to be practical (Koyi, 1997). Conversely, analogue modelling allows for a systematic approach, where different well-constrained variables can be thoroughly (qualitatively and quantitatively) studied individually or in combination; this is paramount for the recognition of empirical patterns that, ideally, are also found in nature, in fact an analogue modeller may more easily recognise patterns in nature if he has already observed them in a model, making use of a common expression – 'the eyes do not see what the mind does not know'. These patterns can sometimes be extrapolated to some *empirical laws* that can allow for a predictive approach.

[(1)] Rheology is an emergent property, this means that it is dependent on the observation scale (both in terms of time and space). Continuous deformation of rocks occurs through the induced propagation of defects in the crystal lattice of its constituent minerals (either diffusion or dislocation creep). A note should be made on the Maxwell time (τ), that can be interpreted as the time needed for tension to decrease to 1/e ($\approx$0.37) of its original value, this means that $\approx$.063 of rock deformation occurred under creep deformation. For mantle rocks τ is in the order of 10^3 years, this means that for times greater than this creep deformation is dominant and the rheology can be considered as viscous (Ranalli, 1995). Another way to somewhat quantify the time dependence of rheology is the Deborah number (*De*), a dimensionless ratio between the *relaxation time* (essentially the time required for a given material to continuously deform to a given amount of strain) and the *observation time* (the time available for the deformation to occur, it can also interpreted as the duration of an experiment). The reader is referred to Ranalli (1995), chapter 8, for further context.

These considerations also hold true for numerical modelling and both methodologies allow the study of the geological object in ways that would otherwise be impossible.

1.2. Historical context

Sir James Hall of Dunglass (1761-1832) is widely acknowledged as the first author to develop a laboratory model with the specific objective of simulating a geological (tectonic) process (Daubrée, 1879; Willis, 1894; Koyi, 1997; Ranalli, 2001; Schellart, 2002); Cadell (1889) called him "the father of experimental geology". Hall was a central figure in the intellectual atmosphere dominating the Royal Society of Edinburg in the late eighteenth century, that was motivated by the Enlightenment and the development of the Huttonian *Theory of the Earth* (Hutton, 1785, 1788, 1795), this would later be called the *Scottish School of Geology* (Ranalli, 2001 and references therein). At the time, the processes that lead to the folding of strata remained unknown, Hall and others such as De Saussure (1779) postulated that this was due to lateral push. In order to test this hypothesis, he built two physical models, the first one was very rough and consisted of layers of cloth, constrained by weights, that where pushed laterally; the second one was more sophisticated and consisted of beds of clay constrained by a box with two opposing walls that moved closer to each other by the action of manual vice screws (see Figure 1.1.). In these experimental works, first read before the Royal Society of Edinburg in 1812 and later published in 1815 (Hall, 1815), Hall compared his experimentally obtained results with the – now famous – folded Silurian greywackes and mudstones fond in the Berwickshire coast of Scotland. The similarity between model and nature was such that it convinced Hall that lateral compression had to be the cause of folding. In spite of some lack of recognition from his contemporary peers, Hall's work on experimental tectonics had a lasting effect, not so much from the conclusions he drew from experimentation, but through the idea that geological-scale processes could be simulated with laboratory models (Ranalli, 2001). Ranalli (2001) noted that Hall's second experiment had all the basic principles of what is now considered a complete model design, as it began with a correct interpretation of natural geometries and structural relations, followed by the postulation of an hypothesis, the building of a laboratory proxy of nature (albeit very roughly and only qualitatively scaled) to test this hypothesis, and the use of experimental results to validate it. Many simple experiments on folding or thrust systems still use the same basic design as Hall's second experiment, with the difference that the walls are now moved by computer controlled motors (Koyi, 1997; Schellart, 2002). Another important contribution to experimental geology, although in the field of petrology, was Hall's proof that igneous-rock texture was controlled by the cooling rate of magma (Hall, 1805). The reader is referred to Ranalli (2001) for an in-depth review of Hall's life and experimental work.

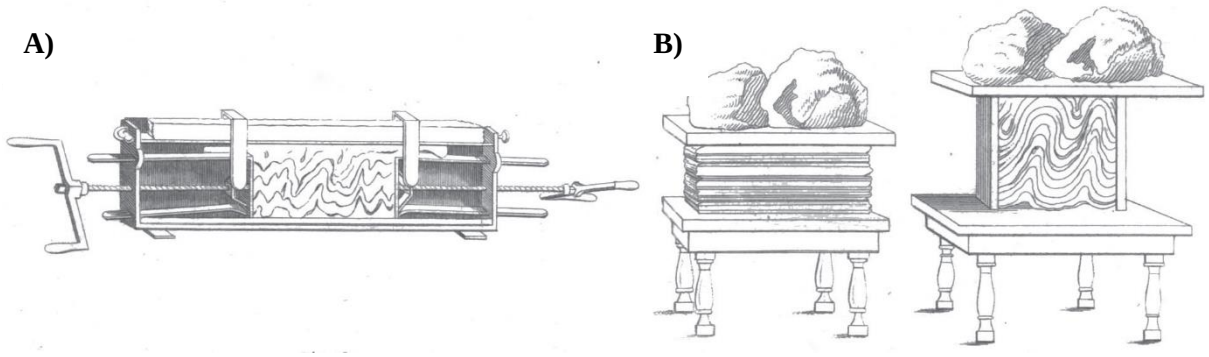

Figure 1.1. A) Drawing of Hall's second experimental apparatus. B) Drawing of Hall's first experiment in the undeformed (left) and deformed (right) states. Adapted from (Hall, 1815)

During the nineteenth century, several authors followed in Hall's footsteps and developed physical models to test a wide range of geological processes. The most prominent of whom was August Daubrée (1814-1896), who was an adamant advocate of geological experimentation, arguing that 'while always maintaining the basis of observation and reasoning, geology must then become experimental; it will now be enlightened by the iron and the fire of experimentation' (Daubrée, 1879) [(2)]. In 1879, Daubrée published a compendium of his life's work (Daubrée, 1879), highlighting experimental work in many areas of geology, including metamorphic petrology, mineral and rock chemistry, ore-forming processes, volcanology, erosion, transport and deposition of sediments, and even the study of meteorites. Most notably to structural geology he experimented on faulting, folding (Figure 1.2), the formation of schistosity, the tectonic deformation of fossils, shear heating and *mountain building*. To account for different deformation styles, he used a wide range of materials such as lead, plaster, wax, resin, turpentine, ice, gypsum, amongst others, sometimes used in combination to widen the scope of material behaviours (Figure 1.2). Daubrée was a truly versatile researcher who was widely acknowledged by his contemporary peers (e.g. Schardt, 1884), Cadell (1889) referred to him as "the greatest living exponent of experimental geology".

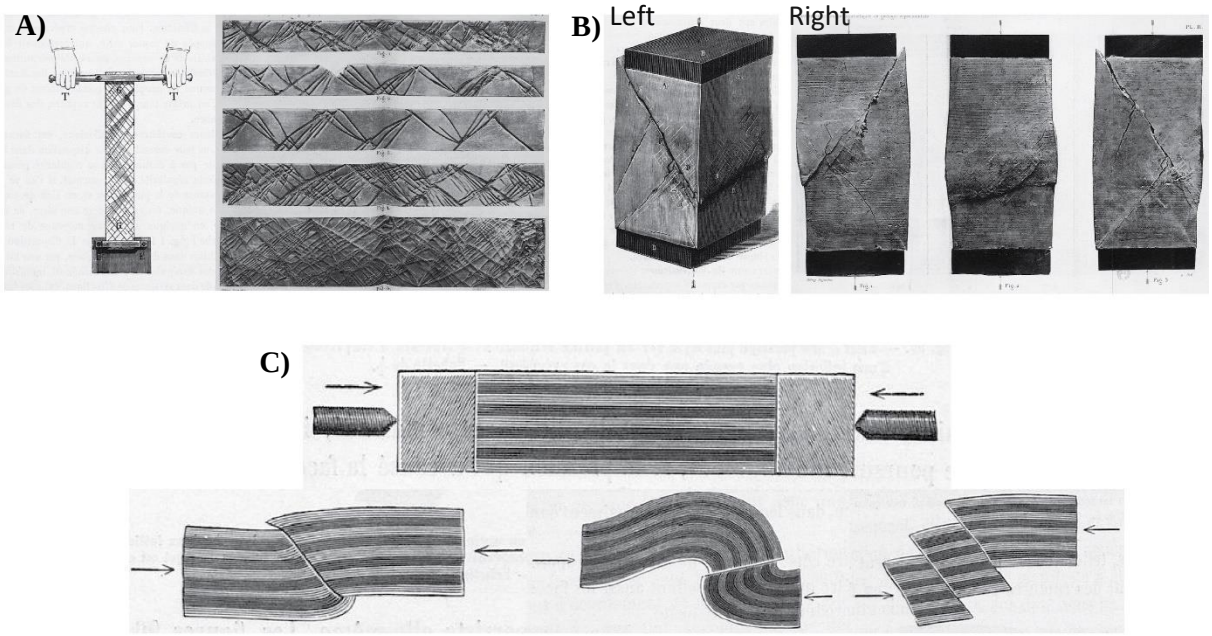

Figure 1.2. Examples of experiments performed by August Daubrée. A) Experiment on fracturing, using ice as a brittle analogue. Left: Experimental setup where a blade of ice was manually twisted; right: photographic print of several experimental results. B) Experiment on fracturing and faulting with a uniaxial compression test on a prism of beeswax mixed with plaster and resin. Left: drawing of experimental results; right: three photographic prints of experimental results. C) Study of *faulting after folding*. Top: experimental setup where coloured layers of wax (which *bends for some time before fracturing*) are horizontally compressed; bottom: three different experimental end-results, depending on the *force* applied to the model. Adapted from Daubrée (1879).

The problems of *mountain building* and folding were, however, the main source of research in the latter half of the century (Bolacha, 2014). Most authors simulated compression through devices similar to that of Hall (1815) (e.g.: Pfaff, 1880; Willis, 1894) (see Fig. 1.3 A), while others constructed models with pre-stretched rubber bases (e.g.: Favre, 1878; Schardt, 1884), as it was the general idea that the deformation of the crust was due to the contraction of a cooling nucleus (Willis, 1894), and others tested with both of these methods (eg: Cadell, 1889). Most of these models employed easily obtainable

[2] From the original 'Tout en conservant toujours comme fondement l'observation et la raisonnement, la géologie doit aussi devenir expérimentale; elle s'éclairera alors […] sous le fer et le feu de l'expérience'.

materials, such as clay (eg: Favre, 1878; Mellard Reade, 1886), loam and *papier-maché* pulp (Pfaff, 1880), stratified layers of sand and clay (Schardt, 1884), sand and plaster (Cadell, 1889), or beeswax and small metal spheres (Willis, 1894). The use of photography allowed, for the first time, the recording of experimental results (e.g.: Cadell, 1889) (Bolacha, 2014) or even natural outcrops (e.g.: Willis, 1894) in an easier and more reliable way (Figs. 1.2 and 1.3).

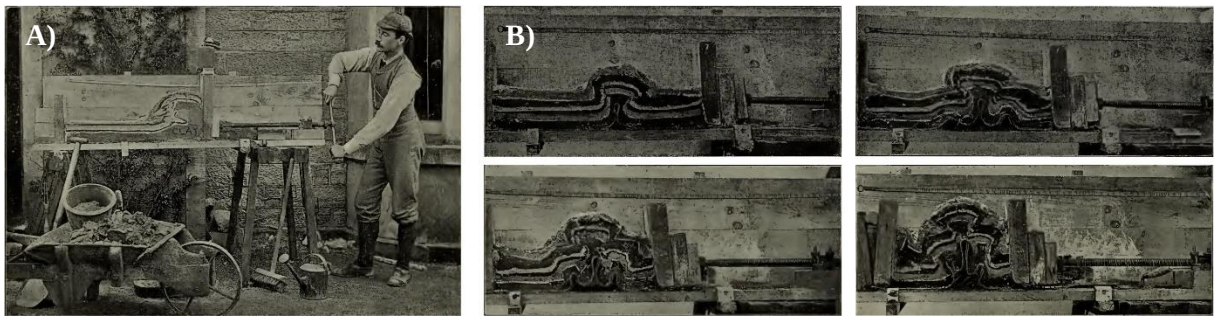

Figure 1.3. A) Photograph of Henry Cadell and his experimental apparatus. B) Photographs taken at different stages (sequence from left to right and top to bottom) of one of Cadell's experiments; in this, lateral compression is applied to a layered pack of stucco and sand, overlaying a sheet of waxcloth. Adapted from Cadell (1889).

The early twentieth century brought further developments to analogue modelling. For example, the first application of the methodology to salt tectonics appeared (Escher and Kuenen, 1928; Link, 1930), and the subjects of folding and faulting were further developed (e.g. Mead, 1920). It was around this time that the first laboratory models of wrench tectonics (strike-slip faulting) were developed, with great relevance to the present thesis, by Hans Cloos (Cloos, 1928) and Wolfgang Riedel (Wolfgang Riedel, 1929). Their models consisted of beds of wet clay laid on top of two adjoining rigid baseplates whose contact surface simulated a pre-existing vertical basement fault. The movement of one baseplate, in relation to the other, along this discontinuity was conveyed upwards into the clay overburden, promoting its deformation. This setup became known as the Riedel experiment (Tchalenko, 1970) and the first faults to usually propagate to the overburden as Riedel shears or R-shears. The models used in the present work are in fact a variation of the Riedel experiment.

The largest contribution to the advance of analogue modelling, however, came with the implementation of rigorous quantitative scaling. Authors had long known that when a model was built with the scaled down dimensions of nature, the strength of the material used also had to be scaled down accordingly; Willis (1894), for example, noted that "of a series of strata hundreds of feet thick and of a pile of layers only inches thick, the bending, breaking, or shearing will obey the same laws, if all the factors of pressure and resistance are proportionate in each case to the dimensions of the pile". Accordingly, authors used materials *softer* than natural rock, such as clay or wax; however, during the nineteenth century, considerations on scaling were always made qualitatively and no attempts were made to quantify either rock rheologies or laboratory material properties, so these were always referred to in a subjective way as *plastic* or *brittle*, for example (e.g. Hall, 1815; Daubrée, 1879; Pfaff, 1880; Cadell, 1889).

Koenigsberger and Morath (1913) made the first attempt to conceive a quantitative scaling of model materials. They argued that if the density of the model material was equal to that of the prototype, then its strength would have to be reduced in the same scale as length (Hubbert, 1937). Cloos (1929) made similar arguments but considering the material's ability to sustain its own weight. It wasn't until Hubbert (1937), however, that the first fully comprehensive and structured theory of scaling applied to analogue modelling appeared. In this theory, Hubbert (op. cit.) defined three degrees of similarity between two bodies: geometrical similarity, kinematic similarity and dynamic similarity. Geometric similarity means that the two bodies have the same geometry, this is, all corresponding lengths are

proportional and all corresponding angles are equal; kinematic similarity is achieved when two geometrically similar bodies undergo the same change in shape and/or position and the time required for this change is proportional, this means that, for every given pair of corresponding points, the velocities and accelerations must be proportional; two geometrically and kinematically similar bodies are also dynamically similar if all corresponding masses (point by point) between them are proportional and all the corresponding forces acting on these masses have the same direction and their magnitude is also proportional. A model is said to be correctly scaled if it shares all three degrees of similarity with the prototype, this means that geometries, masses, velocities, accelerations and both resistive and driving forces are all proportionally scaled. Hubbert's theory of scaling brought not only the ability to choose model materials (and configurations) with added certainty that these would accurately represent nature but, most importantly, the ability to quantify both model conditions and results in a meaningful way that allows extrapolation to nature. Other works have since expanded upon Hubbert's theory, for example Hubbert (1951) set the basis for the scaling of loose sand, several other works have since followed on the scaling of sand and other granular materials (e.g. Horsfield, 1977; Mandl, *et al.*, 1977; Krantz, 1991; Schellart, 2000; Panien, *et al.*, 2006); Ramberg (1967) worked on the scaling of viscosity and density of fluids in centrifuge models and was among the first to use silicone polymers; Weijermars and Schmeling (1986) worked on the scaling of Newtonian and non-Newtonian fluids, Weijermars (1986a, 1986b, 1986c) also introduced the use polydimethylsiloxane (PDMS), a now widely used transparent Newtonian fluid (at low strain rates); Davy and Cobbold (1991) worked on the scaling of thermomechanical models; Ribe and Davaille (2013) revised the scaling of densities or density contrasts; Schellart and Strak, (2016) reviewed and studied the scaling of topography.

1.2.1. Recent advances

The late twentieth century brought with it an enormous variety of advances to analogue modelling, most notably in the application of the methodology to virtually all geodynamic processes, in the availability and application of an ever-increasing diversity of materials, in recording techniques and in the combined use with numerical modelling.

With the introduction in the 1960's of the theory of plate tectonics, modellers started testing on subduction (e.g. Jacoby, 1973, 1976; Shemenda and Grocholsky, 1992; Schellart, 2004, 2008) and rifting (e.g. Shemenda and Grocholsky, 1994; Benes and Davy, 1996; Keep and McClay, 1997; Corti *et al.*, 2003; Corti, 2008) (Schellart and Strak, 2016). The development of centrifuge models also became popular around this time, specially with the work of Ramberg (Ramberg, 1967) that built an entire lab around a centrifuge, other authors further expanded this technique (e.g. Dixon, 1974, 1975; Talbot, 1977; Jackson, 1988; Dixon and Liu, 1992). The use of a centrifuge allows experiments to be conducted with an apparent gravity that can be hundreds or thousands of times greater than earth's. The advantage of this is that analogue materials with greater strength can be used without compromising scaling.

Analogue modelling has now been applied to virtually all geodynamic or tectonic processes, from the smallest outcrop scale in studies of porphyroclast rotation (e.g. Ghosh and Ramberg, 1976; Ildefonse *et al.*, 1992; Rosas *et al.*, 2002; Ceriani *et al.* 2003), shear zone formation (e.g. Grujic and Mancktelow, 1998), folding or boudinage (e.g. Ramberg, 1955; Cobbold and Quinquis, 1980; Davy and Cobbold, 1991; Rosas *et al.*, 2001; Marques *et al.*, 2012), to the regional scale in studies of volcanic systems and magma intrusion (e.g. Donnadieu and Merle, 1998; Donnadieu *et al.*, 2003), strike-slip (e.g. Naylor *et al.*, 1986; Schreurs, 1994; Dooley and Schreurs, 2012), transpression and trastension (e.g. Schreurs and Colletta, 1998), thrust-wrench interference (Duarte *et al.*, 2011; Rosas *et al.*, 2012), fold and trust belts (e.g. Schreurs, *et al.* 2001; Marques and Cobbold, 2002, 2006; Willingshofer and

Sokoutis, 2009), diapirism (e.g. Escher and Kuenen, 1928; Koyi *et al.*, 1993; Weijermars *et al.*, 1993), accretionary wedges (e.g. Gutscher *et al.*, 1998), geomorphology (e.g. Crave *et al.*, 2000), tectonic-sedimentary interference (e.g. Graveleau and Dominguez, 2008; Graveleau *et al.*, 2015), pull-apart basins (e.g. McClay and Dooley, 1995), and to the lithosphere and mantle scales in studies of subduction and mantle flow (e.g. Kincaid and Griffiths, 2004; Schellart, 2004, 2008; MacDougall *et al.*, 2014; Strak and Schellart, 2014), rifting (see references above), lithospheric extension and shortening (e.g. Vendeville *et al.*, 1987; Davy and Cobbold, 1991; Benes and Davy, 1996), plumes (e.g. Griffiths and Campbell, 1990), backarc extension (e.g. Schellart, *et al.*, 2002; Schellart, *et al.*, 2003), amongst other examples (see Schellart and Strak, 2016 and references therein). The all-embracing applicability of analogue modelling to the study of geodynamics certainly attests its importance to earth sciences.

Analogue modellers today have at their disposal a large variety of materials that can simulate different rock rheologies, most notably granular materials such as quartz sand (e.g. Hubbert, 1951), glass microbeads (e.g. Krantz, 1991), clay or feldspar powder (e.g. Corti, 2008), are used to simulate the brittle deformation of the upper-crust, as both are considered to deform according to the Mohr-Coulomb failure criterion (e.g. Schellart, 2000); linear-viscous materials such as silicone polymers (e.g. PDMS) (e.g.Weijermars, 1986a) and syrups (e.g. Schellart, 2008) are used to simulate the geological scale viscous deformation of the lower crust or of the lithospheric mantle or the diffusion creep in the sub-lithospheric mantle, respectively; paraffin wax (e.g. Jacoby, 1976) can be used as a thermal-dependent material and plasticine (e.g. Weijermars, 1986b) as a thermal-dependent plastic material; layers consisting of different materials are often used to simulate natural rheological layering (e.g. Vendeville *et al.*, 1987; Davy and Cobbold, 1991; Shemenda and Grocholsky, 1992; Koyi, *et al.*, 1993; Benes and Davy, 1996; Schellart, 2004, 2008) and different mixtures of these materials can also be used to create complex visco-plastic, non-linear viscous or ductile rheologies (see Schellart and Strak, 2016 and references therein).

Since the advent of this methodology, modellers have recorded the stage-by-stage deformation of their models, first with drawings and later with photographs. Photography continues to be the most widely used recording technique in analogue modelling, as it allows for an easy, inexpensive and reliable way of visualising deformation, in regular intervals of time or displacement. Photographs are usually taken in map (top) view to record the deformation at the surface of the model, or in a side view if the model box has transparent walls (usually made of glass or acrylic). These photographs can be subsequently processed in a quantitative analysis of deformation, either done manually or with the aid of computer algorithms. Manual post-processing consists of measuring, in the image, the deformation or displacement of passive markers in the models, this requires that a scale be present in the image or that pixel size be known (Schellart and Strak, 2016). The markers can be of many kinds, such as lines, grids, points, or differently coloured features (e.g. layers) (see Koyi, 1997; Schellart and Strak, 2016 and references therein). This can be an inexpensive way to quantify deformation, displacements or velocities and is often used as a first approach when conceiving or calibrating a model.

Algorithmic based post-processing uses a variety of techniques and software to analyse the acquired images in order to compute displacement, velocity or strain fields. The most widely applied of these techniques uses algorithms that recognise random groups of particles or textural patterns and track their movements by comparing serially taken photographs, this technique is called Particle Image Velocimetry (PIV) (e.g. Kincaid and Griffiths, 2004). A two-camera oblique array can be used to allow the recording of deformation in 3D, this is called stereo PIV (e.g. Strak and Schellart, 2014). Other similar techniques record movement by tracking individual tracers (Particle Tracking Velocimetry – PTV) or individual particles (Feature Tracking - FT) (Raffel *et al.*, 2007) or by recognising brightness patterns (optical-flow) (e.g. Bernard *et al.*, 2007). Other techniques employ software (such as Dynel,

SSPX, or Matlab) with algorithms that track the deformation imposed on physical marker grids imprinted on the models (e.g. Duarte, *et al.* 2013).

Modellers also frequently slice their models to record deformation in depth; this, however, is a destructive method that only allows the recording of deformation at the prescribed end-state of the experiment. To record the in depth deformation of the model throughout the duration of the experiment modellers must resort to non-destructive methods such as X-ray Computed Tomography (X-ray CT) (e.g. Schreurs, 1994) (see Fig. 1.4 B) or seismic reflection (e.g. Sherlock and Evans, 2001).

The recording of surface deformation (change in topography) through Digital Elevation Models (DEM) is also now commonplace and can be achieved through several different techniques such as fringe projection (e.g. Graveleau and Dominguez, 2008), where a laser interferometer projects lines on the surface that are then photographed, or with stereo photogrammetry (e.g. Schrank and Cruden, 2010), a technique very similar to stereo PIV or, most commonly, using laser scanners (e.g. Dooley and Schreurs, 2012b) (see Fig. 1.4 A).

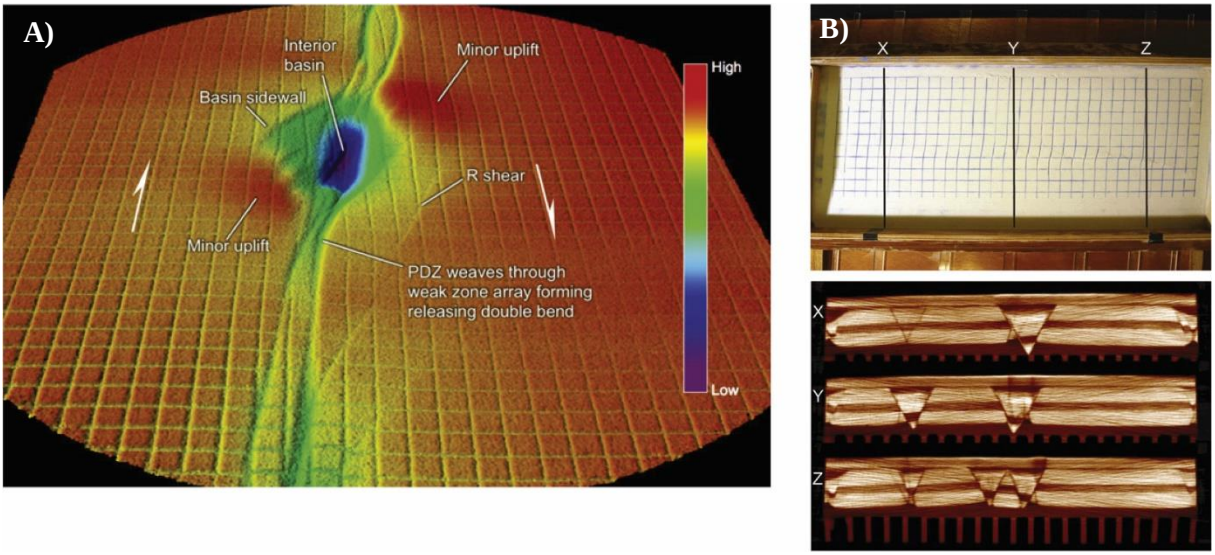

Figure 1.4. A) Example of a laser-scan image showing the end-stage topography of a strike-slip experiment. B) Example of X-ray CT scan taken during the course of a simple shear experiment, along three sections (locations shown in the top image). Adapted from Dooley and Schreurs (2012)

The reader is referred to Schellart and Strak (2016) for a thorough review on scaling, materials used and recording techniques in analogue modelling.

The advent, and widespread use, of numerical modelling brought the opportunity to combine it with analogue modelling in a way that mutually complements both methodologies and enriches results (e.g. Ellis, *et al.*, 2004; Marques *et al.*, 2005; Yamada, *et al.*, 2006; Burliga, *et al.*, 2012; Rosas *et al.*, 2012).

1.3. Different approaches

When envisaging a model, a modeller can follow different approaches regarding experiment design, depending on what process is being investigated and what information is to be extracted from the model. Schellart and Strak (2016) categorized three different general approaches to experiment design based on the driving forces acting on the model. These are: the external, the combined, and the internal approaches. The external approach is adopted when all deformation of the model is imposed by

one or more external actions, this means that the system is open and energy (sometimes also mass) must be externally applied in order to deform the model material. This is usually done by applying a force to one or more moving walls of the model creating a velocity boundary condition (this is called the kinematic external approach). Prescribed boundary condition can also be thermal, in the form an external heat source (thermal external approach) or may result from added material to a boundary (material influx external approach), both of these usually affect the bottom boundary of the model. In the internal approach the system is closed, and no external energy is added to the model. Hence, all deformation occurs due to gravity forces, resulting only from the density layering/configuration of employed materials (buoyancy forces), and from the viscous resistance of this same materials to the implied flow. It is worth noting that in the thermal external approach all deformation in the model is also caused by buoyancy forces, however the density contrasts do not result from the use of different materials but are rather caused by thermal expansion within the same medium. The combined approach results form a combination of externally added energy and buoyancy forces. This means that in addition to forces added externally to the model, materials with different densities causing buoyancy contrast forces are also employed. A large limitation of this approach is that it is difficult to proportionally scale the externally added forces relatively to the internal buoyancy ones. This often results in critically ignoring the possibility of the first group of (external artificially imposed) forces having an unrealistic magnitude, far too great in comparison with in buoyance force equilibrium that drives the large-scale geological processes in nature.

In order to simulate the natural rheological layering of the lithosphere, of the sub-lithospheric mantle or even within a sedimentary basin, modellers use different techniques and build a variety of different model types, following three main "rheological approaches" as defined by Schellart (2002) and later reformulated by Schellart and Strak (2016). The first approach, termed isothermal brittle-viscous, consists of using layers or domains of different materials with different mechanical behaviours in an isothermal model. In these, material properties are homogeneous (if the material is viscous) or are dependant only on normal stress (if the material is granular), the relevant mechanical contrasts are abrupt and exist in the interface between two different materials. In the second approach, the use of model materials with temperature-dependent rheologies combined with an induced, usually vertical, temperature gradient creates a rheological layering in the model, it also allows thermal and rheological readjustments during the course of the experiment. In the third rheological approach, the model is also isothermal, the lithosphere is simulated by a single layer of a highly viscous material, overlying a less viscous material for isostatic compensation or simulating sub-lithospheric mantle flow. The use of models with rheological (mechanical) layering requires that the scaling of both rheology and density is made consistently for every layer (see Schellart and Strak, 2016 and references therein).

An experimenter may also wish to model in fine detail a very specific natural example (prototype), in this case usually great effort is put in giving as much similarity as possible between model and prototype, both in terms of geometry and rheology. The increase in considered variables may, however, mean that the model is poorly constrained, empirical physical relations are hard to extract from the results and that ensuing conclusions may also be difficult to extrapolate to a general case. Alternatively, an experimenter may choose a more conceptual approach and design a relatively simple model, with few and well constrained variables, from where it might be easier to extract empirical physical relations that can be extrapolated to a general case. These model results generally have a less perfect resemblance with any given natural prototype (due to local features) but can be compared to a greater number of them.

The experiments portrayed in this manuscript follow the kinematic external approach as all deformation on the models is imposed by the external force of a stepping motor (see section 2.1.2) and

the isothermal brittle-viscous rheological approach as all models are isothermal and rheological contrasts are simulated through the use of different materials (both approaches as defined by Schellart and Strak, 2016), these experiments also embody a more conceptual approach.

1.4. Remarks on analogue modelling, general limitations and constraints

Any model, be it physical or numerical, is always a simplification of nature and its deformation always lacks the complexity of that undergone by the natural example. This does not mean that models are not useful, but it does mean that the limitations of any given model always need to be well acknowledged in order to give significance to any interpretations. An analogue modeller must always be conscious of what information can or cannot be validly extracted from the model.

The choice of used materials is always paramount when envisaging a model as these must scale as faithfully as possible physical properties from rock to model. As pointed out above (section 1.2.1), modellers can use a wide variety of materials as a proxy to rock rheology, however, these may still be limited in their ability to simulate the whole range of rock properties (Koyi, 1997). Furthermore, the mechanical properties of these materials are often static, meaning that they do not change through the course of the experiment (except for example if materials have thermal dependant properties and the model design features a thermal gradient, or if the mechanical response of the material is strain or strain rate dependant). On the other hand, rock rheology does change through the course of geodynamic processes as it is dependent on temperature, pressure, strain, strain rate and chemical reactions; such changes are often considerably hard to simulate in the lab if not impossible. There is still also a level of uncertainty regarding the large time-scale rheology of natural rocks, this is reflected in an added difficulty in ensuring correct scaling of the model (Koyi, 1997). A great level of attention in now given to the correct scaling and applicability of model materials (e.g. Schellart, 2000) as well as to the detailed description of their properties, additionally the influence of laboratory environment, model preparation techniques, and the human factor have also come under scrutiny (e.g. Krantz, 1991; Schreurs *et al.*, 2006; Schreurs *et al.*,2016) in an effort to increase general reproducibility of results.

Even considering its limitations, analogue modelling is still a valuable, and indispensable tool in the comprehension of geodynamic processes as it allows: 1) to indirectly test hypotheses where direct testing is impossible; 2) to observe and quantify geological processes from onset to conclusion generally in 3D; 3) the ability to study phenomena and individual variables in a systematic way; 4) to constrain certain deformation styles to large scale rock rheology; and its historical significance cannot be understated. The advent, and utilisation, of new recording techniques allows for more an ever more robust quantification of deformation. The ability to construct some experiments in an inexpensive way, that can be replicated with relative ease by pears is also a great advantage of this methodology. Analogue modelling can also be used in combination with numerical modelling in an enriching and complemental way.

2. Submitted Article

A transcript of the article submitted to the *Journal of Structural Geology* is now presented. Minor adaptations were made to chapter numbering, image location, text format and image or table references, in order to suit the stile required for this manuscript.

Author contributions: Afonso S. Gomes conceived the ideas, designed the experimental apparatus, conducted all experiments and wrote the initial manuscript. Filipe M. Rosas also conceived the ideas, participated in the lab work and corrected the initial manuscript. All authors contributed by occasional participation in the experimental work, by analysing and interpreting the experimental results, and by editing of the original manuscript.

Analogue modelling of brittle shear zone propagation across upper crustal morpho-rheological heterogeneities

A.S. Gomes [a]; F.M. Rosas [a, b]; J.C. Duarte [a, b, c]; W.P. Schellart [d]; J. Almeida [a, b]; R. Tomás [e], Strak, V [d].

[a] Departamento de Geologia, Faculdade de Ciências, Universidade de Lisboa, 1749-016 Lisboa, Portugal.
[b] Instituto Dom Luiz, Faculdade de Ciências, Universidade de Lisboa, 1749-016 Lisboa, Portugal.
[c] School of Earth, Atmosphere and Environment, Monash University, Melbourne, VIC 3800, Australia.
[d] Department of Earth Sciences, Vrije Universiteit Amsterdam, Amsterdam, Netherlands
[e] Rock Mechanics Laboratory, School of Earth and Environmental Sciences, University of Portsmouth, Portsmouth, PO1 3QL, UK.

Abstract

Brittle shear propagation across the thickness of a layered sand-cake overlying a strike-slip (rigid) basement fault is systematically investigated by a series of analogue modelling experiments. These were specifically conceived to understand the process through which the existence of different pre-tectonic morphological and rheological perturbations within the upper crust (sand overburden) potentially affect the development of the corresponding surface brittle shear deformation patterns. Three main sets of experiments were performed and compared with a benchmark end-member to account for the following specific constraints: i) The existence of a crustal interstratified viscous body (silicone oblate disc representing a salt pillow or an igneous laccolithic body) above the basement fault trace; ii) The existence of a major topographic crest at a different angle (either 90º or 120º) from the basement fault direction; and iii) The combination of the previous two, i.e. the simultaneous existence of a crustal viscous body and a topographic crest (morpho-rheological perturbation). Experimental results show that the sand surface deformation pattern is fundamentally determined by the interplay between strain accumulation in the (viscous) weak body during the (vertical and horizontal) propagation of the deformation across the brittle overburden, and by the coincidence/mismatch between the main sand-silicone rheological boundaries and existent (topographic crest-related) morphological steps. Furthermore, the potential similitude between experimentally obtained deformation patterns and some natural examples is also preliminarily discussed.

Keywords:

Analogue modelling; Basement strike-slip fault; Brittle shear zone; Upper crustal viscous anomaly; Rheological stratified medium; Structural distribution pattern.

2.1. Introduction

Pure strike-slip faulting and associated brittle shear deformation have been profusely studied through analogue modelling in the last decades, representing one of the most exhaustively investigated subjects from the onset of the application of this methodology to structural geology and tectonics (e.g., An and Sammis, 1996; Casas *et al*., 2001; Cloos, 1930; Dauteuil and Mart, 1998; Dooley and Schreurs, 2012; Emmons, 1969; Le Guerroué and Cobbold, 2006; Mandl *et al*., 1977; McClay and Bonora, 2001; Naylor *et al*., 1986; Richard *et al*., 1991, 1995; Richard and Krantz, 1991; Riedel, 1929; Román-Berdiel *et al*., 1997; Schellart and Nieuwland, 2003; Schrank *et al*., 2008; Schreurs, 1994; Sylvester, 1988). Concerning the same general subject of analogue modelling of brittle wrench systems, several contributions have also dealt with the employment of different geometric basal boundary conditions (releasing and restraining fault-bend geometries) as a means to nucleate corresponding transtensional and transpressive dynamic regimes, which allowed the investigation of processes governing the formation and evolution of oblique pull-apart basins and ridges, respectively (e.g. Atmaoui *et al*., 2006; Cunningham and Mann, 2007; Dooley and Schreurs, 2012; Mann, 2007; McClay and Bonora, 2001; Mitra and Paul, 2011; Naylor *et al*., 1986; Richard *et al*., 1995; Rowley *et al*., 2016; Schellart and Nieuwland, 2003; Wu *et al*., 2009). Conversely, the influence of crustal viscous bodies (e.g., salt walls or diapirs, shallow magma chambers, laccolithic igneous intrusions) intersecting/interfering with a main brittle shear zone have been comparatively less studied through analogue modelling techniques, being mostly focused on specific examples or case studies (Román-Berdiel, Gapais and Brun, 1997; Letouzey and Sherkati, 2004; Corti, Moratti and Sani, 2005; Holohan, Van Wyk de Vries and Troll, 2008; Koyi *et al*., 2008; Dooley and Schreurs, 2012).

Building on these previous inputs, in the present paper we use analogue modelling to systematically investigate the different interference structural patterns that are expected to be formed as a result of the propagation of a brittle shear zone across a pre-existent (i.e. pre-tectonic) rheological crustal anisotropy, and/or across a major topographic crest. We further address the potential recognition of such structural patterns in some natural examples, briefly discussing ensuing main implications for their formation and evolution.

2.1.1. Previous work

Previous contributions regarding the analogue modelling of a brittle shear zone intersecting a crustal rheological anomaly (viscous body) considered in general two main variables: i) the influence of a syntectonic viscous body injection along the main basement fault and associated brittle shear zone structures; and ii) the role of different original angular positions of pre-tectonic inequidimensional viscous bodies relatively to the main brittle shear zone direction.

Regarding the first case, modelling of upper crustal syntectonic (granitic) intrusions was reported in the pioneering work of Román-Berdiel *et al*. (1997). In their experimental original state, a viscous ductile layer (silicone putty) was set within the sandpack, beneath which a less viscous and less dense silicone putty was injected along an active basement strike-slip fault. The authors investigated the influence of the brittle cover thickness and volume of injected material on the overall geometric-kinematic pattern of the intrusions. Their main results showed that the presence of an upper crustal viscous layer strongly controls the intrusion process and its shape, since it locally allows lateral expansion to occur favouring laccolithic geometries. They have also shown that the syntectonic elongation of the intrusions is determined by the principal extension direction of the bulk strain field implied by the main strike-slip regime. Moreover, lateral expansion of the laccolithic intrusions was shown to be limited by arrays of Riedel faults formed in the brittle cover, and this limiting effect was

revealed to be enhanced by the thickness of this cover relatively to the thickness of the ductile viscous layer.

Corti *et al*. (2005) expanded on the previous authors' work by experimentally considering parameters such as the magma injection rate, the velocity of deformation and the total amount of lateral displacement occurring during the intrusion. Their conclusions indicate a feedback relationship between the control exerted by the syntectonic intrusions on the overall development of the brittle shear fault pattern, and in turn the control exerted by these forming faults on the geometry-kinematics of some of the intrusions. More specifically, the authors showed that if the strike-slip fault displacement velocity is high, or the injection velocity low, the intrusion tends to be drop-shaped with its maximum elongation subparallel to the long-axis of the strain ellipsoid. In contrast, if the inverse happens (i.e. high magma injection or low displacement velocity), then the maximum elongation direction of the intrusive bodies is along the compressive quadrants implied by the bulk strike-slip regime, i.e. in this case intrusions tend to be preferentially driven by the mechanical brittle anisotropies that comprise the surface fault pattern.

Koyi *et al*. (2008) carried out a series of 1g (i.e. ambient-gravity) and centrifuge analogue modelling experiments to study the process through which strike-slip faults and associated releasing bends/pull-apart basins can trigger salt diapirism within the tectonic framework evolution of the Zagros fold-thrust belt. In their 1g experiments they used silicone (SGM-36) and dry quartz sand to simulate a basal salt layer and an overlying upper crustal sedimentary cover (overburden), respectively. Basal and interstratified velocity discontinuities simulated by a pre-cut thin plastic sheet were used to create a releasing bend at 45º to the main strike-slip direction. Different ratios between the thickness of the salt layer and the strike-slip displacement, or the thickness of salt layer and the thickness of the sedimentary overburden where considered as variables. In their centrifuge experiments silicone (PDMS) and Plasticine were used instead to simulate the same equivalent units (i.e. salt layer and overburden). Their main results showed that the most plausible explanation for the spatial association between the salt diapirs and the basement strike-slip faults in the Zagros was the formation of oblique-slip pull-apart basins, which drove the salt diapiric intrusions and were induced along the Zagros folds or thrusts by basement strike-slip faulting.

Holohan *et al*. (2008) focused on the study of the effects of strike-slip deformation on the development of volcanic calderas. The authors preformed a series of analogue modelling experiments to better understand the interactions between strike-slip regional structures (R-and Y-shears) and volcano-tectonic caldera subsidence. They modelled this process by means of placing an interbedded honey layer (simulating a pre-tectonic sill-like magma reservoir) to be crosscut by a main brittle strike-slip shear zone. In a different set of experiments the same material was also injected to simulate a recharge of the magma chamber under syntectonic to post-tectonic collapse conditions. Their study showed that the geometry of the magma chamber (i.e. the geometry of the honey viscous anomaly) strongly controls the tectonic pattern developed on the surface, namely the pattern of the subsidence faults bounding the developing caldera structure. When cutting the centre of the magma chamber, such roof-dissecting faults also serve as magma ascent pathways. Additionally, the same results have also shown that long-lived (passive) magma chambers are able to localize marginal faults, resulting from the rheological contrast between the magmatic chamber and the surrounding crust.

Regarding the study of the interference between pre-tectonic crustal anomalies and brittle shear zones, Dooley and Schreurs (2012) investigated the influence of different original orientations (i.e. angular positions) of viscous bodies on the resulting structural pattern of either pure strike-slip or highly oblique transtensional brittle shear zones. In their work, an inequidimensional viscous anomaly (made of PDMS) was set in the original experimental state to make a 45º angle (clockwise or counterclockwise) with the main shear plane direction. The same authors also considered in different experiments the

influence of viscous anomalies corresponding to a double cylinder array (also silicone), with each cylinder being placed tangentially on opposite sides of the fault zone (mimicking a left lateral offset). Their experimental results showed that the presence of viscous bodies clearly perturbs the normal sequence of formation of the structures comprising a brittle shear zone, constituting barriers to the rupture-propagation and linkage of such structures, and thus promoting brittle shear zone segmentation. The viscous bodies were shown to localize strain, preferably as the centre of restraining stepovers, originating pop-up structures bounded by oblique-slip Riedel-fault segments. The overall geometry of the resulting structural pattern was shown to vary essentially as a function of the original position of the viscous body relatively to the main brittle shear zone direction. Viscous bodies with a counterclockwise 45º angle favoured lazy S-shaped restraining-bend geometries, whereas those with a clockwise 45º angle developed rhomboidal to Z-shaped restraining-bend geometries. Releasing stepovers were also shown to form in association with viscous zones, although less commonly, since they required both a combination of (counterclockwise 45º) weak zone orientation and a degree of divergence (i.e. transtension) to develop.

2.1.2. Present work

In this paper we build on previous contributions (see section above) to understand the main processes governing the structural/tectonic interference between a main brittle shear zone (developed above a basement strike-slip fault) and an interbedded pre-tectonic rheological anomaly (crustal weak body). Accordingly, in our experiments we consider an equidimensional PDMS viscous anomaly (oblate disc of PDMS with an original axial ratio = 1 and a thickness of ≈2cm), interstratified within the sand layers, with its centre aligned above the basement strike-slip fault (Figs. 2.1 and 2.2) and representing a crustal low viscosity body (e.g. shallow magma chamber, igneous laccolithic body, salt pillow). Since the occurrence of these upper crustal viscous anomalies is often associated with some type of morphological expression, the combination with differently orientated topographic crests is also analysed. Our intent was not to model a specific natural example, but rather to comply with a more systematic analysis of the type of structural pattern that is generally expected to develop as a result of brittle shear propagation across pre-existent (i.e. pre-tectonic) rheological/morphological obstacles. However, we did take into account one specific case (see below section 2.4) in which the interference angle between a main strike-slip fault and a major topographic crest is of approximately 120º clockwise. We thus considered the following different experimental sets:

a) A strike-slip brittle shear zone cutting through a rheological (viscous) anomaly (a discoidal body of PDMS) interbedded within the sand centred above the basement fault direction (BFD, Fig. 2.2);

b) Strike-slip brittle shear propagation across differently orientated topographic crests making an angle of either 90º or 120º (clockwise) with the basement fault direction – BFD (in this case without any rheological viscous body, Fig. 2.3);

c) A strike-slip brittle shear zone propagating across a morpho-rheological anomaly corresponding to a viscous body and a topographic crest (also at either 90º or 120º to the BFD, Fig. 2.4).

We further used as an end-member term of comparison a benchmark pure strike-slip standard experiment, in which none of the previous (neither morphological, nor rheological) perturbations were considered (see Fig. 2.1 B). An experiment with a viscous weak anomaly exposed at the surface was also carried out for the sake of discussion (see section 2.4.4) and made available in the supplementary data (Figs. 2.18 and movie MSupp.mp4).

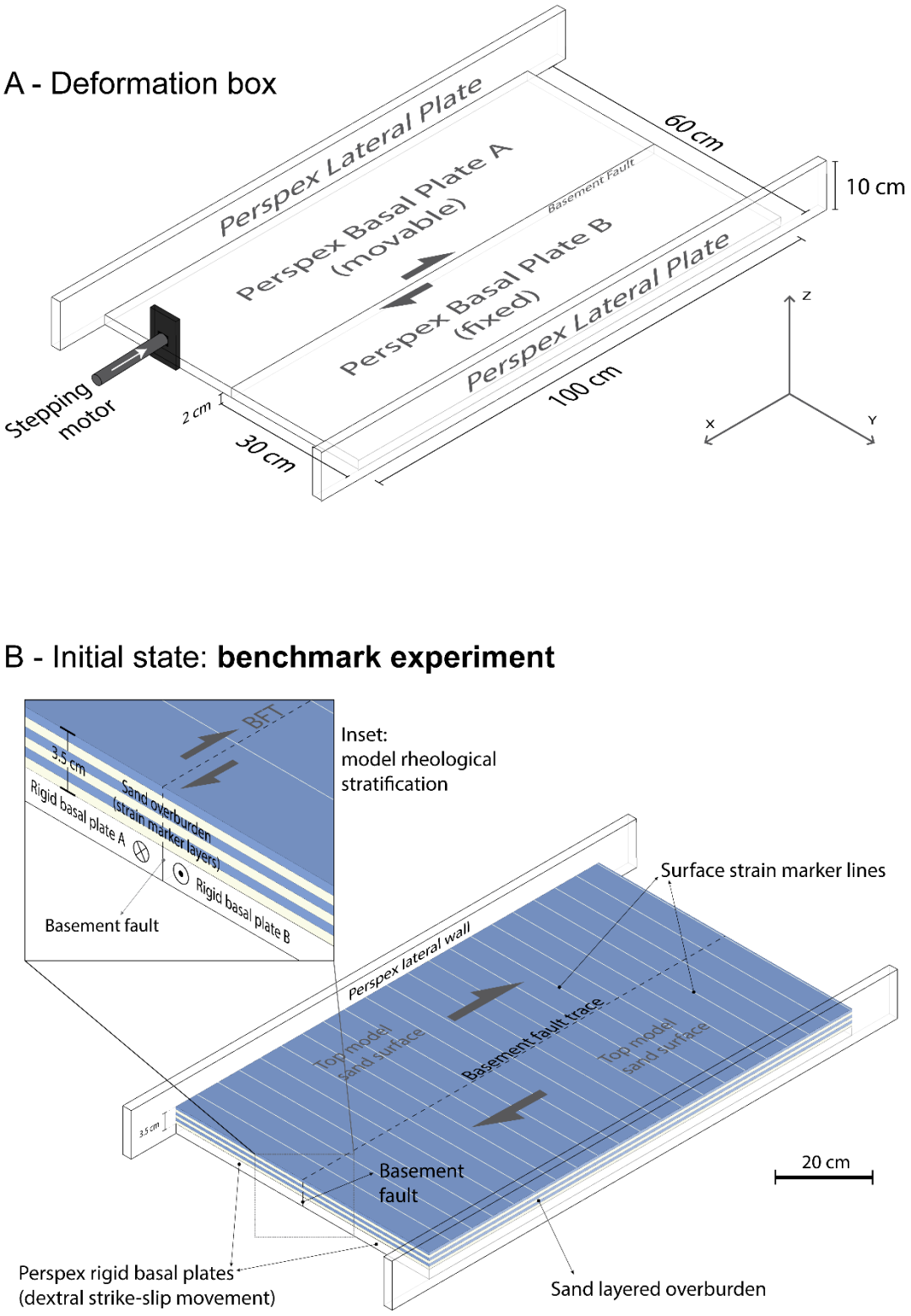

Figure 2.1. Experimental apparatus. A: Perspex deformation box; B: Initial state of the classical Riedel experiment used as an end member comparison benchmark in the present study. Inset in B shows the thickness of the sand overburden. BFT – Basement fault trace. Halved arrows indicate bulk strike-slip kinematics along basement fault direction.

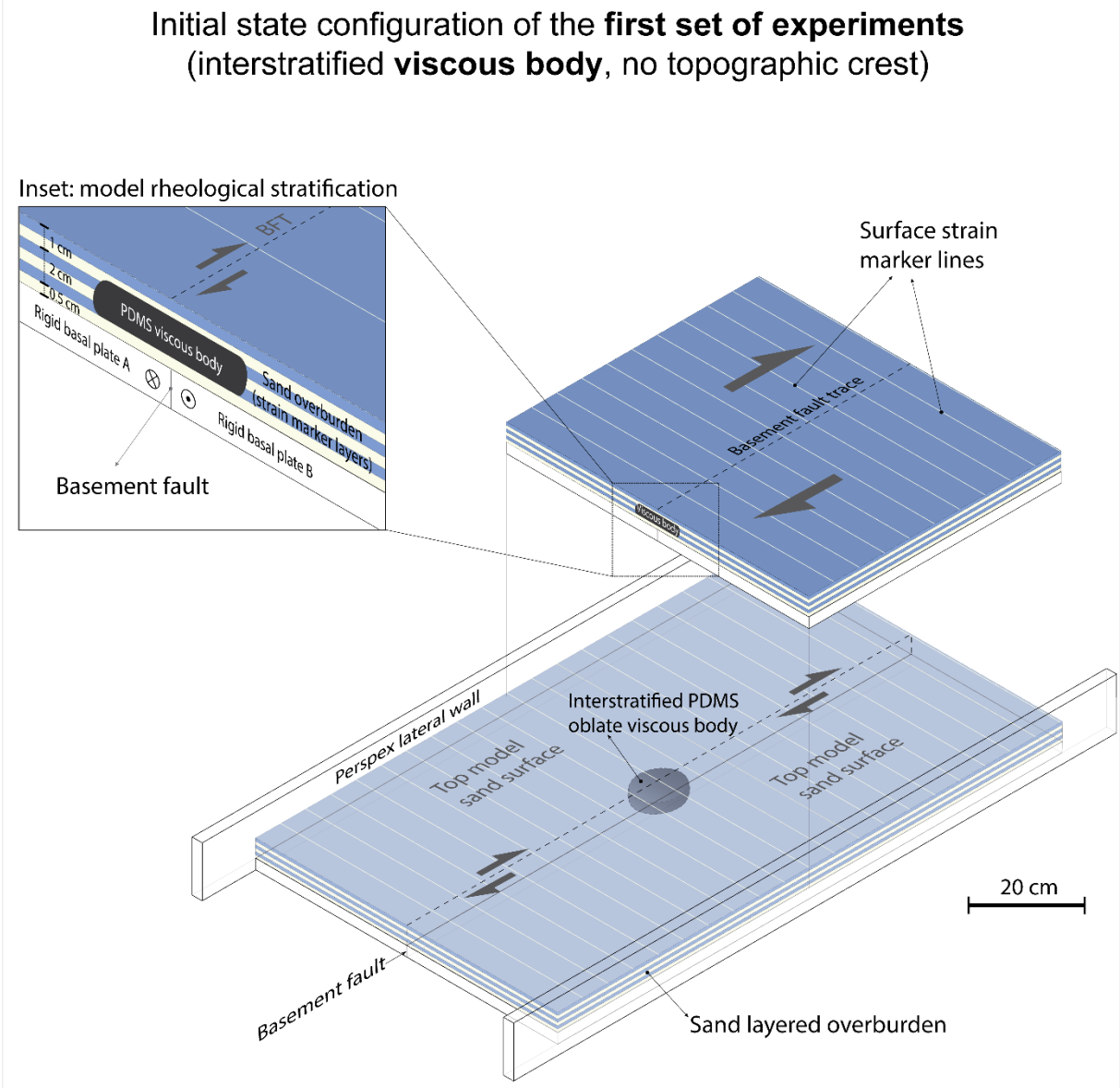

Figure 2.2. Initial state configuration of the first set of experiments (interstratified viscous body, no topographic crest). Inset depicts the detailed rheological stratigraphy of the model along a section cutting the viscous body. BFT – Basement fault trace. Halved arrows indicate bulk strike-slip kinematics along basement fault direction.

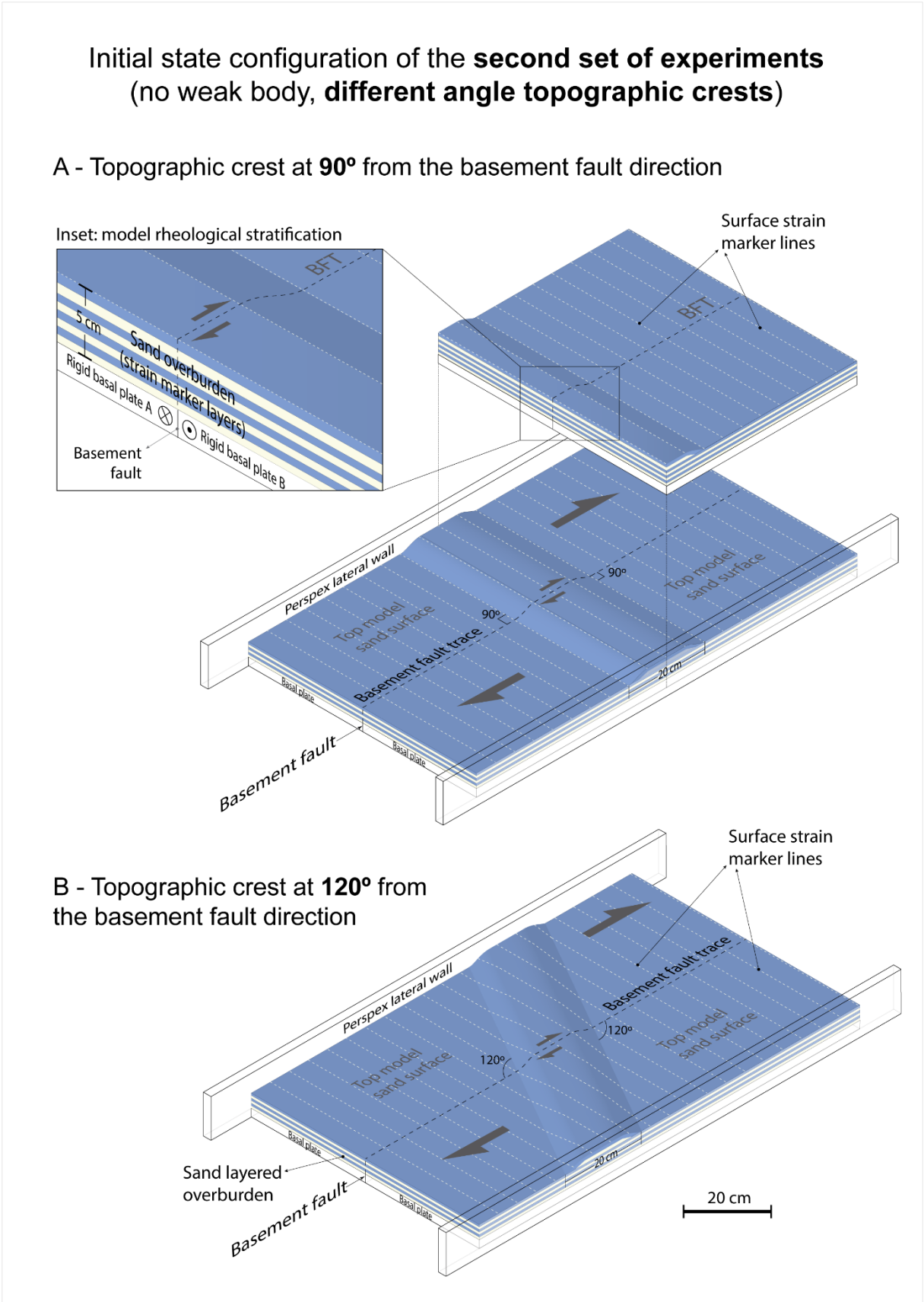

Figure 2.3. Initial state configuration of the second set of experiments (no viscous body, different angle topographic crests). A: topographic crest at 90º from the basement fault direction; B: topographic crest at 120º (clockwise) from the basement fault direction. Inset in A shows the higher thickness (5 cm) of the sand overburden across the topographic crest. BFT – Basement fault trace. Halved arrows indicate bulk strike-slip kinematics along basement fault direction.

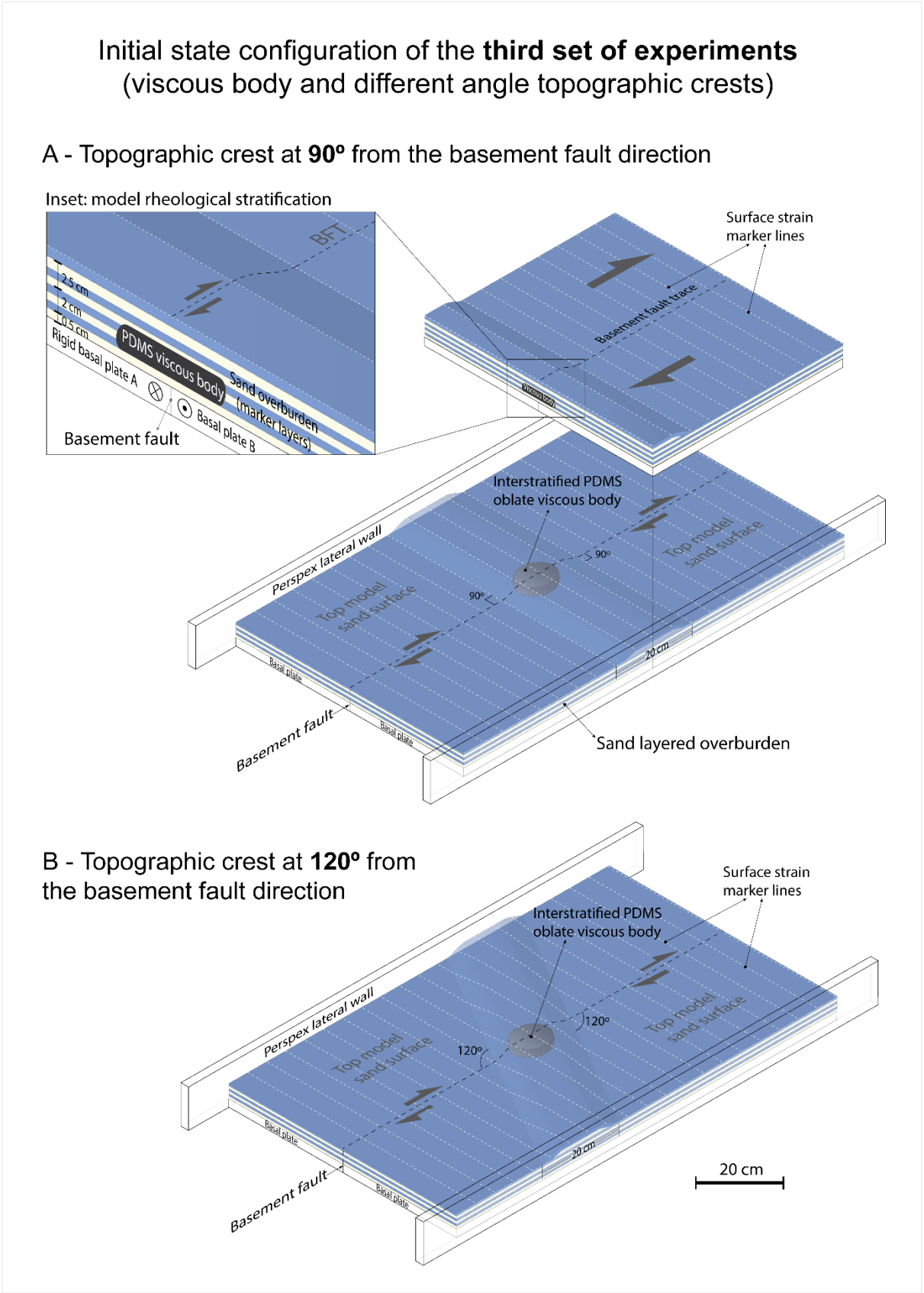

Figure 2.4. Initial state configuration of the third set of experiments (viscous body and different angle topographic crests). A: topographic crest at 90º from the BFD; B: topographic crest at 120º (clockwise) from the BFD. Inset in A shows the detailed rheological stratigraphy of the model along a section cutting the viscous body and the topographic crest. BFT – Basement fault trace. Halved arrows indicate bulk strike-slip kinematics along basement fault direction.

2.2. Methodology

2.2.1. Material properties and scaling

Dry quartz sand (SIFRACO NE34) was used in all our experiments to account for the mechanical behaviour of upper crustal rocks (see Table 1 and supplementary data of Rosas *et al*., 2017 for detailed sand properties). Sand is a classical analogue modelling material that deforms in a brittle way following the Coulomb failure criterion (e.g. Davis *et al*., 1983; Hubbert, 1951, 1937; Mandl, 1988; Mandl *et al*., 1977; Schellart, 2000) and has been extensively used in similar analogue modelling studies to simulate the rheological behaviour of brittle crustal and upper crustal rocks (e.g., Dooley and Schreurs, 2012; Rosas *et al*., 2017). Likewise, transparent silicone putty has also been classically used to simulate Newtonian rheologies accounting for (relatively low viscosity) upper lithospheric viscous layers/bodies (e.g., Corti *et al*., 2005; Dooley and Schreurs, 2012; Keppler *et al*., 2013; Koyi *et al*., 2008). In the present case polydimethyl-siloxane or PDMS (manufactured by Dow Corning of Great Britain under the trade name SGM 36, Weijermars, 1986; Weijermars and Schmeling, 1986) was used to simulate the viscous behaviour of a crustal viscous anomaly with a general viscosity of 10^{17} Pa.s (see Table 2.2 for SGM 36 properties and model/nature ratios). In the present experiments we are assuming a crustal viscous body *in general*, and this value (10^{17} Pa.s) corresponds to the lower limit of the viscosity interval assumed for a salt diapir (i.e. between 10^{17} and 10^{21} Pa.s, e.g. Mukherjee *et al*., 2010; Weijermars *et al*., 1993), which could also account for the viscosity of a cooled pre-tectonic shallow magma chamber. Likewise, the general value assumed for the density of the viscous body was 2200 kg/m^3, which is in the range of densities assumed for salt (between 2000 and 2200 kg/m^3, Koyi, 2001; Mukherjee *et al*., 2010) and for rhyolitic magma (between 2180 and 2250 kg/m^3). As in other previous approaches (e.g., Edwards *et al*., 2015; Keppler *et al*., 2013) the silicone was mixed with a high-density powder (in this case Wolframite) in the right proportion to properly tune the density ratio between this material and the crustal viscous anisotropy (see Table 2.2).

According to the scaling theory of Hubbert (1937) proper dynamic scaling is only achieved when model/natural ratios for the three main fundamental units of length, time and mass are independently established (see Appendix A. for scaling procedure details). Following these same theoretical premises in the present experiments the length model/nature ratio was assumed in view of the dimensions of the used apparatus (see section 2.2 below). The mass ratio was deduced indirectly from the model/nature density ratio. The time ratio was also obtained from the corresponding model/nature viscosity ratio, assuming inertial accelerations to be negligible when compared to gravity acceleration *g* (see Appendix A. and Tables 2.1 and 2.2).

2.2.2. Apparatus, initial stage and experimental procedure

All the experiments were performed using the Perspex deformation box depicted in figure 2.1 A, orientated relatively to the Cartesian X, Y, Z reference frame as illustrated. In the initial experimental state, a layered sandpack with a total thickness of approximately 3.5 cm was placed on top of two laterally juxtaposed Perspex basal plates. No rheological contrast exists between different layers in the sandpack, since these were meant to be used strictly as a strain-markers along section planes containing the Z direction. The layers were obtained by pouring similar amounts of alternating normal and blue-dyed sand from a moving wide hopper, placed 20 cm above the basal plates and running parallel to the longest dimension of the deformation box (i.e. along the X direction). No scrapping or compaction was applied to the model surface or to any of the layers to avoid possible local compaction effects and resulting heterogeneities in the sand mechanical properties, which could influence the experimental outcomes and thereby affect the reproducibility of the experiments (e.g. Panien *et al*., 2006; Schreurs *et*

al., 2016). Also, no significant differences regarding grain-size distribution and internal friction were detected between dyed and non-dyed batches of sand (see supplementary data of Rosas *et al*., 2017 for further details), although such differences have been reported as potentially relevant in other instances (depending on the adopted dying methodology, Klinkmüller *et al*., 2016). In all experiments equally spaced (5 cm) parallel marker lines were imprinted on the top surface of the model (perpendicularly to the BFD), and top-view photographs were taken at regular time intervals of 30 seconds.

The experiments were always initiated by using a stepping motor to push (along the X direction) one of the rigid Perspex basal plates relatively to the other at a constant velocity of 1.44 cm/hr, (see Fig. 2.1 A). This simulated a right-lateral strike-slip movement along a pre-existent (i.e. pre-cut) vertical basement fault. Since the overlying layered sandpack was in frictional contact with both rigid basal plates, the basement strike-slip kinematics was conveyed upwards to the brittle overburden being accommodated by the progressive development of a brittle shear zone in the sand.

While our benchmark experiment corresponded just to the situation described above (Fig. 2.1B), in our first set of experiments a disc of PDMS with a thickness of ~2 cm and a radius of ~4.2 cm was interstratified within the sand, 0.5 cm above the basement fault trace in the centre of the model (see Fig. 2.2). Since the deformation propagates upwards from the moving basal rigid plates (basement) to the overlying sandpack (brittle overburden), the aim was to evaluate the potential obstructing role of a low viscosity anomaly (crustal viscous body) in this propagation, and its expression in the resulting surface structural pattern.

Conversely, in the second set of experiments no weak (viscous) anomaly was considered, but instead a major morphological crest was prescribed in the model by adding (along a ~20 cm wide strip) an extra 1.5 cm thickness to the sand pack (Fig. 2.3). In this case the objective was to understand the potential effect of such a major topographic anomaly in the upward propagation of the basement strike-slip deformation to the overlying brittle cover. Furthermore, the crosscut angle between the topographic crest and the main direction of the basement fault was also investigated within this second set of experiments, by considering either an orthogonal (90º), or a 120º (clockwise) angle of interference between both these features (see Fig. 2.3 A and B).

In the final third set of experiments both the existence of a crustal weak body (low viscosity anisotropy) and of a topographic crest were considered (Fig. 2.4), to evaluate the combined effect of a morpho-rheological anomaly in the brittle shear zone propagation across the thickness of the sandpack. Accordingly, both the interstratified PDMS disc prescribed in the first experimental set and the topographic crest considered in the second (at 90º and 120º angles with the BFD) were used in this case (see Fig. 2.4 A and B).

In one additional experiment the top sand layer thickness above the silicone viscous body was absent to allow direct observation of wrenching strain accommodation by this viscous anomaly above the basement strike-slip fault (see additional experiment - Fig. 2.18 in the supplementary data [(3)]).

All experiments ended after reaching a strike-slip offset of approximately 5 cm (~14.3 km). In all cases the end-state model was humidified and several YZ sections were serially cut and thoroughly photographed.

[(3)] In the case of the present manuscript, this figure was placed after chapter 2.5.

2.3. Experimental results

The results of the three sets of experiments referred above are here presented by comparison with the typical results of a classical Riedel sand-box experiment (Riedel, 1929), which are used as a benchmark (Fig. 2.5 and movie MBenchMK.mp4 in the supplementary data). Accordingly, we start by presenting the experimental results of this benchmark example, followed by the ones regarding the three sets of newly performed experiments. Our focus is thus on the denoted deviations from the classical results of Riedel (1929), caused by the prescribed different constraints in the new experiments.

2.3.1. Benchmark classical Riedel experiment

In early experimental stages (for dextral offset values < 1cm) the basement strike-slip movement is accommodated in the overlying sandpack essentially by the early development of an elongated linear morphologic high (with an ~8 cm width), coinciding with the basement fault trace direction (Fig. 2.5 A). Subsequently, a set of left-stepping en-échelon Riedel shears starts to develop, with Riedel structures partially overlapping and making characteristic angles of 17º to 20º with the basement fault trace (Fig. 2.5 B). Riedel shears display a dominant (dextral) strike-slip component of movement, although a minor reverse dip-slip component is also observed accommodating ongoing dilation and consequent uplift between adjacent overlapping Riedel structures (e.g. Le Guerroué and Cobbold, 2006). Lower angle synthetic shears (LAS shears) start to form shortly after the formation of the original Riedel shears (dextral offset of 1.4 cm) intersecting them along the basement fault trace direction (Fig. 2.5 C). Subsequent progressive coalescence of the lower angle shears produces the definition of an initial Y-shear (Morgenstern and Tchalenko, 1967), which gradually develops substituting the original Riedel structures in the accommodation of the main (dextral) strike-slip movement along the brittle shear zone (Figs. 2.5 D and E). The original Riedel shears eventually become inactive and are passively offset along the main Y-shear, giving rise to a complex anastomosed fault pattern (Fig. 2.5 E). In the final experimental stage, the offset superposition of different (somewhat uplifted) Riedel-fault bounded domains on opposite sides of the main Y-shear often originates a conspicuous bowtie-shaped structural pattern (see zoomed area – Inset of Fig. 2.5 E).

Obtained YZ cross-sections also reveal the characteristic flower structure configuration described for brittle shear zones in classical Riedel experiments (Fig. 2.5 F). The specific type of flower structure configuration depends on the position of the cross section, and although tulip-shape configurations are dominant, geometric-kinematic patterns implied in reverse slip accommodation of compressive stress are also common (see Fig. 2.5 F - cross section D-D'). Based on the en-échelon Riedel configuration seen in horizontal XY sections, and on the fact that Riedel shears root in the basement fault at depth (as seen in cross sections), a 3D helicoidal geometry has been previously proposed for these structures by different authors (Naylor, Mandl and Supesteijn, 1986; Mandl, 1988; Richard, Naylor and Koopman, 1995; Ueta, Tani and Kato, 2000).

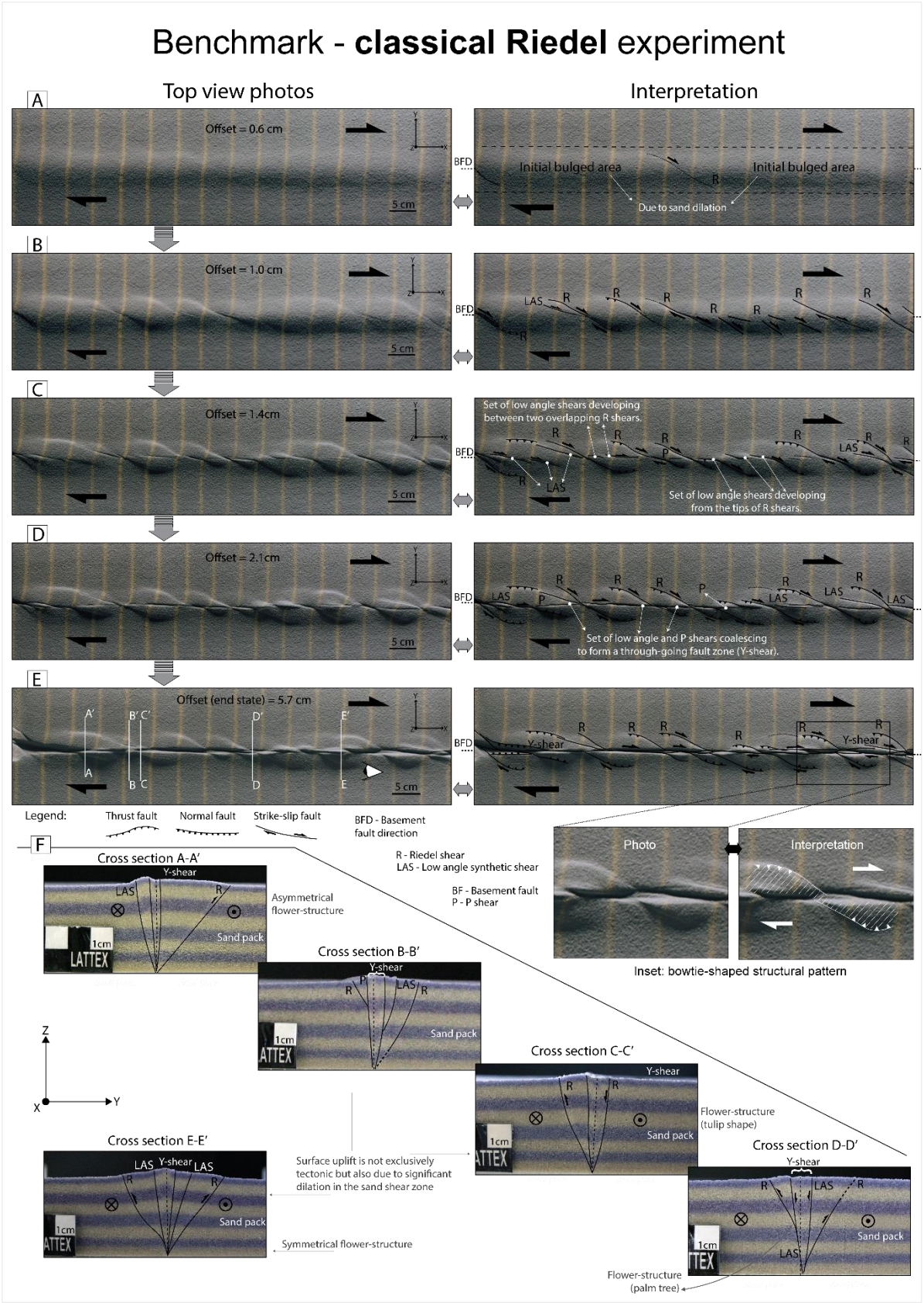

Figure 2.5. Results of the benchmark Riedel of experiment (see also movie MBenchMK.mp4 in the repository). A to E: Successive XY top view photographs (left column) and corresponding line drawing interpretations (right column) obtained for different increasing amounts of bulk strike-slip offset along the basement fault. View in E shows a detail of a bowtie-shaped structural pattern. F: Interpreted YZ cross-sections obtained in the experimental end state across the X direction (see exact location of the several sections in E).

2.3.2. First set of experiments: interstratified viscous body

The results of this first set of experiments are illustrated in detail in figure 2.6 (see also the movie M1Set.mp4 made available in the supplementary data). From the onset of the experiment a separation of the brittle shear zone in two main segments is readily observed directly above the viscous (silicone) body (Fig. 2.6 A-B). This segmentation is shown by the absence of Riedel shears (or any other type of structures) in this area at this early stage. Also, the strike-slip offset accommodation in the sand atop the weak (viscous) anomaly occurs along a wider shear domain contrasting with the discrete Riedel shear accommodation along the rest of the main brittle shear zone (Figs. 2.6 B-C). As in the benchmark experiment LAS shears are formed shortly after the Riedel structures and start to coalesce to form Y-shears (Fig. 2.6 C). For a bulk (total) offset of ~2 cm the main Y-shear forms along the length of the brittle shear zone, except in the area above the viscous anisotropy domain (Fig. 2.6 C). In this domain few LAS shears start to propagate to the interior of the viscous zone, still without cutting it completely. For further increments of strike-slip offset (between 3.5 and 5.7 cm - Figs. 2.6 D and E), the implied dextral kinematics is seen to be mostly accommodated by a well-defined linear trough corresponding to the main Y-shear that offsets all previously formed *Riedels*. The exception to this occurs in the area above the viscous body, in which the linkage between both (left and right) main brittle shear zone segments is represented, not by a single discrete structure (main Y-shear), but instead by a higher number of more delocalized shears (synthetic low angle shears above the viscous zone in Fig. 2.6 D and E). The viscous zone domain is also seen to be bounded by two normal faults orientated sub-perpendicularly to the σ_3 principal stress direction (see Fig. 2.6 C, D and F cross sections A-A' and E-E').

As in the benchmark experiment, the obtained (YZ) cross sections that cut the brittle shear zone without intersecting the viscous anisotropy show a typical flower structure geometry, intersecting the main Y-shear, as well as the LAS shears and the Riedel faults (Fig. 2.6 F). Similarly orientated cross sections sequentially cutting the viscous (silicone) body across the X-axis from the left edge to the right (see exact positions in Fig. 2.6 E), allow the reconstruction of the top view contour geometry of this anisotropy in its deformed end stage (Fig. 2.6 G). The evolving geometry of the viscous body was further clarified in the additional experiment in which the sand above the viscous anisotropy is absent (experiment in supplementary data – Fig. 2.18). This revealed an overall stretched viscous body with a sigmoidal shape, and with its longest axis closely aligned with the σ_3 principal stress direction implied by the bulk simple shear strain.

Accordingly, in the successive YZ sections cutting across the viscous silicone body this anisotropy is firstly observed only to one side of the main brittle shear zone (corresponding to the first of the intersected stretching quadrants implied by the bulk strike-slip deformation - see Fig. 2.6 F - cross section B-B'). In its inner boundary the viscous body exhibits a concave (inner verging) geometry and the silicone is seen to be slightly injected into the bounding fault (see bounding R shear in Fig. 2.6 F - cross section B-B').

In YZ sections cutting across the middle part of the viscous silicone body this anisotropy is observed continuously to both sides of the basement fault trace (Fig. 2.6 F – cross section C-C'), rendering the overall structural pattern a more symmetrical geometry. In this case, in the sand layer beneath the silicone body one or two faults propagate upwards from the basement fault trace until reaching the lower limit of the viscous body, where they die out and do not propagate across its thickness. Additionally, in the sand layers above the viscous body, a much larger number of shears is observed spreading along a wider area, corresponding to a more delocalized fault pattern (see Fig. 2.6 F – cross section C-C').

In the YZ sections cutting across the other end of the silicone body (Fig. 2.6 F – cross section D-D'), the overall structures are similar, although with a symmetrically opposite vergence, relatively to the ones described above (compare cross sections B-B' and D-D' in Figs. 2.6 F). As such, the viscous silicone body is only observed to the opposite side of the main brittle shear zone (also the one corresponding to the extensional quadrant), limited by inner bounding faults with slightly injected silicone material.

2.3.3. Second set of experiments: different angle morphological crests

The obtained results in this second set of experiments are similar regardless of the angle (90º or 120º clockwise) between the crest and the BFD (Figs. 2.7 and 2.8 and movies M2Set_90.mp4 and M2Set_120.mp4 in the supplementary data). As in the benchmark experiment, a pervasive pattern of left-stepping Riedel shears and incipient LAS shears is initially formed in the model surface away from the morphological crest (Figs. 2.7 and 2.8 A to B). In contrast, on top of the same morphological crest, the bulk strike-slip kinematics is in both cases mostly accommodated by a main synthetic shear (making an angle α with the BFD between 9º and 17º - Figs. 2.7 and 2.8 A to B). Likewise, in both experiments, from 2 cm of offset onwards, LAS shears coalesce and link defining the main Y-shear (Figs. 2.7 and 2.8 C to D) that eventually accommodates all dextral wrenching kinematics (passively offsetting all previously formed structures, Figs. 2.7 and 2.8 E).

In both 90º and 120º angle experiments the obtained YZ sections across the several Riedel, low-angle and Y shears allow a straightforward correlation with corresponding structures seen in top view (Figs. 2.7 and 2.8 F), revealing the same dominant tulip-shape characteristic geometry observed in the benchmark case.

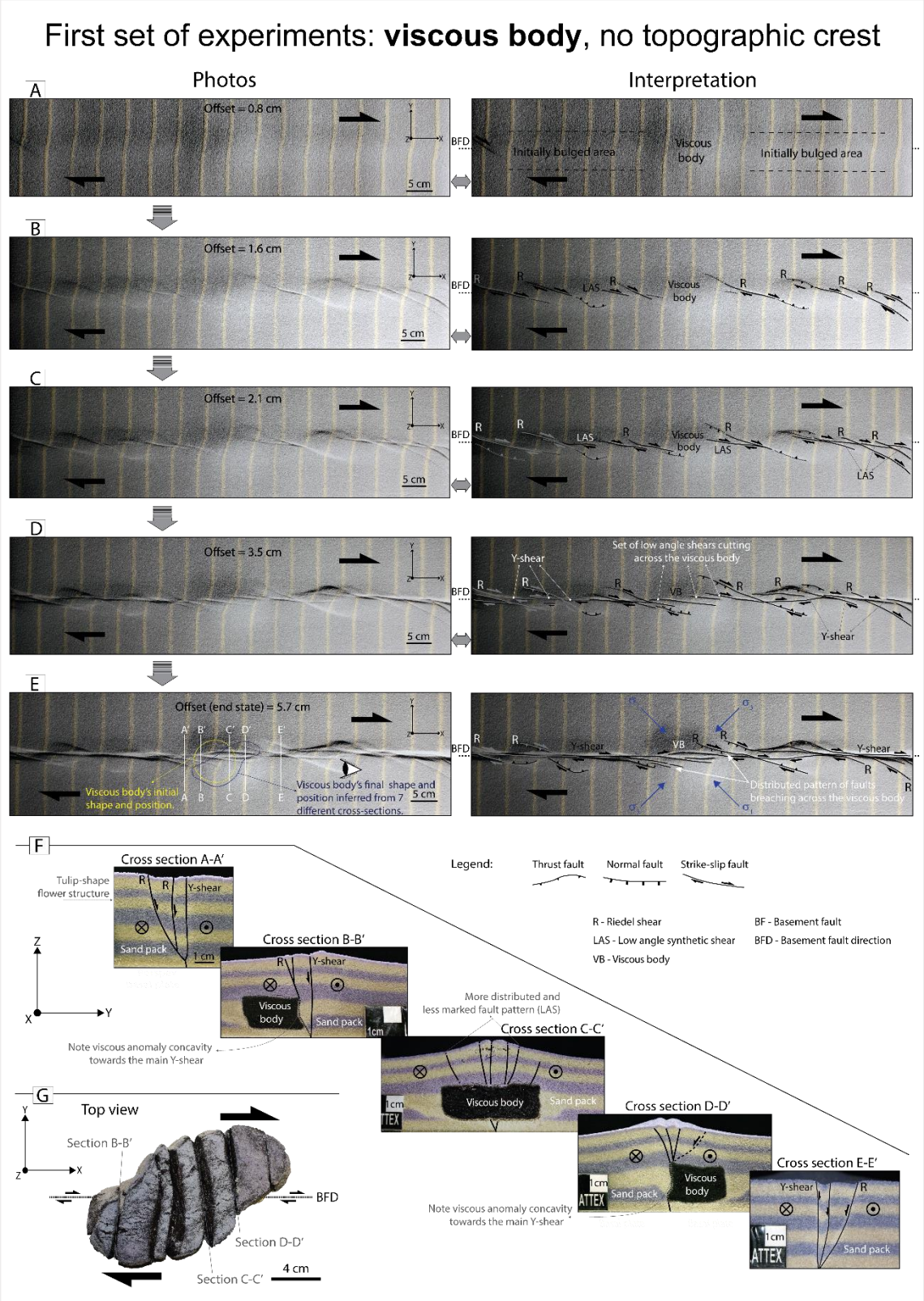

Figure 2.6. Results of the first set of experiments: interstratified viscous anisotropy and absence of topographic crest (see also movie M1Set.mp4 in the repository). A to E: Successive XY top view photographs (left column) and corresponding line drawing interpretations (right column) obtained for different increasing amounts of bulk strike-slip offset along the basement fault. Contour coloured dashed lines in E correspond to the inferred XY geometry of the viscous anomaly in the initial (yellow) and final (blue) experimental end-state. F: Interpreted YZ cross-sections obtained in the experimental end state across the X direction (exact locations in E). G: Top view photograph of the reconstruction of the viscous body approximate geometry in the experimental end stage (E), obtained by reassembling the several slices produced while cutting the cross-sections depicted in F (note the resemblance with the depicted outlined geometry in E – blue contour dashed line).

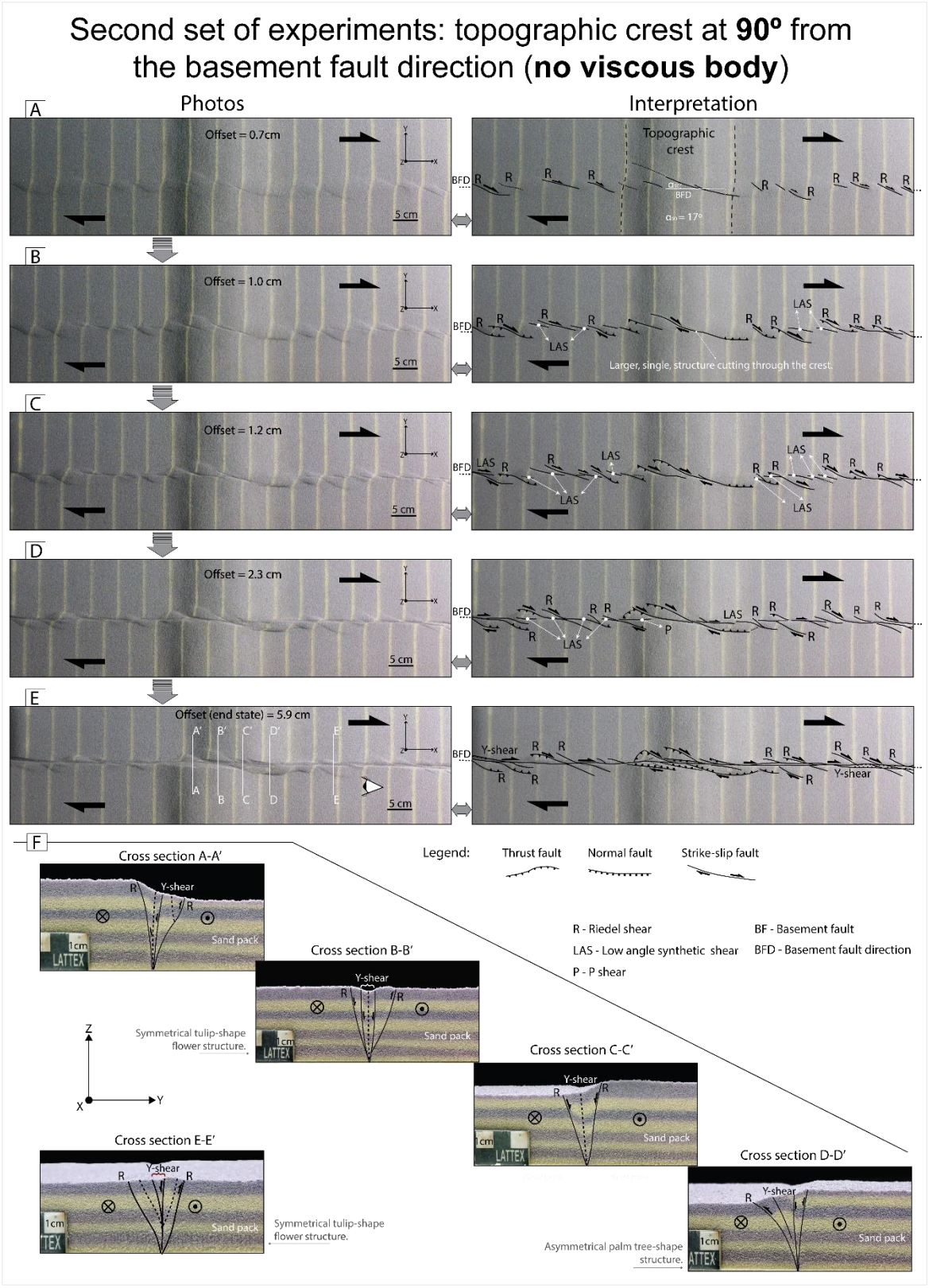

Figure 2.7. Results of the second set of experiments: topographic crest at 90º from the basement fault direction and absence of interstratified viscous anisotropy (see also movie M2Set_90.mp4 in the repository). **A to E**: Successive XY top view photographs (left column) and corresponding line drawing interpretations (right column) obtained for different subsequent increments of bulk strike-slip offset along the basement fault. **F**: Interpreted YZ cross-sections obtained in the experimental end state across the X direction (exact locations in E). α_{90} – angle between the main shear atop the topographic crest and the basement fault direction (BFD).

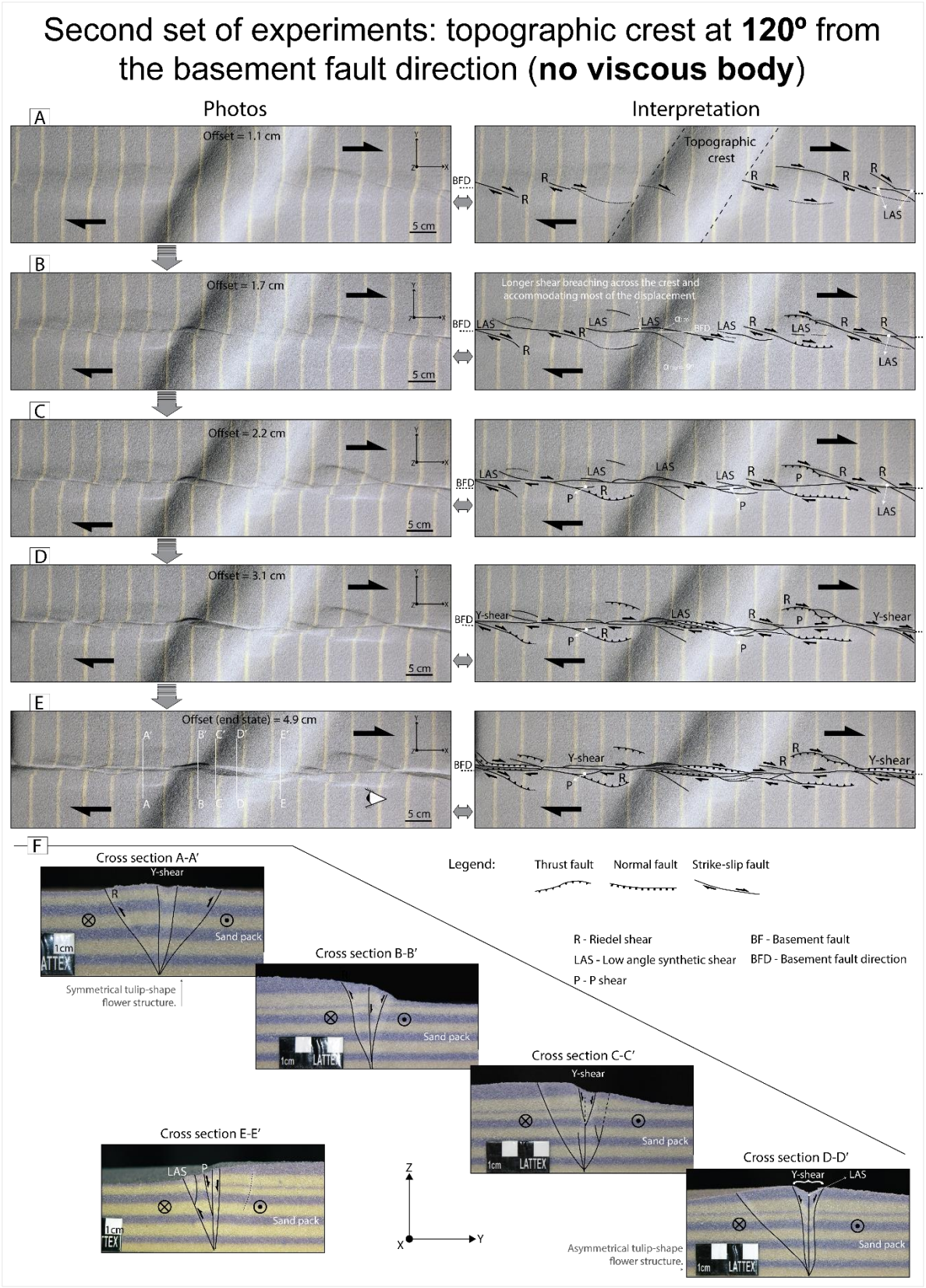

Figure 2.8. Results of the second set of experiments: topographic crest at 120º from the basement fault direction and absence of interstratified viscous anisotropy (see also movie M2Set_120.mp4 in the repository). **A to E**: Successive XY top view photographs (left column) and corresponding line drawing interpretations (right column) obtained for different subsequent increments of bulk strike-slip offset along the basement fault. **F**: Interpreted YZ cross-sections obtained in the experimental end state across the X direction (exact locations in E). $\boldsymbol{\alpha_{120}}$ – angle between the main shear atop the topographic crest and the basement fault direction (BFD).

2.3.4. Third set of experiments: viscous body and different angle morphological crests

The results of this third set of experiments are illustrated in detail in figures 2.9 and 2.10 (see also movies M3Set_90.mp4 and M3Set_120.mp4 in the supplementary data). The comparison of both 90º and 120º angle experiments with the corresponding ones obtained in the second set of experiments (similarly oriented topographic crests, but no silicone anisotropy, see Figs. 2.7 and 2.8) reveals a delay in the propagation of the Riedel and LAS shears across the morpho-rheological perturbation. Accordingly, for similar small amounts of strike-slip offset, a main low angle shear is generally readily observed in experiments without the silicone anomaly, while in the ones with this interbedded viscous anomaly no crosscutting shears are observed at this same stage (compare Figs. 2.9 A-C with 2.7 A-C and Figs. 2.10 B-C with 2.8 B-C). Hence, in the topographic crest above the viscous body the bulk strike-slip offset is rather accommodated by a wider shear zone than by any discrete structures absent at this stage.

Moreover, in the end stage of this third set of experiments pull apart basins formed orthogonally to σ_3, being distributed around opposite sides (extensional quarters) of the viscous body anisotropy - Figs. 2.9 F (Inset) and 2.10 F (Inset). In the 120º angle experiments reverse faults also nucleate at opposite (compressive) quarters of the viscous (silicone) body orthogonally to σ_1 - Fig. 2.10 F (Inset). This structural association is better developed in the 120º angle experiments than in the 90º angle ones, in which the bounding reverse faults are much less developed (compare Figs. 2.9 F and 2.10 F). Conversely, in the second set of experiments (without the silicone body), no compressive vs. extensional quarter structures of this type were observed to form (compare Figs. 2.9 and 2.10 with Figs. 2.7 and 2.8, respectively).

Relatively to the first experimental set, the results of this third set also show a consistently more localized pattern of deformation breaching across the morpho-rheological anomaly (i.e. preferably represented by a few or a single main through-going Y-shear). As referred above (see section 2.3.2), equivalent deformation in the first experiments was always preferably accommodated by a set of more numerous and more distributed shears (compare Figs. 2.9 F and 2.10 F with Fig. 2.6 E).

The serially cut sections obtained from the end-stage models allow a clear correlation between the structures observed along these sections and the ones observed in top view photos (Figs. 2.9 G and 2.10 G). The same sigmoidal contour geometry observed in the first experimental set is also deduced for the viscous (silicone) body anisotropy from these sections (Figs. 2.9 F and 2.10 F). Silicone injection along fault planes, as well as an overall structural vergence to the interior of the model (i.e. towards the main Y-shear) is likewise observed in the end stage of 90º angle experiments (in sections cutting the edges of the silicone anisotropy - Fig. 2.9 G – sections B-B' and D-D'). Conversely, in YZ sections cutting across the centre of the model (through the middle of the viscous body anisotropy) both 90º and 120º angle silicone-crest experiments show a somewhat more localized pattern of faulting above the silicone anisotropy near the surface, comparatively to the one observed in the first experimental set in which this pattern tends to be more distributed (compare Fig. 2.9 G - section C-C' and Fig. 2.10 G - section B-B' with Fig. 2.6 F - section C-C'). Additionally, in the 120º angle case, the obtained cross-sections also show pull-apart basin normal faults (perpendicular to σ_3) nucleating along the (lateral) sand-silicone contact (i.e. along the subvertical contact interface between the viscous body and the sand layers - Fig. 2.10 G, pull-apart basins in sections C-C' and D-D'). The same was also observed for the reverse faults that also bound the viscous body along the orthogonal direction (i.e. perpendicularly to σ_1 - Fig. 2.10 G, section A-A' and B-B').

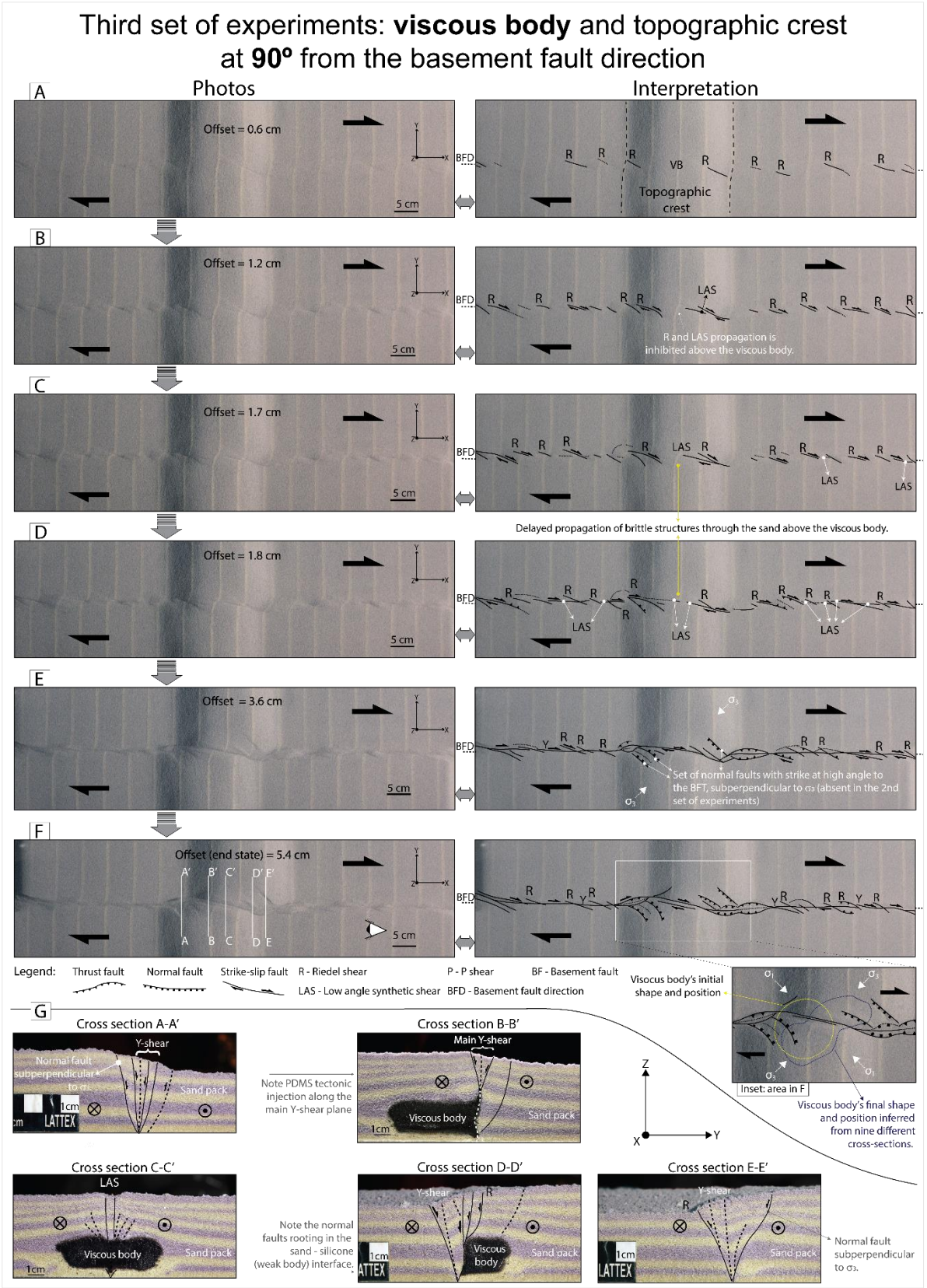

Figure 2.9. Results of the third set of experiments: interstratified viscous anisotropy and topographic crest at 90º from the basement fault direction - BFD (see also movie M3Set_90.mp4 in the repository). A to F: Successive XY top view photographs (left column) and corresponding line drawing interpretations (right column) obtained for different increasing amounts of bulk strike-slip offset along the basement fault. Contour coloured dashed lines in F (Inset) correspond to the inferred XY geometry of the viscous anomaly in the initial (yellow) and final (blue) experimental end-state. G: Interpreted YZ cross-sections obtained in the experimental end state across the X direction (exact locations in F).

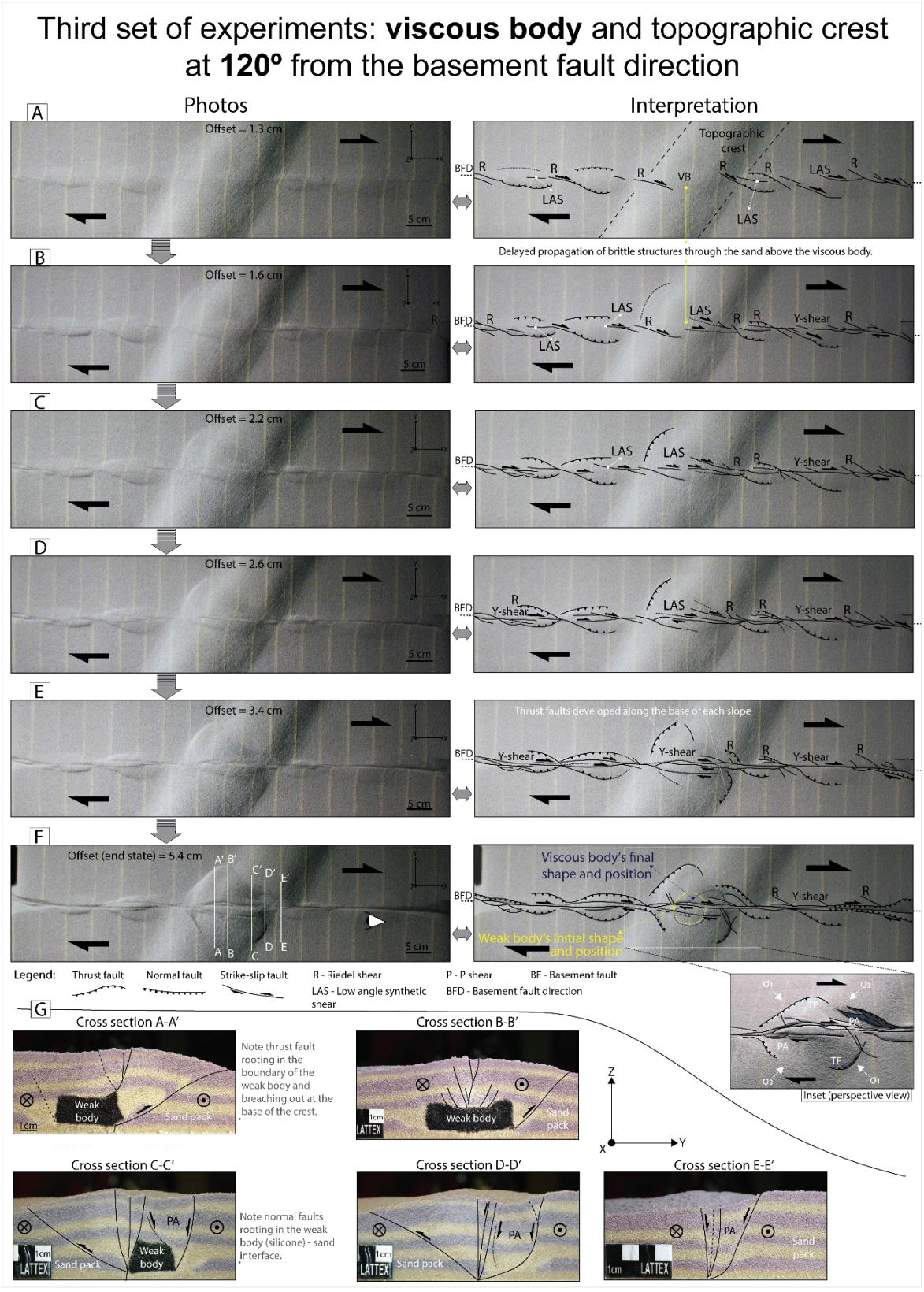

Figure 2.10. Results of the third set of experiments: interstratified viscous anisotropy and topographic crest at 120º from the basement fault direction - BFD (see also movie M3Set_120.mp4 in the repository). **A to F**: Successive XY top view photographs (left column) and corresponding line drawing interpretations (right column) obtained for different increasing amounts of bulk strike-slip offset along the basement fault. Contour coloured dashed lines in F correspond to the inferred XY geometry of the viscous anomaly in the initial (yellow) and final (blue) experimental end-state. **Inset** F: Detail of shortening vs. extensional structures around opposite quarters of the viscous body. **G**: Interpreted YZ cross-sections obtained in the experimental end state across the X direction (exact locations in F).

2.4. Discussion

2.4.1. The effects of an interstratified viscous body anisotropy

The results from the first experimental set show two main differences relatively to the benchmark experiment: an initial delay in the formation of the brittle structures in the sand above the viscous body (compare Figs. 2.5 CD and 2.6 BC); and a much more delocalized pattern of these structures in the experimental end stage, represented by a higher number of smaller, more distributed, low angle shears (compare the corresponding end stages: Fig. 2.5 E with Fig 2.6 E).

The upward propagation of strike-slip accommodating brittle structures (across the thickness of the model overburden above the basement fault) is strongly delayed in the sand layers overlying the viscous body. This delay is caused by the viscous response (strain accommodation) of the interstratified body (Fig. 2.11). In the beginning of the experiment the bulk dextral strike-slip kinematics implied by the basement plate relative movement is readily conveyed to the frictional overlying (0.5 cm thick) sand layer, where it is accommodated by the formation of a few upwards splaying dextral strike-slip Riedel shears. However, when this upward propagation of dextral movement reaches the base of the silicone body the different rheology of the latter responds by promoting a delayed viscous strain accumulation throughout its thickness, rather than a more efficient upward stress propagation as in the case of the brittle sand (Fig. 2.11). Because of the viscous rheology of the silicone body, upward shearing propagation across the basal sand-silicone contact surface is delayed, possibly due to viscous resistance of this body. This seemingly suggests that the shear stress implied by the frictional yielding in the underlying sand layer would not be enough to produce immediately (corresponding) viscous yielding in the silicone (at the prescribed velocity). In any case, the different shear-accommodating response given by sand and silicone must imply some degree of strain accumulation along the highly frictional basal contact between both. In the silicone body, local stress is thus preferably dissipated by the gradual straining of its original oblate shape, undergoing shortening along the main direction of compression and stretching along the orthogonal extensional one (Fig. 2.12 A). This, together with the internal rotation (i.e. vorticity) implied by the non-coaxial nature of the bulk (simple shear) deformation leads to the sigmoidal shape observed in the experimental end state (see Fig. 2.6 G and supplementary data – Fig. 2.18). Delayed whole body viscous strain is eventually transmitted to the overlying sand layers, where it is accommodated in a more delocalized manner by the development of the observed more distributed set of low angle shears (see Fig. 2.6 E and F – cross section C-C'). It should be noted that the deformation affecting the top sand layers overlying the silicone body is also controlled by the displacement of the confining sand, which may explain the bulging of the sand above this viscous body.

This stress/strain vertical (upward) propagation also controls the surface distribution of shortening and extensional structures around opposite quarters of the viscous body (orthogonally to σ_1 and σ_3 respectively, see Fig. 2.12 A). Accordingly, localization of compressive stress and associated reverse faults is favoured along sub-vertical sand-silicone (lateral contact) interfaces, oriented sub-perpendicularly to σ_1, with the faults rooting in this surface of rheological contrast (Fig. 2.12 B). Along this same type of boundary but orthogonally to σ_3 normal faults are instead preferably formed (Fig. 2.12 C). This is because the silicone also resists the lateral push exerted by the confining sand, resulting in different displacement velocities in the sand and silicone (see Fig. 2.12).

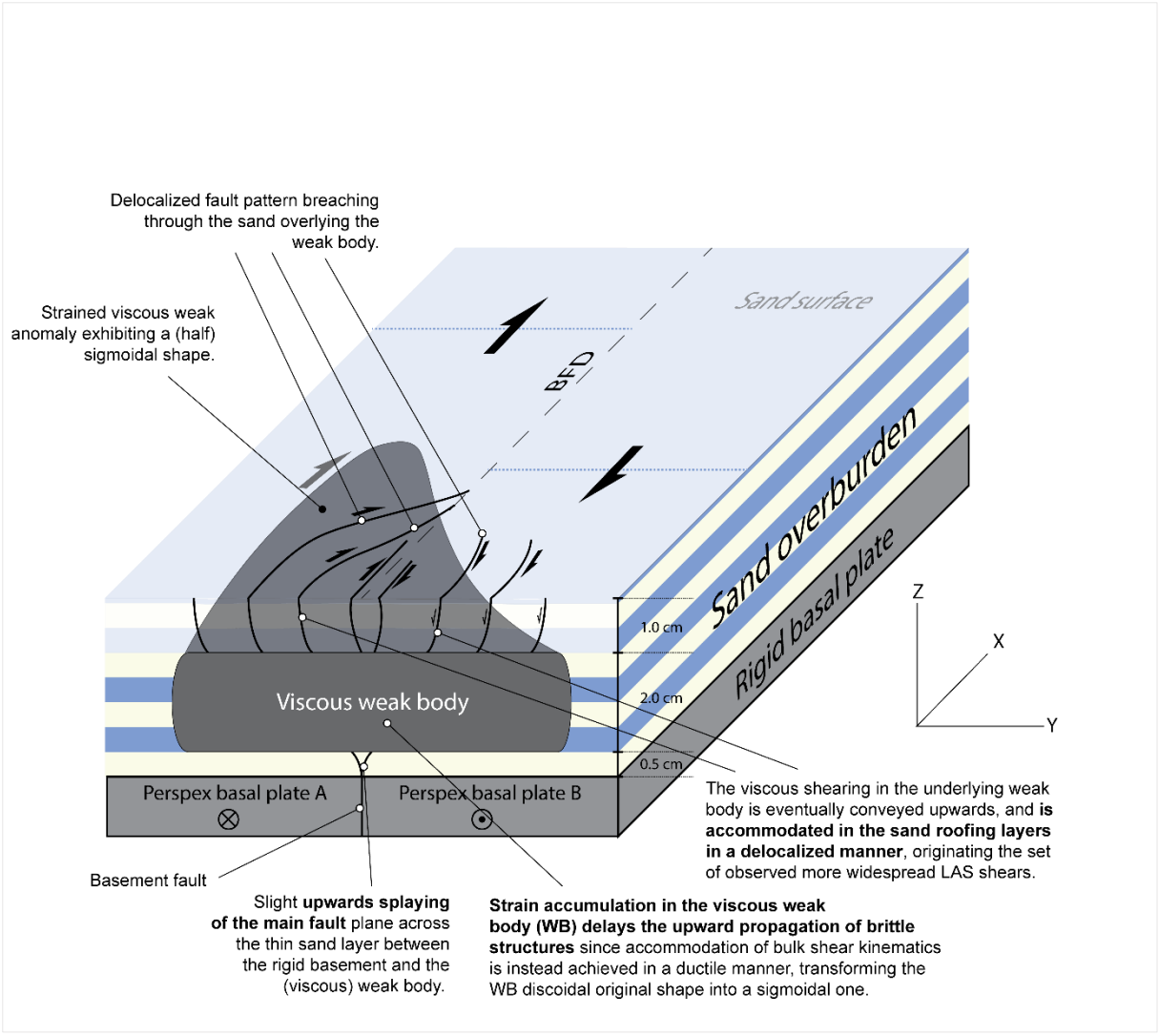

Figure 2.11. General schematic representation of the way through which the different prescribed model material rheologies control the upwards shear stress-strain propagation (implied by the dextral strike-slip basement faulting) across the whole model thickness.

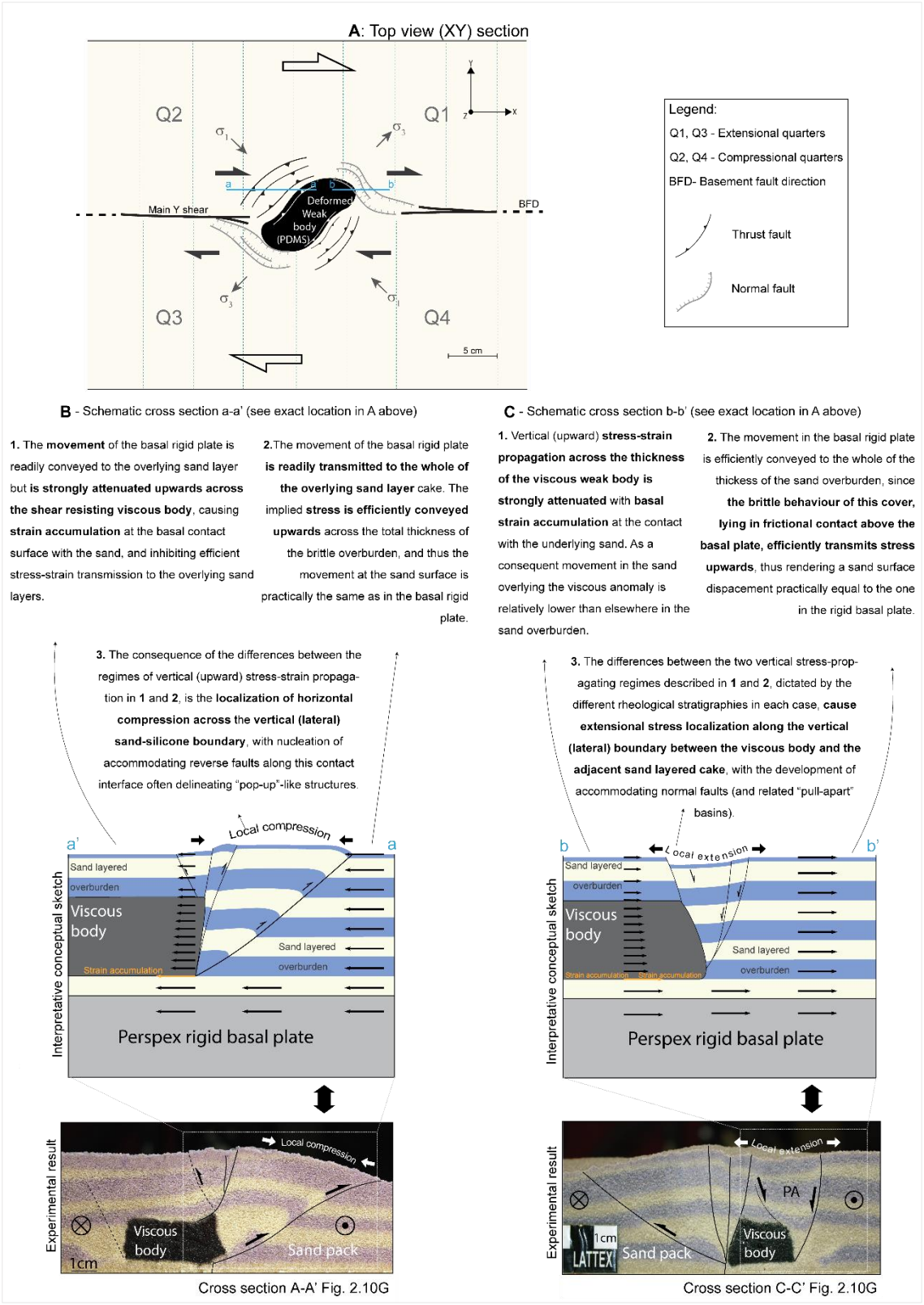

Figure 2.12. Schematic interpretation of the way through which different model rheological stratigraphies determine the distribution of different types of structures around opposite (extensional vs. compressive) quarters of the viscous weak body. **A:** top view line drawing of an experimental end stage (removed rooftop sand layers - see repository of supplementary data - Fig. *2.18*) ; **B and C:** Schematic cross sections (along σ_1 and σ_3 directions, a-a' and b-b', respectively) illustrating the strain accumulation effect caused by the interstratified viscous weak body, and its role in localizing compressive vs. tensile accommodating structures along (lateral) sand-silicon boundaries. Note that the depicted (photos corresponding to cross sections A-A' and C-C' of Fig. 2.10) are not parallel to any of the principal stress directions but are instead orthogonal to the basement fault direction (BFD).

2.4.2. The effects of a strictly morphological barrier (major morphological crest)

The results of the second set of experiments show that the main change in the surface structural pattern arising from prescribing a morphological crest (at different angles from the main shear zone) is the development of fewer, longer, low angle shears breaching across this morphological high (compare Fig. 2.5 C-D with Figs. 2.7 C-D and 2.8 B-C). This is interpreted simply as the result of the increase in the thickness of the brittle overburden above the basement fault implied by the existence of a morphological crest (see Fig. 2.3 A and B). Accordingly, for a brittle overburden with the same internal friction, the higher the sandpack thicknesses, the longer the initial Riedel shears and the wider the brittle shear zone that is formed at the surface (Naylor *et al*., 1986). These empirical relationships were reported by the cited authors, revealing (for a brittle medium with an internal frictional angle of φ = 35º to 40º) that the length of first *Riedels* is nearly 1.6 times the thickness of the brittle overburden, and the surface width of the brittle fault zone approximately equals that same thickness. When considering the data of this second set of experiments, taking into account the thickness of the brittle cover both away and above the morphological high (for both 90º and 120º angle experiments), these relationships show to hold qualitatively (see Table 2.3). Accordingly, an increase in the thickness of the sand overburden is always matched by an increase in the length of the Riedel shears, together with an increase on the width of the main shear zone. However, the obtained quantitative ratios differ ~48% for R1 and ~14% for R2 relatively to the corresponding ones reported by the cited authors (see Table 2.3).

2.4.3. The combined effects of a morpho-rheological obstacle

In the end stage of the third set of experiments, pull-apart structures are formed around the viscous body anisotropy, orthogonally to σ_3 least principal stress (see insets of Figs. 2.9 F and 2.10 F, and cross-sections C-C', D-D' and E-E' in Fig. 2.10 G). In the same experimental end stage, reverse faults have also formed bounding opposite quarters of the same anisotropy, with direction sub-perpendicularl to σ_1 (see Figs. 2.10 F and cross-sections A-A', C-C' and D-D' in Fig. 2.10 G). This structural configuration/distribution is here interpreted taking into account the strain localization effect of the interstratified viscous anomaly and specifically considering, not only the upward propagation of the deformation (from the basement fault to the viscous-frictional overburden), but also the consequences of this in terms of the diachronic lateral distribution of the deformation across two juxtaposed different rheological mediums (from viscous to frictional or vice-versa, Fig. 2.12). In the performed experiments σ_1 principal stress is at 45º from the basement fault trace. The delayed upward propagation of the deformation, caused by the viscous body basal strain localization effect, promotes horizontal compression and complying reverse-fault accommodation along σ_1 and across the lateral contact interface between the sand and the silicone viscous body (around opposite, compressive, quarters of this viscous anisotropy - see Fig. 2.12 A and B). For similar reasons, along the σ_3 direction, extensional structures (normal faults) also form between the sand layers and the silicone viscous body, eventually producing the observed graben-like structures and pull-apart basins (distributed around opposite, extensional, quarters of this same viscous anomaly - see Fig. 2.12 A and C).

Viscous body -bounding reverse faults are much better developed in the 120º angle experiments than in the 90º angle ones (compare Figs. 2.9 F, G and 2.10 F, G). This shows that in this third set of experiments the nucleation of these type of structures is not exclusively controlled by the rheological contrast along preferably oriented sand-silicone interfaces, but also by the orientation of the prescribed morphological steps (Fig. 2.13). In the 120º angle case the orientation of the crest is more orthogonal to σ_1 (at 75º) than in the 90º angle case (at 45º – see Fig. 2.13 A and B). This morphological step represents an abrupt transition between adjacent domains of different thickness (i.e. different lithostatic load and

compaction), and thus, strain tends to concentrate at this morphological boundary. Accordingly, in the 120º case the propensity for nucleating bounding reverse faults with a certain strike is going to be controlled not only by the orientation of the sand-silicone rheological boundary, but also by a more favourable (i.e. more orthogonal) orientation of the topographic step (Fig. 2.13 B and C).

These same experimental results show that the breaching of the morpho-rheological obstacle is represented by a main localized through-going Y-shear that accommodates most of the bulk dextral wrenching kinematics in the experimental end stage (Fig. 2.14 C, D and Figs. 2.9 G – cross section C-C', 2.10 G – cross section B-B'). This is in clear contrast with what is observed in the end-stage of the first set of experiments, in which the deformation pattern affecting the sand layers above the viscous anisotropy was much more distributed, comprising a set of smaller low angles synthetic shears (Fig. 2.14 B and Fig. 2.6 F – cross section C-C'). This is interpreted as the result of the different original thickness of the sand layers overlying the silicone viscous anisotropy in each case (Fig. 2.15 A). In the initial state of the first set of experiments the viscous anomaly is originally only at a depth of about 1 cm beneath the sand surface. Since deformation is propagated upwards through the thickness of the model, this relatively thinner sand cover is going to accommodate the ductile strain affecting the whole of the underlying viscous anisotropy also in a somewhat distributed manner. This accommodation corresponds to a mechanical brittle response to the wide spread ductile viscous strain conveyed from below and is manifested by the development of the observed set of relatively smaller low angle synthetic shears distributed along a wider area above the viscous body. Conversely, in the third set of experiments the sand above the viscous weak body is 2.5 times thicker (Fig. 2.15 B). The mechanical influence of the ductile straining viscous anisotropy in the way deformation is accommodated across the overlying, relatively thicker, sand cover decreases as the depth distance to this viscous body increases. As a result, the fault-distributed deformation pattern is attenuated towards the surface and is progressively replaced by the narrower main (through-going) Y-shears observed at the surface of the model in the experimental end stage.

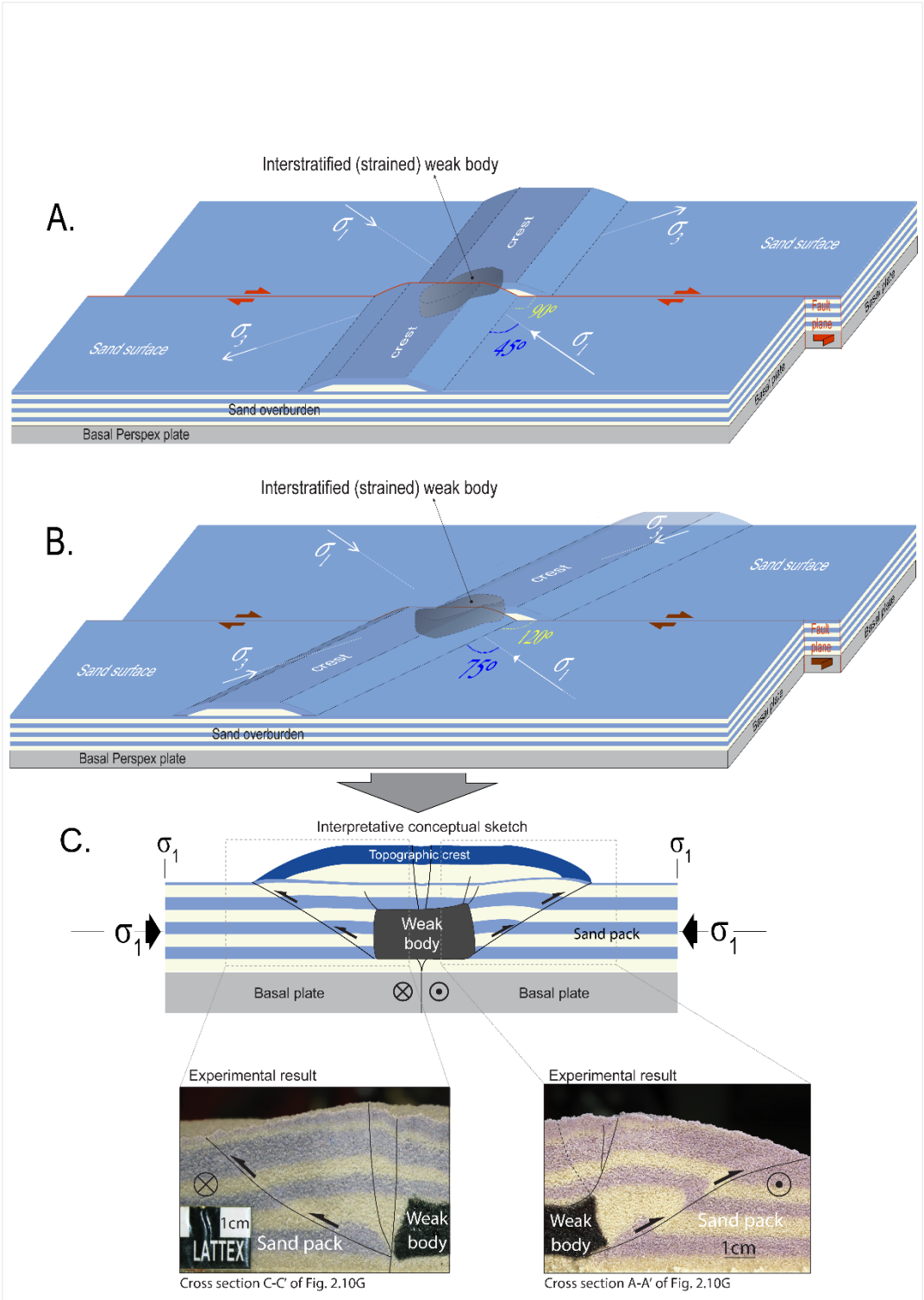

Figure 2.13 Schematic illustration of the combined effect exerted by both morphological and rheological obstacles/anisotropies on the formation and distribution of pop-up bounding reverse faults around opposite quarters of the viscous body anisotropy. **A**: Topographic crest at 90º from the basement fault trace and at 45º from σ_1. This more oblique disposition relatively to σ_1 is less prone to reverse-fault shortening accommodation. **B**: Topographic crest at 120º (clockwise) from the basement fault trace, and at 75º from σ_1. This more orthogonal disposition relatively to σ_1 favours reverse-fault shortening accommodation. **C**: Schematic cross section intersecting the viscous body anisotropy along σ_1, illustrating the nucleation of viscous body -bounding reverse faults at the sub-perpendicular sand-silicone contact interfaces. Zoomed photos show the correspondence with obtained experimental results.

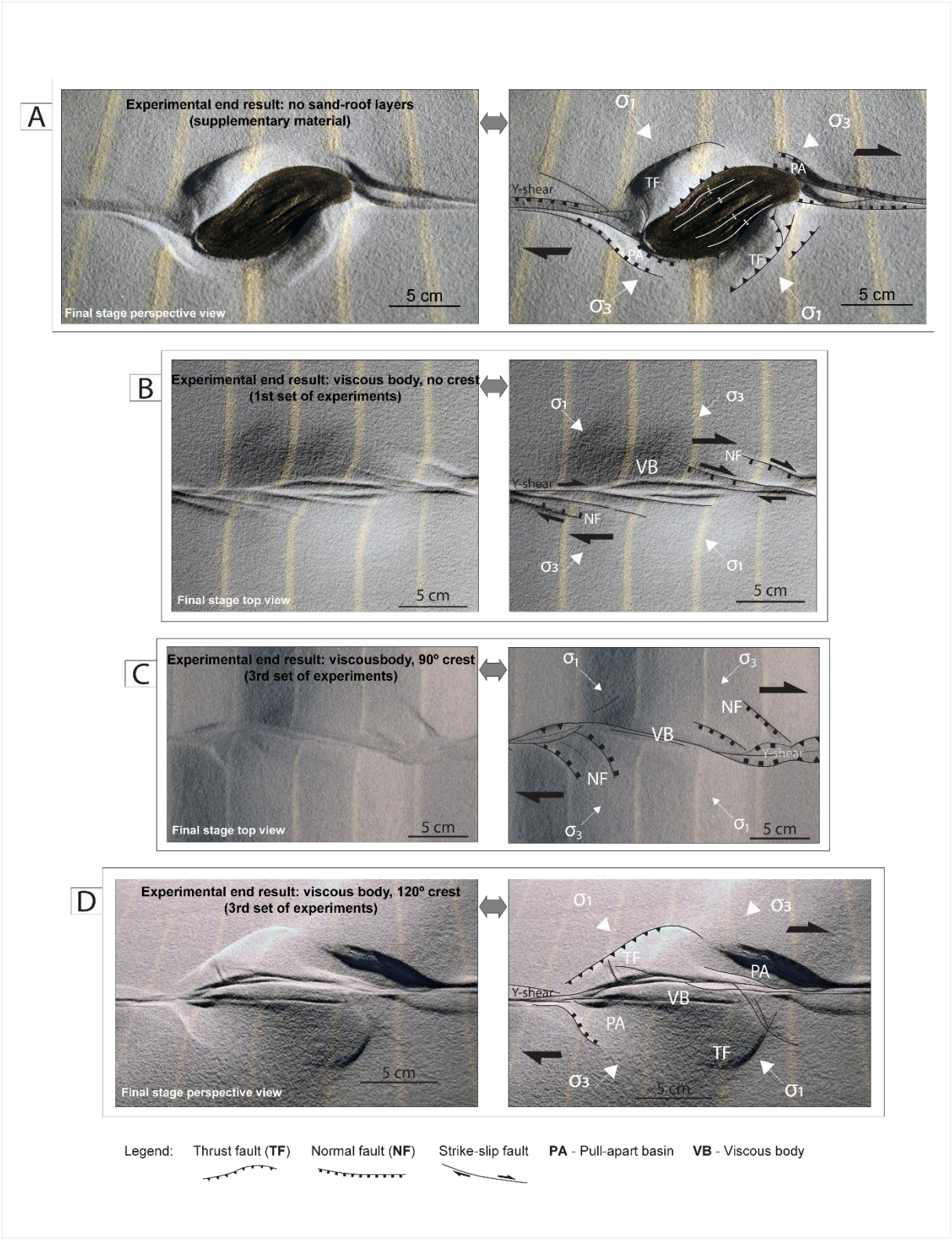

Figure 2.14. Comparative illustration of all end-stage experimental results with a prescribed viscous body anisotropy. A: supplementary experiment (see Fig. 2.18) without rooftop sand layers. B: interstratified viscous body (first set of experiments). C and D: interstratified viscous body, third set of experiments (90º and 120º angle topographic crest, respectively).

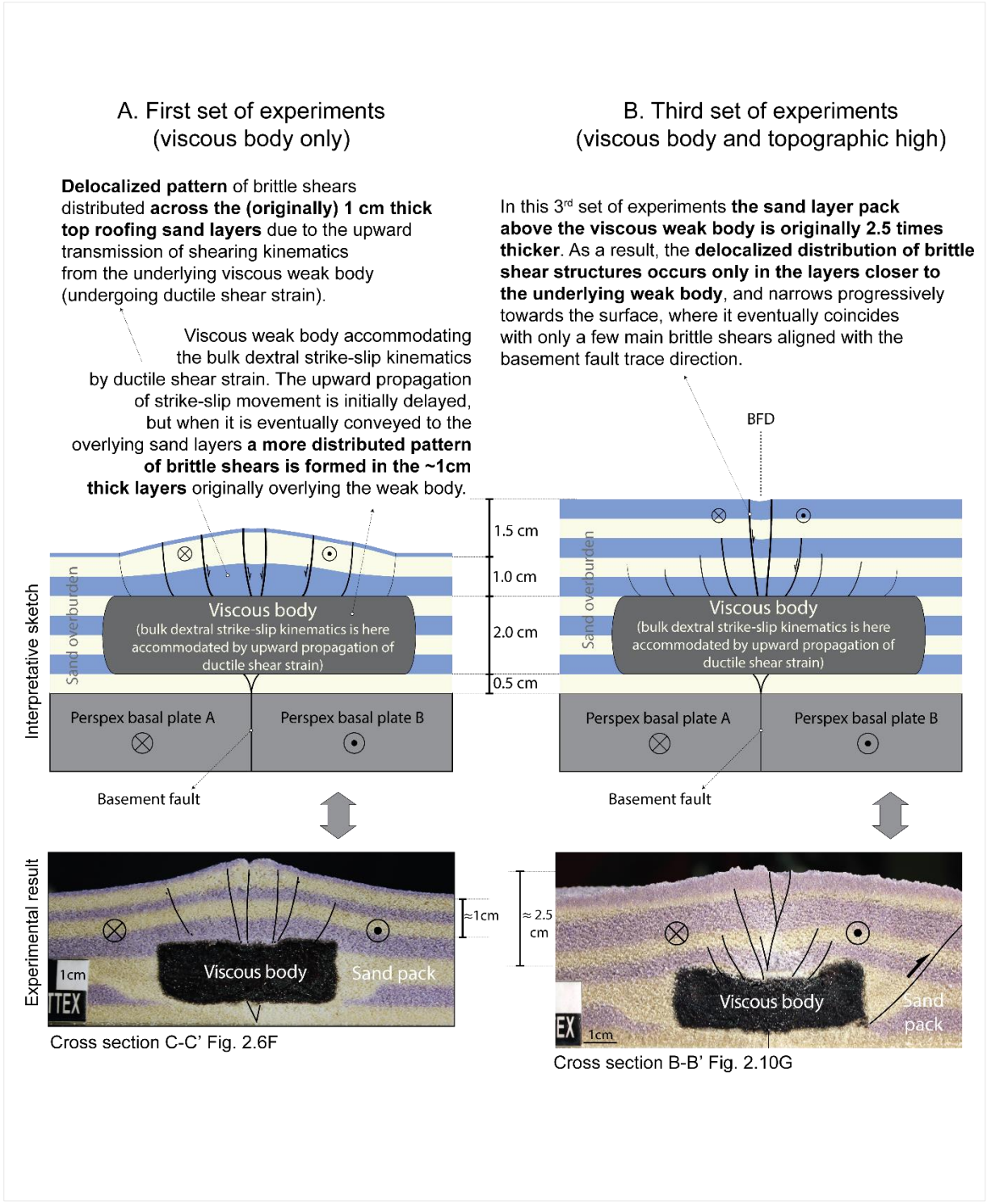

Figure 2.15 Schematic representation of the way through which different prescribed thicknesses for the model top sand layers (overlying the viscous weak body) are interpreted to determine either: more distributed (A), or more localized (B) near surface (brittle) shear patterns. A. First set of experiments: interstratified viscous body at ~1 cm depth. B. Third set of experiments - interstratified viscous body at a 2.5 higher depth (thicker sand-layered cover).

2.4.4. Natural examples

As explained above (section 2.1.2) the intent of the performed experiments was not to model a single specific natural example, but rather to conceptually investigate the way through which either a morphological obstacle (i.e. a topographic crest), or an interstratified viscous body (i.e. a viscous rheological anisotropy at depth), can modify the general upper crustal structural pattern resulting from a typical (brittle) strike-slip shear zone.

In nature there are several examples illustrating the segmentation of a strike-slip fault structural pattern caused by an intersecting viscous body anisotropy. In the West Portuguese Mesozoic Lusitanian basin (Vimeiro diapir, Chaminé *et al*., 2004), or in central and SW Iran (e.g. Jahani *et al*., 2017), several precursor salt diapirs are affected by strike-slip faults, exhibiting sigmoidal geometries (e.g. Great Kavir diapir - Fig. 2.16 A) complying with the morpho-structural configuration observed in the preformed experiments. The same geometry and implied structural pattern is also observed associated to pre-tectonic igneous intrusions (e.g. Teixeira batholith in NE Brazil, Archanjo *et al*., 2008 – Fig. 2.16 B). In other situations, it is also possible to recognize the modelled alternate distribution of compressive (pop-up bounding reverse faults) and extensional (pull-apart basins) structures around the viscous body anisotropy (see Fig. 2.14 D). This is the case of the Sedom diapir in the Dead Sea basin associated with the left-lateral transform system that separates the Arabian and African plates in the middle east region (e.g. Al-Zoubi *et al*., 2002; Larsen *et al*., 2002), although in this situation stress field modifications associated to rock volume accommodation changes (implied by the salt diapirism) might interfere with the otherwise "strictly tectonic" structures related to the strike-slip faulting (Alsop *et al*., 2018).

One of the most striking examples of the experimentally investigated (morphotectonic rheological) interference is illustrated by the tectonic-bathymetric configuration of a specific segment of the Eurasia–Nubia plate boundary in the NE Atlantic (Fig. 2.17, Batista *et al*., 2017; Neres *et al*., 2016; Omira *et al*., 2019; Rosas *et al*., 2014). Here, Azores-Gibraltar Fracture Zone (AGFZ extending from the Azores triple junction to the Gibraltar Straits - see inset of Fig. 2.17 A) crosscuts a major bathymetric crest that corresponds to a ~3800 m high submarine rise, extending along ~1000 km between the Madeira archipelago and the Tore seamount. This so-called Tore-Madeira Rise makes a ~120º (clockwise) angle with the major Gloria transform fault (Fig. 2.17 B), and in the intersection domain several active volcanic plugs (with reported isotopic ages locally varying between 16 and 0.5 My, Geldmacher *et al*., 2006; Grange *et al*., 2010; Merle *et al*., 2009) suggest the existence of one (or more) shallow upper crustal magma chambers. The observed natural morpho-structural pattern shows an obvious resemblance with the results obtained in the 120º third set of experiments (Fig. 2.17 C – left), with similar opposite quarter distribution of shortening vs. extensional structures subperpendicular to the σ_1 and σ_3 principal stress directions, respectively (as implied by the regional dextral strike-slip regime). The comparison of this same morpho-structural pattern with the second set of experiments (absence of viscous body, Fig. 2.17 C – right) also shows the formation of a major single fault developing across the crest in both model and natural example. However, the distribution of bounding thrust and normal faults along alternate shortening and extensional quarters is absent in the case of these experiments, illustrating the probable role of a shallow (upper crustal) viscous anomaly in the formation of the observed natural morpho-tectonic pattern in this specific domain.

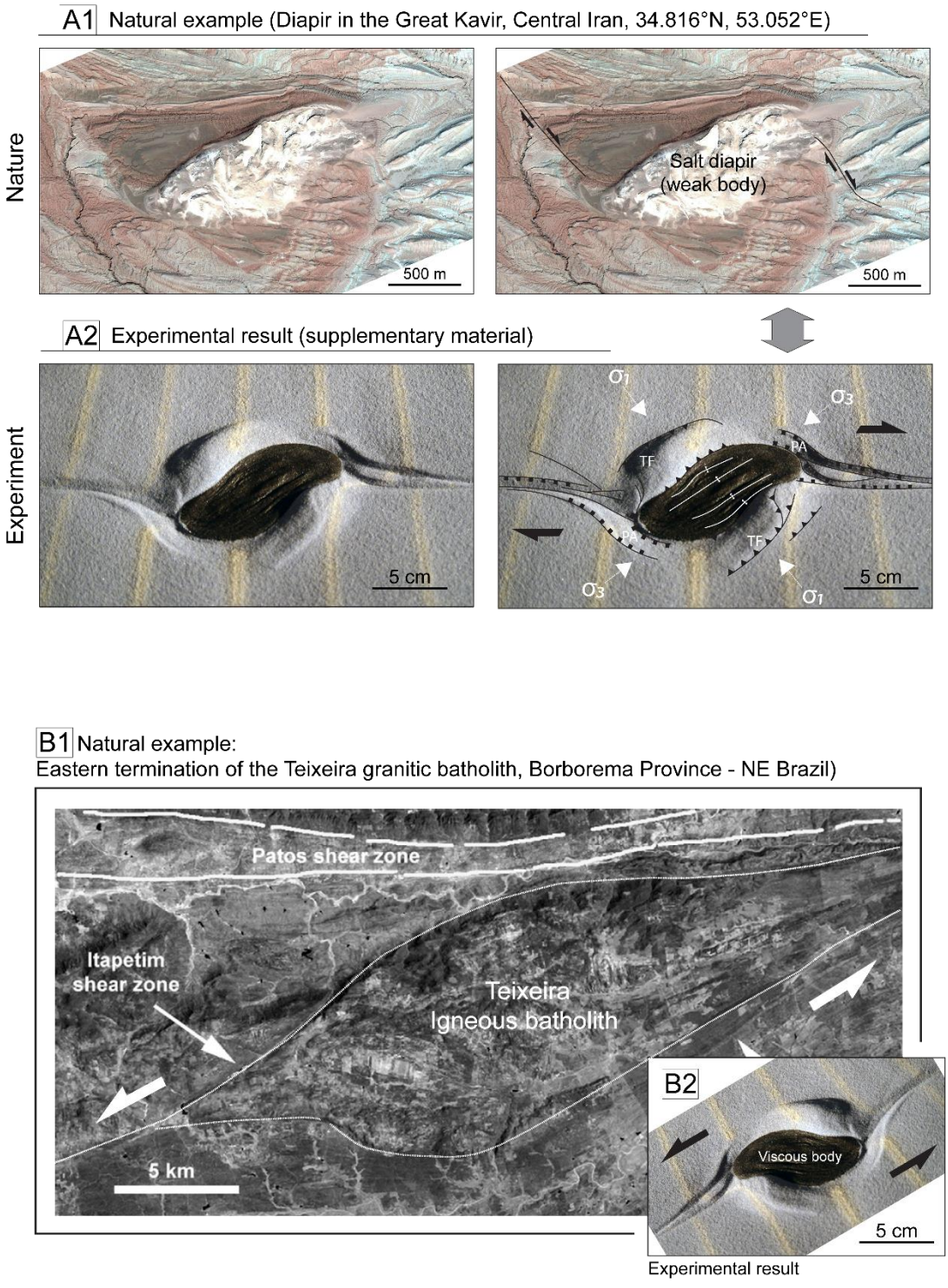

Figure 2.16. Examples of the natural structural interference between major (upper-crustal) strike-slip faults and: (A) precursor salt-diapir (Great Kavir Diapir, Central Iran, 34.816°N, 53.052°E, aerial photo from Google Earth, adapted from Dooley and Schreurs, 2012); (B) pre-tectonic batholitic igneous intrusion (Teixeira granitic batholith, Borborena Province – NE Brazil, adapted from Archanjo *et al*., 2008).

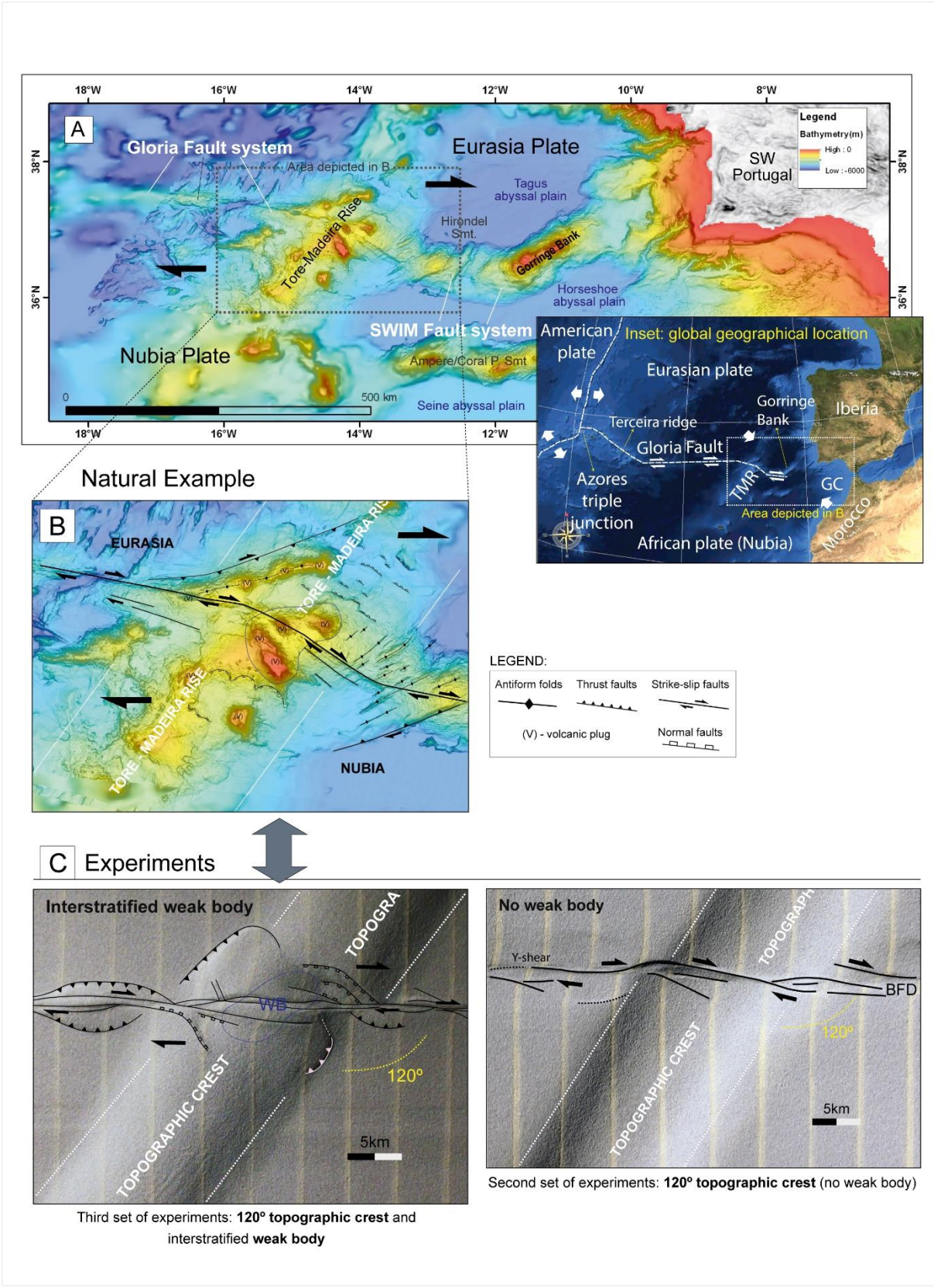

Figure 2.17. A: General tectonic setting of the dextral transcurrent Eurasia - Nubia plate boundary in the NE Atlantic (see low-right inset for geographical location). B: Morphotectonic setting of the Tore-Madeira vs. Gloria Fault interference area. C: Obtained experimental results for comparison with the natural example. Left: third set of experiments (viscous anomaly and 120º crest); Right: second set of experiments (120º crest, no viscous anomaly). GC – Gulf of Cadiz; TMR – Tore-Madeira Rise; SWIM – SW Iberian Margin fault-system; WB – Viscous body; BFD - Basement fault direction. Bathymetry from GEBCO (General Bathymetric Chart of the Oceans).

2.5. Conclusions

The following main conclusions can be drawn from the obtained experimental results:

1) The typical structural pattern of an upper crustal shear zone accommodating wrenching deformation in a brittle overburden atop a basement strike-slip fault can be significantly modified by both rheological and/or morphological major crustal heterogeneties (interstratified viscous bodies, and/or topographic crests, respectively).

2) The mechanical control exerted by a pre-tectonic viscous rheological anomaly (e.g. a salt bed/diapir or a cooling magma chamber) interstratified in the brittle cover sediments can be envisaged as the result of two main causes:

   - The different accommodation response of the (brittle-viscous-brittle) rheologically stratified medium to the upward propagation of the wrenching deformation above the basement strike-slip fault. This difference is essentially determined by a viscous delay effect caused the silicone body, contrasting with the brittle behaviour of the confining upper crustal sediments that transmit stress much more efficiently and yield according with the Mohr-Coulomb criteria.

   - The consequences of this different mechanical response, not only in the vertical direction (i.e. across the thickness of the mechanically stratified upper crust), but also along the horizontal one (i.e. across the sub-vertical sand-silicone rheology boundaries representing the lateral contact surfaces between the upper crustal sediments and the viscous body).

3) The first cause mentioned in the point above explains the delay in the upward propagation of the deformation across the viscous anomaly, leading initially to a segmentation of the main brittle shear zone at the surface of the model (with no brittle structures breaching across the area above the viscous anomaly), and later evolving to a more distributed pattern of smaller low angle synthetic shears.

4) The second cause mentioned in point 2 above explains the distribution of pop-up versus pull-apart basins around opposite quarters of the viscous body anisotropy, along the alternating compressive and extensional quadrants implied by the bulk non-coaxial (brittle) shear deformation.

5) The perturbation of the structural pattern typical of an upper crust brittle shear zone can also occur due to a strictly morphological anomaly (a topographic crest intersecting the main shear zone with different orientations) and is essentially determined by a thickness scaling effect. Accordingly, fewer longer LAS and Riedel shears are preferably formed above the thicker domains that correspond to the topographic highs, comparatively with the more pervasive distribution of relatively shorter shears in the domains of normal thickness.

6) A combined morphological and rheological effect is also shown to significantly modify the main strike-slip shear pattern, since the geometrical (spatial) coincidence of sub-vertical rheological boundaries with abrupt surface morphological steps (displaying a favoured orientation relatively to the principal horizontal stress directions) both concur to localize strain along such morpho-rheological boundaries, promoting nucleation of upper crustal brittle structures at these sites.

7) The main (geo)mechanical processes (referred to above) unveiled by the carried-out experiments are seemingly recognized in different natural examples, in which analogue

structural distribution patterns and resulting tectonic configurations are coherent with experimental results.

Acknowledgments

This work was sponsored by the Fundação para a Ciência e a Tecnologia (FCT) through project UID/GEO/50019/2013-IDL and project SPIDER - PTDC/GEO-FIQ/2590/2014. Jaime Almeida acknowledges a Ph.D. grant by Lisbon Earth-Systems Doctoral School ref: PD/BD/135067/2017. A. Simões and M. Roque are acknowledged for helping with lab work.

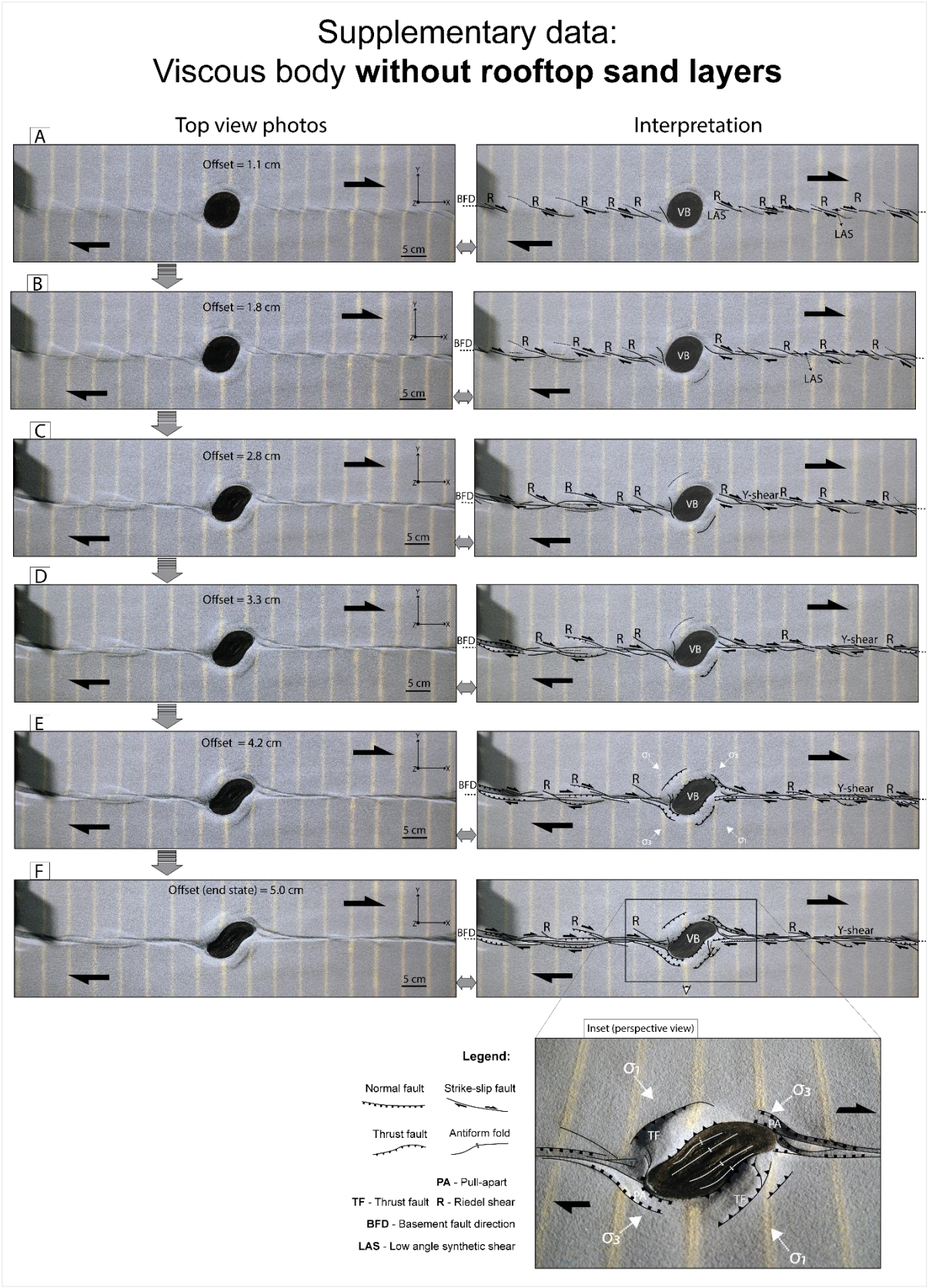

Figure 2.18. Results of the supplementary set of experiments: viscous anisotropy without sand overburden (see also movie MSupp.mp4 in the repository). A to F: Successive XY top view photographs (left column) and corresponding line drawing interpretations (right column) obtained for different increasing amounts of bulk strike-slip offset along the basement fault. Inset: end stage perspective view of the detailed distribution of pull-apart basins (PA) vs. thrust faults (TF) around opposite quarters (tensile and compressive, respectively) of the viscous body anisotropy.

2.6. Appendix A. Scaling

The scaling theory of Hubbert (1937) contends that dynamic scaling is only achieved when model/natural prototype ratios are independently established for the three fundamental units of length (*L*), time (*T*) and mass (*M*). In the present experiments the length ratio (λ) resulted directedly from considering model dimensions relatively to nature (e.g. a sandpack thickness of 3.5 cm in the model corresponding to 10 km of upper crust thickness in nature see Table 2.2) giving:

$$\lambda = L_m/L_n = 3.5 \times 10^{-6} \qquad (2.1)$$

(in which *L* is the length, *m* and *n* refer to model and nature, respectively)

The mass ratio (μ) was obtained from the model/nature ratio for density (δ), using the known densities of the employed viscous and frictional materials (PDMS and sand, see Tables 2.1 and 2.2) and the density ascribed to the considered crustal viscous anomaly (within the interval of densities considered for salt diapirs or acidic magmas, see Table 2.2). In accordance, the obtained density ratio was:

$$\delta = D_m/D_n = 0.62 \qquad (2.2)$$

(in which *D* is the density)

and since

$$\delta = \mu/\lambda^3 \qquad (2.3)$$

the mass ratio (μ) was readily obtained by using the values of λ and δ (calculated above in equations 2.1 and 2.2, respectively) in equation 2.3:

$$\mu = M_m/M_n = 2.6 \times 10^{-17} \qquad (2.4)$$

(in which *M* is the mass).

Proper tuning of model/nature density ratio was achieved by altering the PDMS density from 965 kg/m^3 to 1350 kg/m^3 by means of mixing this silicone putty with Wolframite powder in adequate proportion (less than ca. 6% of the total volume of the silicone body corresponding to ca. 31% of its total mass).

The time ratio (τ) was calculated from the viscosity ratio (ψ) between the PDMS and the considered viscous crustal anisotropy (see values in Table 2.2):

$$\psi = \eta_m/\eta_n = 2.5 \times 10^{-13} \qquad (2.5)$$

(in which η is the viscosity)

Note that in the present case inertial accelerations are considered negligible when compared with the acceleration of gravity (g), since the former correspond to tectonic movements in the order of a few centimetres per year (i.e. n x 10^{-9} m/s) varying significantly only along millions of years (n x 10^{13} s), and thus, are at least 22 orders of magnitude lower than the latter (g $\approx$ 10 m/s^2). As a consequence, the acceleration ratio (γ) can be simplified as being equal to the gravity acceleration ratio (γ_g):

$$\gamma = \gamma_g = \frac{g_m}{g_n} = 1 \qquad (2.6)$$

and thus, the viscosity ratio corresponding to:

$$\psi = \frac{\mu.\gamma.\tau}{\lambda^2} = \frac{\mu.\gamma.\tau.\lambda}{\lambda^2.\lambda} = \delta.\gamma.\tau.\lambda \quad (2.7)$$

can be defined as:

$$\psi = \delta.\tau.\lambda \quad (2.8)$$

(by substituting the value of γ from equation 2.6 in equation 2.7).

Finally, by substituting in equation A8 the values of λ, δ and ψ from equations 2.1, 2.2 and 2.5 respectively, the time ratio (τ) is readily obtained:

$$\tau = \frac{T_m}{T_n} = 1.2 \times 10^{-7} \quad (2.9)$$

(in which *T* is the time).

Material properties and scaling parameter	Quartz sand * (model)	Upper crust (nature)	Ratio: model/nature
Grain shape	Well-rounded	-	-
Grain size (mm)	< 0.30	-	-
Density (kg/m^3)	1600	2600	δ=0.62
Internal friction angle f (º)	~ 30	-	-
Coefficient of internal friction, μ_c	~ 0.6	0.6 – 0.85	-
Cohesion, C_0 (Pa)	Negligible (~100)	40x10^6	-
Gravity acceleration (m/s^2)	9.81	9.81	γ_g=1
Length, L (m)	0.35 (3.5 cm)	10^3 (10 km)	**λ=3.5x10^{-6}**
Mass, M (kg)	-	-	**μ=2.6x10^{-17}**
Time, T (s)	3.7x10^4 (~10 hrs)	3.2x10^{13} (~1 Myrs)	**τ =1.2x10^{-9}**

Table 2.1 - Analogue modelling material properties and scaling: upper crust. Scaled fundamental units are in bold. A mean cohesion of C_0=40 MPa was assumed for the natural prototype (e.g. Weijermars *et al.*, 1993). *Sand used in our models is SIFRACO NE34 (see supplementary data of Rosas *et al.*, 2017 for detailed sand properties).

Material properties and scaling parameter	PDMS - SGM 36 (model)	Viscous anisotropy (nature)	Ratio: model/nature
Density (kg/m^3)	1350*	2200	δ=0.62
Viscosity (Pa.s)	2.5x10^4	10^{17}	ψ=2.5x10^{-13}
Gravity acceleration (m/s^2)	9.81	9.81	γ_g=1
Length, L (m)	0.35 (3.5cm)	10^3 (10 km)	**λ=3.5x10^{-6}**
Mass, M (kg)	-	-	**μ=2.6x10^{-17}**
Time, T (s)	3.6x10^3 (1hrs)	3.1x10^{10} (~1Kyrs)	**τ =1.2x10^{-7}**

Table 2.2 - Analogue modelling material properties and scaling: crustal viscous anisotropy. Scaled fundamental units are in bold.* Mixed with Wolframite powder (original density of the PDMS-SGM 36 is 965 kg/m3)

Table 3 –

	90º to the BFD		120º to the BFD	
	Normal height	Crest	Normal height	Crest
Thickness (cm)	3.5	5.0	3.5	5.0
SZ width (cm)	4.4	5.5	6.7	7.9
Length of 1st R-fault (cm)	5.0	6.0	5.3	7.0
R1 = SZ width / Thickness	1.3	1.1	1.9	1.6
R2 = 1st R-fault / Thickness	1.4	1.2	1.5	1.4

Table 2.3 - Naylor's *et al*. (1986) empirical parameters obtained for the 2nd set of experiments. Note that accordingly with Naylor's *et al*. (1986) proposal: R1 ≈ 1 and R2 ≈ 1.6

3. References

Al-Zoubi, A., Shulman, H. and Ben-Avraham, Z. (2002) 'Seismic reflection profiles across the southern Dead Sea basin', *Tectonophysics*, 346(1–2), pp. 61–69. doi: 10.1016/S0040-1951(01)00228-1.

Alsop, G. I. *et al.* (2018) 'Fault and fracture patterns around a strike-slip influenced salt wall', *Journal of Structural Geology*. Elsevier, 106(November 2017), pp. 103–124. doi: 10.1016/j.jsg.2017.10.010.

An, L.-J. and Sammis, C. G. (1996) 'Development of strike-slip faults: shear experiments in granular materials and clay using a new technique', *Journal of Structural Geology*. Pergamon, 18(8), pp. 1061–1077. doi: 10.1016/0191-8141(96)00012-0.

Archanjo, C. J. *et al.* (2008) 'Fabrics of pre- and syntectonic granite plutons and chronology of shear zones in the Eastern Borborema Province, NE Brazil', *Journal of Structural Geology*, 30(3), pp. 310–326. doi: 10.1016/j.jsg.2007.11.011.

Atmaoui, N. *et al.* (2006) 'Initiation and development of pull-apart basins with Riedel shear mechanism: Insights from scaled clay experiments', *International Journal of Earth Sciences*, 95(2), pp. 225–238. doi: 10.1007/s00531-005-0030-1.

Batista, L. *et al.* (2017) 'Crustal structure of the Eurasia–Africa plate boundary across the Gloria Fault, North Atlantic Ocean', *Geophysical Journal International*, 209(2), pp. 713–729. doi: 10.1093/gji/ggx050.

Benes, V. and Davy, P. (1996) 'Modes of continental lithospheric extension: experimental verification of strain localization processes', *Tectonophysics*. Elsevier, 254(1–2), pp. 69–87. doi: 10.1016/0040-1951(95)00076-3.

Bernard, S. *et al.* (2007) 'Kinematics of fault-related folding derived from a sandbox experiment', *Journal of Geophysical Research*. John Wiley & Sons, Ltd, 112(B3), p. B03S12. doi: 10.1029/2005JB004149.

Bolacha, E. (2014) *Modelos de dinâmica da Terra aplicados à geologia de Portuga l: relevância da experimentação análoga no ensino e na divulgação da geologia*. Lisboa. Available at: http://hdl.handle.net/10451/10964.

Burliga, S., Koyi, H. A. and Chemia, Z. (2012) 'Analogue and numerical modelling of salt supply to a diapiric structure rising above an active basement fault', *Geological Society, London, Special Publications*, 363(1), pp. 395–408. doi: 10.1144/SP363.18.

Cadell, H. M. (1889) 'VII.—Experimental Researches in Mountain Building.', *Transactions of the Royal Society of Edinburgh*, 35(01), pp. 337–357. doi: 10.1017/S0080456800017658.

Casas, A. M. *et al.* (2001) 'Analogue models of transpressive systems', *Journal of Structural Geology*, 23(5), pp. 733–743. doi: 10.1016/S0191-8141(00)00153-X.

Ceriani, S., Mancktelow, N. S. and Pennacchioni, G. (2003) 'Analogue modelling of the influence of shape and particle/matrix interface lubrication on the rotational behaviour of rigid particles in simple shear', *Journal of Structural Geology*. Pergamon, 25(12), pp. 2005–2021. doi: 10.1016/S0191-8141(03)00098-1.

Chaminé, H. I. *et al.* (2004) 'Diapiric geometry, kinematics and dynamics of Vimeiro morphostructure (Torres Vedras, central Portugal): implications for a hydrogeological model', *CADERNOS DO LABORATORIO XEOLÓXICO DE LAXE*, 29, pp. 11–30.

Cloos, H. (1928) 'Experimente zur inneren Tektonik', *Centralblatt für Mineral. Geol. und Paläontol.*, (12), pp. 609–621.

Cloos, H. (1929) 'Künstliche Gebirge', *Natur und Museum. Senckenbergische Naturforschende*

Gesellschaft, (5), pp. 225–243.

Cloos, H. (1930) 'Zur experimentellen Tektonik - Methodik und Beispiele', *Die Naturwissenschaften*, 18(34), pp. 741–747. doi: 10.1007/BF01493341.

Cobbold, P. R. and Quinquis, H. (1980) 'Development of sheath folds in shear regimes', *Journal of Structural Geology*. Pergamon, 2(1–2), pp. 119–126. doi: 10.1016/0191-8141(80)90041-3.

Corti, G. *et al.* (2003) 'Analogue modelling of continental extension: a review focused on the relations between the patterns of deformation and the presence of magma', *Earth-Science Reviews*. Elsevier, 63(3–4), pp. 169–247. doi: 10.1016/S0012-8252(03)00035-7.

Corti, G. (2008) 'Control of rift obliquity on the evolution and segmentation of the main Ethiopian rift', *Nature Geoscience*. Nature Publishing Group, 1(4), pp. 258–262. doi: 10.1038/ngeo160.

Corti, G., Moratti, G. and Sani, F. (2005) 'Relations between surface faulting and granite intrusions in analogue models of strike-slip deformation', *Journal of Structural Geology*, 27(9), pp. 1547–1562. doi: 10.1016/j.jsg.2005.05.011.

Crave, A. *et al.* (2000) 'Analogue modelling of relief dynamics', *Physics and Chemistry of the Earth, Part A: Solid Earth and Geodesy*. Pergamon, 25(6–7), pp. 549–553. doi: 10.1016/S1464-1895(00)00084-3.

Cunningham, W. D. and Mann, P. (2007) 'Tectonics of strike-slip restraining and releasing bends', *Geological Society, London, Special Publications*, 290(1), pp. 1–12. doi: 10.1144/SP290.1.

Daubrée, A. (1879) *Etudes synthétiques de géologie expérimentale*. Paris: Dunod.

Dauteuil, O. and Mart, Y. (1998) 'Analogue modeling of faulting pattern, ductile deformation, and vertical motion in strike-slip fault zones', *Tectonics*, p. 303. doi: 10.1029/97TC03410.

Davis, D., Suppe, J. and Dahlen, F. A. (1983) 'Mechanics of fold-and-thrust belts and accretionary wedges', *Journal of Geophysical Research*, 88(B2), p. 1153. doi: 10.1029/JB088iB02p01153.

Davy, P. and Cobbold, P. R. (1991) 'Experiments on shortening of a 4-layer model of the continental lithosphere', *Tectonophysics*. Elsevier, 188(1–2), pp. 1–25. doi: 10.1016/0040-1951(91)90311-F.

Dixon, J. M. (1974) 'A new method of determining finite strain in models of geological structures', *Tectonophysics*. Elsevier, 24(1–2), pp. 99–114. doi: 10.1016/0040-1951(74)90132-2.

Dixon, J. M. (1975) 'Finite strain and progressive deformation in models of diapiric structures', *Tectonophysics*. Elsevier, 28(1–2), pp. 89–124. doi: 10.1016/0040-1951(75)90060-8.

Dixon, J. M. and Liu, S. (1992) 'Centrifuge modelling of the propagation of thrust faults', in *Thrust Tectonics*. Dordrecht: Springer Netherlands, pp. 53–69. doi: 10.1007/978-94-011-3066-0_5.

Donnadieu, F. *et al.* (2003) 'Digital photogrammetry as a tool in analogue modelling: applications to volcano instability', *Journal of Volcanology and Geothermal Research*. Elsevier, 123(1–2), pp. 161–180. doi: 10.1016/S0377-0273(03)00034-9.

Donnadieu, F. and Merle, O. (1998) 'Experiments on the indentation process during cryptodome intrusions: New insights into Mount St. Helens deformation', *Geology*. GeoScienceWorld, 26(1), p. 79. doi: 10.1130/0091-7613(1998)026<0079:EOTIPD>2.3.CO;2.

Dooley, T. P. and Schreurs, G. (2012) 'Analogue modelling of intraplate strike-slip tectonics: A review and new experimental results', *Tectonophysics*. Elsevier, 574–575, pp. 1–71. doi: 10.1016/j.tecto.2012.05.030.

Duarte, J. C. *et al.* (2011) 'Thrust–wrench interference tectonics in the Gulf of Cadiz (Africa–Iberia plate boundary in the North-East Atlantic): Insights from analog models', *Marine Geology*. Elsevier, 289(1–4), pp. 135–149. doi: 10.1016/J.MARGEO.2011.09.014.

Duarte, J. C., Schellart, W. P. and Cruden, A. R. (2013) 'Three-dimensional dynamic laboratory models of subduction with an overriding plate and variable interplate rheology', *Geophysical Journal International*. Oxford University Press, 195(1), pp. 47–66. doi: 10.1093/gji/ggt257.

Edwards, S. J., Schellart, W. P. and Duarte, J. C. (2015) 'Geodynamic models of continental subduction and obduction of overriding plate forearc oceanic lithosphere on top of continental crust', *Tectonics*, 34(7), pp. 1494–1515. doi: 10.1002/2015TC003884.

Ellis, S., Schreurs, G. and Panien, M. (2004) 'Comparisons between analogue and numerical models of thrust wedge development', *Journal of Structural Geology*, 26(9), pp. 1659–1675. doi: 10.1016/j.jsg.2004.02.012.

Emmons, R. C. (1969) 'Strike-slip rupture patterns in sand models', *Tectonophysics*, 7(1), pp. 71–87. doi: 10.1016/0040-1951(69)90065-1.

Escher, B.G. ; Kuenen, P. H. (1928) 'Experiments in connection with Salt Domes', *Leidse Geologische Mededelingen*. Geologisch en Mineralogisch Instituut der Rijksuniversiteit te Leiden, 3(1), pp. 151–182. Available at: http://repository.naturalis.nl/record/505826 (Accessed: 6 February 2019).

Favre, A. (1878) 'Expériences sur les effets des refoulements ou écrasements latéraux en géologie', in *Archives des sciences physiques et naturelles*. T. 62. Genève: Biliothèque Universelle, pp. 193–211. Available at: https://www.e-periodica.ch/digbib/view?pid=bsv-002:1884:20#3.

Geldmacher, J. *et al.* (2006) 'Origin and geochemical evolution of the Madeira-Tore Rise (eastern North Atlantic)', *Journal of Geophysical Research: Solid Earth*, 111(9). doi: 10.1029/2005JB003931.

Ghosh, S. K. and Ramberg, H. (1976) 'Reorientation of inclusions by combination of pure shear and simple shear', *Tectonophysics*. Elsevier, 34(1–2), pp. 1–70. doi: 10.1016/0040-1951(76)90176-1.

Grange, M. *et al.* (2010) 'Plume-lithosphere interaction during migration of cretaceous alkaline magmatism in SW Portugal: Evidence from U-Pb Ages and Pb-Sr-Hf isotopes', *Journal of Petrology*, 51(5), pp. 1143–1170. doi: 10.1093/petrology/egq018.

Graveleau, F. *et al.* (2015) 'Experimental modelling of tectonics–erosion–sedimentation interactions in compressional, extensional, and strike–slip settings', *Geomorphology*. Elsevier, 244, pp. 146–168. doi: 10.1016/J.GEOMORPH.2015.02.011.

Graveleau, F. and Dominguez, S. (2008) 'Analogue modelling of the interaction between tectonics, erosion and sedimentation in foreland thrust belts', *Comptes Rendus Geoscience*. Elsevier Masson, 340(5), pp. 324–333. doi: 10.1016/J.CRTE.2008.01.005.

Griffiths, R. W. and Campbell, I. H. (1990) 'Stirring and structure in mantle starting plumes', *Earth and Planetary Science Letters*. Elsevier, 99(1–2), pp. 66–78. doi: 10.1016/0012-821X(90)90071-5.

Grujic, D. and Mancktelow, N. S. (1998) 'Melt-bearing shear zones: analogue experiments and comparison with examples from southern Madagascar', *Journal of Structural Geology*. Pergamon, 20(6), pp. 673–680. doi: 10.1016/S0191-8141(98)00006-6.

Le Guerroué, E. and Cobbold, P. R. (2006) 'Influence of erosion and sedimentation on strike-slip fault systems: insights from analogue models', *Journal of Structural Geology*, 28(3), pp. 421–430. doi: 10.1016/j.jsg.2005.11.007.

Gutscher, M.-A. *et al.* (1998) 'Episodic imbricate thrusting and underthrusting: Analog experiments and mechanical analysis applied to the Alaskan Accretionary Wedge', *Journal of Geophysical Research: Solid Earth*. John Wiley & Sons, Ltd, 103(B5), pp. 10161–10176. doi: 10.1029/97JB03541.

Hall, J. (1805) 'III. Experiments on Whinstone and Lava', *Transactions of the Royal Society of Edinburgh*. Royal Society of Edinburgh Scotland Foundation, 5(01), pp. 43–75. doi: 10.1017/S0080456800008449.

Hall, J. (1815) 'II. On the Vertical Position and Convolutions of certain Strata, and their relation with

Granite', *Transactions of the Royal Society of Edinburgh*, 7(01), pp. 79–108. doi: 10.1017/S0080456800019268.

Holohan, E. P., Van Wyk de Vries, B. and Troll, V. R. (2008) 'Analogue models of caldera collapse in strike-slip tectonic regimes', *Bulletin of Volcanology*, 70(7), pp. 773–796. doi: 10.1007/s00445-007-0166-x.

Horsfield, W. T. (1977) 'An experimental approach to basement-controlled faulting.', *Geologie en Mijnbouw*, 56(4), pp. 363–370. Available at: https://www.researchgate.net/publication/27710982_An_experimental_approach_to_basement-controlled_faulting_Geologie_En_Mijnboyw.

Hubbert, M. K. (1937) 'Theory of scale models as applied to the study of geologic structures', *Geological Society of America Bulletin*, 48(10), pp. 1459–1520. doi: 10.1130/GSAB-48-1459.

Hubbert, M. K. (1951) 'Mechanical basis for certain familiar geologic structures.', *Geological Society of America Bulletin*. GeoScienceWorld, 62(4), pp. 355–372. doi: 10.1130/0016-7606(1951)62[355:mbfcfg]2.0.co;2.

Hutton, J. (1785) 'Abstract of a Dissertation Read in the Royal Society of Edinburgh, upon the Seventh of March, and Fourth of April, MDCCLXXXV, Concerning the System of the Earth, its Duration, and Stability.', *Royal Society of Edinburgh*, p. 30.

Hutton, J. (1788) 'Theory of the Earth;or an investigation of the laws observable in the composition, dissolution, and restoration of land upon the globe', *Transactions of the Royal Society of Edinburgh*, (1), pp. 209–304. doi: 10.1017/S0080456800029227.

Hutton, J. (1795) *Theory of the Earth, with Proofs and Illustrations, Vols I & II*. Edinburgh: Cadell & Davies.

Ildefonse, B., Sokoutis, D. and Mancktelow, N. S. (1992) 'Mechanical interactions between rigid particles in a deforming ductile matrix. Analogue experiments in simple shear flow', *Journal of Structural Geology*. Pergamon, 14(10), pp. 1253–1266. doi: 10.1016/0191-8141(92)90074-7.

Jackson, M. P. A. (1988) *Centrifuge modeling of the effects of aggradation and progradation on syndepositional salt structures /*. Austin, Tex. : Bureau of Economic Geology, University of Texas at Austin,. Available at: https://searchworks.stanford.edu/view/229131 (Accessed: 8 February 2019).

Jacoby, W. R. (1973) 'Model Experiment of Plate Movements', *Nature Physical Science*, 242(122), pp. 130–134. doi: 10.1038/physci242130a0.

Jacoby, W. R. (1976) 'Paraffin model experiment of plate tectonics', *Tectonophysics*. Elsevier, 35(1–3), pp. 103–113. doi: 10.1016/0040-1951(76)90031-7.

Jahani, S. *et al.* (2017) 'Salt tectonics and tear faulting in the central part of the Zagros Fold-Thrust Belt, Iran', *Marine and Petroleum Geology*. Elsevier Ltd, 86, pp. 426–446. doi: 10.1016/j.marpetgeo.2017.06.003.

Keep, M. and McClay, K. R. (1997) 'Analogue modelling of multiphase rift systems', *Tectonophysics*. Elsevier, 273(3–4), pp. 239–270. doi: 10.1016/S0040-1951(96)00272-7.

Keppler, R., Rosas, F. and Nagel, T. (2013) 'Thin viscous middle-crust and evolving fault distribution during continental rifting: Insights from analog modeling experiments', *Tectonophysics*. Elsevier B.V., 608, pp. 161–175. doi: 10.1016/j.tecto.2013.10.001.

Kincaid, C. and Griffiths, R. W. (2004) 'Variability in flow and temperatures within mantle subduction zones', *Geochemistry, Geophysics, Geosystems*. John Wiley & Sons, Ltd, 5(6). doi: 10.1029/2003GC000666.

Klinkmüller, M. *et al.* (2016) 'Properties of granular analogue model materials: A community wide survey', *Tectonophysics*. Elsevier B.V., 684, pp. 23–38. doi: 10.1016/j.tecto.2016.01.017.

Koenigsberger, J. and Morath, O. (1913) 'Theoretische Grundlagen der experimentellen Tektonik.', *Zeitschrift der Deutschen Geologischen Gesellschaft*. Schweizerbart'sche Verlagsbuchhandlung, (65), pp. 65–86. Available at: https://www.schweizerbart.de/papers/zdgg_alt/detail/65/67110/Theoretische_Grundlagen_der_experimentellen_Tektonik.

Koyi, H. (1997) 'ANALOGUE MODELLING: FROM A QUALITATIVE TO A QUANTITATIVE TECHNIQUE — A HISTORICAL OUTLINE', *Journal of Petroleum Geology*, 20(2), pp. 223–238. doi: 10.1111/j.1747-5457.1997.tb00774.x.

Koyi, H. A. (2001) 'Modeling the influence of sinking anhydrite blocks on salt diapirs targeted for hazardous waste disposal', *Geology*, 29(5), p. 387. doi: 10.1130/0091-7613(2001)029<0387:MTIOSA>2.0.CO;2.

Koyi, H. A. *et al.* (2008) 'The mechanical relationship between strike-slip faults and salt diapirs in the Zagros fold-thrust belt', *Journal of the Geological Society*, 165(6), pp. 1031–1044. doi: 10.1144/0016-76492007-142.

Koyi, H., Talbot, C. J. and Tørudbakken, B. O. (1993) 'Salt diapirs of the southwest Nordkapp Basin: analogue modelling', *Tectonophysics*. Elsevier, 228(3–4), pp. 167–187. doi: 10.1016/0040-1951(93)90339-L.

Krantz, R. W. (1991) 'Measurements of friction coefficients and cohesion for faulting and fault reactivation in laboratory models using sand and sand mixtures', *Tectonophysics*. Elsevier, 188(1–2), pp. 203–207. doi: 10.1016/0040-1951(91)90323-K.

Larsen, B. D., Ben-Avraham, Z. and Shulman, H. (2002) 'Fault and salt tectonics in the southern Dead Sea basin', *Tectonophysics*, 346(1–2), pp. 71–90. doi: 10.1016/S0040-1951(01)00229-3.

Letouzey, J. and Sherkati, S. (2004) 'Salt Movement, Tectonic Events, and Structural Style in the Central Zagros Fold and Thrust Belt (Iran)', in *Salt Sediment Interactions and Hydrocarbon Prospectivity: Concepts, Applications, and Case Studies for the 21st Century: 24th Annual*. SOCIETY OF ECONOMIC PALEONTOLOGISTS AND MINERALOGISTS, pp. 753–778. doi: 10.5724/gcs.04.24.0753.

Link, T. A. (1930) 'Experiments Relating to Salt-Dome Structures', *AAPG Bulletin*. American Association of Petroleum Geologists, 14(4), pp. 483–508. Available at: http://archives.datapages.com/data/bulletns/1917-30/data/pg/0014/0004/0450/0483.htm#purchaseoptions (Accessed: 6 February 2019).

MacDougall, J. G. *et al.* (2014) 'The impact of slab dip variations, gaps and rollback on mantle wedge flow: insights from fluids experiments', *Geophysical Journal International*. Oxford University Press, 197(2), pp. 705–730. doi: 10.1093/gji/ggu053.

Mandl, G. (1988) 'Mechanics of Tectonic Faulting', in. Elsevier, p. 407.

Mandl, G., Jong, L. N. J. and Maltha, A. (1977) 'Shear zones in granular material', *Rock Mechanics Felsmechanik Mécanique des Roches*. Springer-Verlag, 9(2–3), pp. 95–144. doi: 10.1007/BF01237876.

Mann, P. (2007) 'Global catalogue, classification and tectonic origins of restraining- and releasing bends on active and ancient strike-slip fault systems', *Geological Society, London, Special Publications*, 290(1), pp. 13–142. doi: 10.1144/SP290.2.

Marques, F. O. *et al.* (2005) 'Effects of confinement on matrix flow around a rigid inclusion in viscous simple shear: insights from analogue and numerical modelling', *Journal of Structural Geology*, 27(3), pp. 379–396. doi: 10.1016/j.jsg.2004.11.005.

Marques, F. O. *et al.* (2012) 'Boudinage in nature and experiment', *Tectonophysics*. Elsevier, 526–529, pp. 88–96. doi: 10.1016/J.TECTO.2011.08.017.

Marques, F. O. and Cobbold, P. R. (2002) ‘Topography as a major factor in the development of arcuate thrust belts: insights from sandbox experiments’, *Tectonophysics*. Elsevier, 348(4), pp. 247–268. doi: 10.1016/S0040-1951(02)00077-X.

Marques, F. O. and Cobbold, P. R. (2006) ‘Effects of topography on the curvature of fold-and-thrust belts during shortening of a 2-layer model of continental lithosphere’, *Tectonophysics*. Elsevier, 415(1–4), pp. 65–80. doi: 10.1016/J.TECTO.2005.12.001.

McClay, K. and Bonora, M. (2001) ‘Analog models of restraining stepovers in strike-slip fault systems’, *AAPG Bulletin*, 85(2), pp. 233–260. doi: 10.1306/8626C7AD-173B-11D7-8645000102C1865D.

McClay, K. and Dooley, T. (1995) ‘Analogue models of pull-apart basins’, *Geology*, 23(8), p. 711. doi: 10.1130/0091-7613(1995)023<0711:AMOPAB>2.3.CO;2.

Mead, W. J. (1920) ‘Notes on the Mechanics of Geologic Structures’, *The Journal of Geology*. University of Chicago Press , 28(6), pp. 505–523. doi: 10.1086/622731.

Mellard Reade, T. (1886) *The origin of mountain ranges considered experimentally, structurally, dynamically, and in relation to their geological history*. London: Taylor and Francis. Available at: https://hdl.handle.net/2027/uc1.b4182708.

Merle, R. *et al.* (2009) ‘Evidence of multi-phase Cretaceous to Quaternary alkaline magmatism on Tore-Madeira Rise and neighbouring seamounts from 40Ar/39Ar ages’, *Journal of the Geological Society*, 166(5), pp. 879–894. doi: 10.1144/0016-76492008-060.

Mitra, S. and Paul, D. (2011) ‘Structural geometry and evolution of releasing and restraining bends: Insights from laser-scanned experimental models’, *AAPG Bulletin*, 95(7), pp. 1147–1180. doi: 10.1306/09271010060.

Morgenstern, N. R. and Tchalenko, J. S. (1967) ‘Microscopic Structures in Kaolin Subjected to Direct Shear’, *Géotechnique*, 17(4), pp. 309–328. doi: 10.1680/geot.1967.17.4.309.

Mukherjee, S., Talbot, C. J. and Koyi, H. A. (2010) ‘Viscosity estimates of salt in the Hormuz and Namakdan salt diapirs, Persian Gulf’, *Geological Magazine*, 147(4), pp. 497–507. doi: 10.1017/S001675680999077X.

Naylor, M. ., Mandl, G. and Supesteijn, C. H. . (1986) ‘Fault geometries in basement-induced wrench faulting under different initial stress states’, *Journal of Structural Geology*. Pergamon, 8(7), pp. 737–752. doi: 10.1016/0191-8141(86)90022-2.

Neres, M. *et al.* (2016) ‘Lithospheric deformation in the Africa-Iberia plate boundary: Improved neotectonic modeling testing a basal-driven Alboran plate’, *Journal of Geophysical Research: Solid Earth*, 121(9), pp. 6566–6596. doi: 10.1002/2016JB013012.

Omira, R., Neres, M. and Batista, L. (2019) ‘The Gloria Transform Fault—NE Atlantic: Seismogenic and Tsunamigenic Potential’, in *Transform Plate Boundaries and Fracture Zones*. Elsevier, pp. 157–167. doi: 10.1016/B978-0-12-812064-4.00008-6.

Panien, M., Schreurs, G. and Pfiffner, A. (2006) ‘Mechanical behaviour of granular materials used in analogue modelling: insights from grain characterisation, ring-shear tests and analogue experiments’, *Journal of Structural Geology*. Pergamon, 28(9), pp. 1710–1724. doi: 10.1016/J.JSG.2006.05.004.

Pfaff, F. (1880) *Der Mechanismus der Gebirgsbildung*. Heidelberg: Carl Winter. Available at: https://archive.org/details/dermechanismusd00pfafgoog.

Raffel, M. *et al.* (2007) *Particle image velocimetry: a practical guide*. Springer Science & Business Media.

Ramberg, H. (1955) ‘Natural and Experimental Boudinage and Pinch-and-Swell Structures’, *The Journal of Geology*, 63(6), pp. 512–526. doi: 10.1086/626293.

Ramberg, H. (1967) ‘Model Experimentation of the Effect of Gravity on Tectonic Processes’, *Geophysical Journal of the Royal Astronomical Society*, 14(1–4), pp. 307–329. doi: 10.1111/j.1365-246X.1967.tb06247.x.

Ranalli, G. (1995) *Rheology of the Earth*. 2nd edn. London: Chapman & Hall.

Ranalli, G. (2001) ‘Experimental tectonics: from Sir James Hall to the present’, *Journal of Geodynamics*, 32(1–2), pp. 65–76. doi: 10.1016/S0264-3707(01)00023-0.

Ribe, N. M. and Davaille, A. (2013) ‘Dynamical similarity and density (non-) proportionality in experimental tectonics’, *Tectonophysics*. Elsevier, 608, pp. 1371–1379. doi: 10.1016/J.TECTO.2013.06.005.

Richard, P. D., Naylor, M. a. and Koopman, A. (1995) ‘Experimental models of strike-slip tectonics’, *Petroleum Geoscience*, 1(1), pp. 71–80. doi: 10.1144/petgeo.1.1.71.

Richard, P. and Krantz, R. (1991) ‘Experiments on fault reactivation in strike-slip mode’, *Tectonophysics*, (188), pp. 117–131.

Richard, P., Mocquet, B. and Cobbold, P. R. (1991) ‘Experiments on simultaneous faulting and folding above a basement wrench fault’, *Tectonophysics*, pp. 133–141.

Riedel, W. (1929) ‘Zur Mechanik geologischer Brucherscheinungen (Ein Beitrag zum Problem der Fiederspalten)’, *Centralblatt für Mineralogie*, Abteilung(Geologie und Palaontologie), pp. 354–368.

Riedel, W. (1929) ‘Zur Mechanik geologischer Brucherscheinungen ein Beitrag zum Problem der Fiederspatten.’, *Centralblatt für Mineral. Geol. und Paläontol.*, pp. 354–368.

Román-Berdiel, T., Gapais, D. and Brun, J. P. (1997) ‘Granite intrusion along strike-slip zones in experiment and nature’, *American Journal of Science*, 297(6), pp. 651–678. doi: 10.2475/ajs.297.6.651.

Rosas, F. *et al.* (2002) ‘Sheath folds formed by drag induced by rotation of rigid inclusions in viscous simple shear flow: nature and experiment’, *Journal of Structural Geology*. Pergamon, 24(1), pp. 45–55. doi: 10.1016/S0191-8141(01)00046-3.

Rosas, F. M. *et al.* (2001) ‘Sheath fold development in bulk simple shear: Analogue modeling of natural examples from the Southern Iberian Variscan fold belt’, in *Memoir 193: Tectonic Modeling: A Volume in Honor of Hans Ramberg*. Geological Society of America, pp. 101–110. doi: 10.1130/0-8137-1193-2.101.

Rosas, F. M. *et al.* (2012) ‘Thrust–wrench interference between major active faults in the Gulf of Cadiz (Africa–Eurasia plate boundary, offshore SW Iberia): Tectonic implications from coupled analog and numerical modeling’, *Tectonophysics*, 548–549, pp. 1–21. doi: 10.1016/j.tecto.2012.04.013.

Rosas, F. M. *et al.* (2014) ‘Analog modelling of strike-slip fault (lateral) propagation from an elastic to a viscous medium: Insights from trial experiments’, *Comunicacoes Geologicas*, 101(Special Issue 3), pp. 1429–1432.

Rosas, F. M. *et al.* (2017) ‘Analogue modelling of thrust systems: Passive vs. active hanging wall strain accommodation and sharp vs. smooth fault-ramp geometries’, *Journal of Structural Geology*, 99, pp. 45–69. doi: 10.1016/j.jsg.2017.05.002.

Rowley, D. B. *et al.* (2016) ‘Kinematics and dynamics of the east pacific rise linked to a stable, deep-mantle upwelling’, *Science Advances*, 2(12), pp. 1–19. doi: 10.1126/sciadv.1601107.

De Saussure, H.-B. (1740-1799) (1779) *Voyages dans les Alpes, précédés d’un Essai sur l’histoire naturelle des environs de Genève.* Edited by S. Fauche. Neuchâtel: Imprimeur et Libraire du Roi. Available at: https://gallica.bnf.fr/ark:/12148/bpt6k102951m.texteImage (Accessed: 7 February 2019).

Schardt, H. (1884) ‘Études géologiques sur le Pays-d’Enhaut vaudois’, *Bulletin de la Société Vaudoise des Sciences Naturelles*, 20, pp. 1–183. doi: http://doi.org/10.5169/seals-260130.

Schellart, W. P. (2000) ‘Shear test results for cohesion and friction coefficients for different granular materials: scaling implications for their usage in analogue modelling’, *Tectonophysics*. Elsevier, 324(1–2), pp. 1–16. doi: 10.1016/S0040-1951(00)00111-6.

Schellart, W. P. (2002) ‘Analogue modelling of large-scale tectonic processes: an introduction’, *Journal of the Virtual Explorer*, 07. doi: 10.3809/jvirtex.2002.00045.

Schellart, W. P. (2004) ‘Kinematics of subduction and subduction-induced flow in the upper mantle’, *Journal of Geophysical Research: Solid Earth*. John Wiley & Sons, Ltd, 109(B7). doi: 10.1029/2004JB002970.

Schellart, W. P. (2008) ‘Kinematics and flow patterns in deep mantle and upper mantle subduction models: Influence of the mantle depth and slab to mantle viscosity ratio’, *Geochemistry, Geophysics, Geosystems*. John Wiley & Sons, Ltd, 9(3), p. n/a-n/a. doi: 10.1029/2007GC001656.

Schellart, W. P., Jessell, M. W. and Lister, G. S. (2003) ‘Asymmetric deformation in the backarc region of the Kuril arc, northwest Pacific: New insights from analogue modeling’, *Tectonics*. John Wiley & Sons, Ltd, 22(5), p. n/a-n/a. doi: 10.1029/2002TC001473.

Schellart, W. P., Lister, G. S. and Jessell, M. W. (2002) ‘Analogue modeling of arc and backarc deformation in the New Hebrides arc and North Fiji Basin’, *Geology*. GeoScienceWorld, 30(4), p. 311. doi: 10.1130/0091-7613(2002)030<0311:AMOAAB>2.0.CO;2.

Schellart, W. P. and Nieuwland, D. A. (2003) ‘3D evolution of a pop-up structure above a double basement strike-slip fault: Some insights from analogue modelling’, *Geological Society Special Publication*, 212(June 2007), pp. 169–179. doi: 10.1144/GSL.SP.2003.212.01.11.

Schellart, W. P. and Strak, V. (2016) ‘A review of analogue modelling of geodynamic processes: Approaches, scaling, materials and quantification, with an application to subduction experiments’, *Journal of Geodynamics*, 100, pp. 7–32. doi: 10.1016/j.jog.2016.03.009.

Schrank, C. E., Boutelier, D. a. and Cruden, A. R. (2008) ‘The analogue shear zone: From rheology to associated geometry’, *Journal of Structural Geology*, 30(2), pp. 177–193. doi: 10.1016/j.jsg.2007.11.002.

Schrank, C. E. and Cruden, A. R. (2010) ‘Compaction control of topography and fault network structure along strike-slip faults in sedimentary basins’, *Journal of Structural Geology*. Pergamon, 32(2), pp. 184–191. doi: 10.1016/J.JSG.2009.11.003.

Schreurs, G. (1994) ‘Experiments on strike-slip faulting and block rotation’, *Geology*. GeoScienceWorld, 22(6), p. 567. doi: 10.1130/0091-7613(1994)022<0567:EOSSFA>2.3.CO;2.

Schreurs, G. *et al.* (2006) ‘Analogue benchmarks of shortening and extension experiments’, *Geological Society, London, Special Publications*. Geological Society of London, 253(1), pp. 1–27. doi: 10.1144/GSL.SP.2006.253.01.01.

Schreurs, G. *et al.* (2016) ‘Benchmarking analogue models of brittle thrust wedges’, *Journal of Structural Geology*. Pergamon, 92, pp. 116–139. doi: 10.1016/J.JSG.2016.03.005.

Schreurs, G. and Colletta, B. (1998) ‘Analogue modelling of faulting in zones of continental transpression and transtension’, *Geological Society, London, Special Publications*, 135(1), pp. 59–79. doi: 10.1144/GSL.SP.1998.135.01.05.

Schreurs, G., Hänni, R. and Vock, P. (2001) ‘Four-dimensional analysis of analog models: Experiments on transfer zones in fold and thrust belts’, in *Memoir 193: Tectonic Modeling: A Volume in Honor of Hans Ramberg*. Geological Society of America, pp. 179–190. doi: 10.1130/0-8137-1193-2.179.

Shemenda, A. I. and Grocholsky, A. L. (1992) ‘Physical modelling of lithosphere subduction in collision zones’, *Tectonophysics*. Elsevier, 216(3–4), pp. 273–290. doi: 10.1016/0040-1951(92)90401-Q.

Shemenda, A. I. and Grocholsky, A. L. (1994) ‘Physical modeling of slow seafloor spreading’, *Journal*

of Geophysical Research: Solid Earth. John Wiley & Sons, Ltd, 99(B5), pp. 9137–9153. doi: 10.1029/93JB02995.

Sherlock, D. H. and Evans, B. J. (2001) 'The development of seismic reflection sandbox modeling', *AAPG Bulletin*. American Association of Petroleum Geologists, 85(9), pp. 1645–1659. Available at: http://archives.datapages.com/data/bulletns/2001/09sep/1645/1645.htm (Accessed: 7 February 2019).

Strak, V. and Schellart, W. P. (2014) 'Evolution of 3-D subduction-induced mantle flow around lateral slab edges in analogue models of free subduction analysed by stereoscopic particle image velocimetry technique', *Earth and Planetary Science Letters*. Elsevier, 403, pp. 368–379. doi: 10.1016/J.EPSL.2014.07.007.

Sylvester, A. G. (1988) 'Strike-slip faults', *Geological Society of America Bulletin*, (November), pp. 1–38. doi: 10.1130/0016-7606(1988)100<1666.

Talbot, C. J. (1977) 'Inclined and asymmetric upward-moving gravity structures', *Tectonophysics*. Elsevier, 42(2–4), pp. 159–181. doi: 10.1016/0040-1951(77)90166-4.

Tchalenko, J. S. (1970) 'Similarities between Shear Zones of Different Magnitudes', *GSA Bulletin*. GeoScienceWorld, 81(6), pp. 1625–1640. doi: 10.1130/0016-7606(1970)81[1625:sbszod]2.0.co;2.

Ueta, K., Tani, K. and Kato, T. (2000) 'Computerized X-ray tomography analysis of three-dimensional fault geometries in basement-induced wrench faulting', in *Developments in Geotechnical Engineering*, pp. 233–246. doi: 10.1016/S0165-1250(00)80019-X.

Vendeville, B. *et al.* (1987) 'Physical models of extensional tectonics at various scales', *Geological Society, London, Special Publications*. Geological Society of London, 28(1), pp. 95–107. doi: 10.1144/GSL.SP.1987.028.01.08.

Weijermars, R. (1986a) 'Finite strain of laminar flows can be visualized in SGM36-polymer', *Naturwissenschaften*. Springer-Verlag, 73(1), pp. 33–34. doi: 10.1007/BF01168803.

Weijermars, R. (1986b) 'Flow behaviour and physical chemistry of bouncing putties and related polymers in view of tectonic laboratory applications', *Tectonophysics*. Elsevier, 124(3–4), pp. 325–358. doi: 10.1016/0040-1951(86)90208-8.

Weijermars, R. (1986c) 'Polydimethylsiloxane flow defined for experiments in fluid dynamics', *Applied Physics Letters*. American Institute of Physics, 48(2), pp. 109–111. doi: 10.1063/1.97008.

Weijermars, R., Jackson, M. P. A. and Vendeville, B. (1993) 'Rheological and tectonic modeling of salt provinces', *Tectonophysics*, 217(1–2), pp. 143–174. doi: 10.1016/0040-1951(93)90208-2.

Weijermars, R. and Schmeling, H. (1986) 'Scaling of Newtonian and non-Newtonian fluid dynamics without inertia for quantitative modelling of rock flow due to gravity (including the concept of rheological similarity)', *Physics of the Earth and Planetary Interiors*. Elsevier, 43(4), pp. 316–330. doi: 10.1016/0031-9201(86)90021-X.

Willingshofer, E. and Sokoutis, D. (2009) 'Decoupling along plate boundaries: Key variable controlling the mode of deformation and the geometry of collisional mountain belts', *Geology*. GeoScienceWorld, 37(1), pp. 39–42. doi: 10.1130/G25321A.1.

Willis, B. (1894) 'The mechanics of Appalachian structure', in *USGS Annual Report*. Vol. 13. US Government Printing Office.

Wu, J. *et al.* (2009) '4D analogue modelling of transtensional pull-apart basins', *Marine and Petroleum Geology*. Elsevier Ltd, 26(8), pp. 1608–1623. doi: 10.1016/j.marpetgeo.2008.06.007.

Yamada, Y., Baba, K. and Matsuoka, T. (2006) 'Analogue and numerical modelling of accretionary prisms with a décollement in sediments', *Geological Society, London, Special Publications*, 253(1), pp. 169–183. doi: 10.1144/GSL.SP.2006.253.01.09.

Appendix B.

An earlier version of this work was presented in the European Geoscience Union (EGU) General Assembly (2018), an international conference on Geoscience held annualy in Vienna. Here I present the abstract subbmited, as featured in the conference proceedings.

Geophysical Research Abstracts
Vol. 20, EGU2018-443, 2018
EGU General Assembly 2018

Strike-slip fault propagation across crustal (interbedded) low viscosity anomalies: new insight from analogue modelling results

Afonso Gomes (1), Filipe Rosas (1,2), João Duarte (1,2,3), Ricardo Tomás (4), Jaime Almeida (1,2), Vincent Strak (5), and Wouter Schellart (5)

(1) University of Lisbon, IDL, Faculty of Science , Geology, Portugal (agomes@alunos.fc.ul.pt), (2) Instituto Dom Luiz, Faculdade de Ciências, Universidade de Lisboa, Portugal, (3) School of Earth, Atmosphere and Environment, Monash University, Melbourne, Australia, (4) School of Earth and Environmental Sciences, University of Portsmouth, Portsmouth, UK, (5) Faculty of Earth and Life Sciences, Vrije Universiteit Amsterdam, Amsterdam, Netherlands

Upper crustal propagation of sub-vertical strike-slip faults across relatively softer (i.e. low viscosity) bodies is investigated through a series of analogue modelling experiments. The low viscosity bodies are here generally considered in *sensu lato* and could potentially represent crustal magmatic chambers, evaporitic dome-like structures, or other mechanically soft anomalies occurring in nature, interbedded in upper-crustal rocks, generally exhibiting sill-like or inverted drop geometries. The aim of the experiments was to investigate the type of structures that are expected to be developed as a result of the interference arising from brittle strike-slip propagation across a topographical and/or mechanical barrier.

Four main different types of experiments were systematically carried out to evaluate the either isolated or combined effect of rheological and morphological (i.e. topographical) anomalies: 1) A benchmark experiment (essentially used to gauge the results arising from the rest of the experimental sets) comprising vertical strike slip faulting cutting across an isotropic brittle medium (represented by a colour-layered sand-cake); 2) A vertical strike-slip fault propagating across the same brittle medium, but cutting across a relatively small central rheological barrier (low viscosity body), represented by different mixtures of silicone putty (PDMS) and high-density powders (e.g. Wolframite powder); 3) The same experimental setting as before, except for the fact that in this case no mechanical/rheological anomaly exists, but instead a morphological barrier (i.e. a topographic central elevated domain) was prescribed; 4) Finally, the same vertical strike-slip fault was set to propagate across both a rheological and a

morphological barrier (i.e. consisting in an elevation with an inner low viscosity body).

Differently orientated slices of the resulting sand-silicone models were obtained to reconstruct the 3D geometry of the resulting surface structures (Y-shears, Riedel faults, etc.) and of the deformed low viscosity body.

Preliminary results show that a specific structural pattern is developed in each case, which could potentially be used as a proxy for the governing geological/geodynamic (general) setting at stake. The main effect produced by the low viscosity rheological anomaly is represented by a delay in the propagation to the surface of typical brittle shear structures (Y-shears and Riedels) above the anomaly area. These structures are hence sparser, or event absent in this domain, since a significant part of the ongoing deformation is here accommodated by viscous strain. Additionally, the structural pattern perturbation caused by the existence of a (strictly) morphological anomaly is essentially manifested by a local deflection (synthetic rotation) of the same main brittle shear structures, which are also generally wider (less penetrative) above the topographic high.

In the experiments in which the combined (morpho-mechanical) effect of a local perturbation was investigated, the resulting structural patterns reflected the conjugated effects of both low viscosity and topography, namely depicting rotation of structures in the sand surface due to shear synthetic bulk vorticity in the underlying low viscosity anomaly.

These results, and all specifically obtained structural patterns were further discussed based on comparison with different selected natural examples.